


5-2018

# Functional Similarity of PRD-Containing Virulence Regulators in *Bacillus anthracis*

Malik Raynor

Follow this and additional works at: [https://digitalcommons.library.tmc.edu/utgsbs\\_dissertations](https://digitalcommons.library.tmc.edu/utgsbs_dissertations)

 Part of the [Bacteriology Commons](#), [Biochemistry Commons](#), [Molecular Biology Commons](#), [Molecular Genetics Commons](#), and the [Pathogenic Microbiology Commons](#)

---

## Recommended Citation

Raynor, Malik, "Functional Similarity of PRD-Containing Virulence Regulators in *Bacillus anthracis*" (2018). *UT GSBS Dissertations and Theses (Open Access)*. 857.

[https://digitalcommons.library.tmc.edu/utgsbs\\_dissertations/857](https://digitalcommons.library.tmc.edu/utgsbs_dissertations/857)

This Dissertation (PhD) is brought to you for free and open access by the Graduate School of Biomedical Sciences at DigitalCommons@TMC. It has been accepted for inclusion in UT GSBS Dissertations and Theses (Open Access) by an authorized administrator of DigitalCommons@TMC. For more information, please contact [laurel.sanders@library.tmc.edu](mailto:laurel.sanders@library.tmc.edu).

FUNCTIONAL SIMILARITY OF PRD-CONTAINING VIRULENCE REGULATORS IN

*BACILLUS ANTHRACIS*

by

*Malik Jamaal Raynor, B.S.*

APPROVED:

---

Theresa M. Koehler, Ph.D.  
Advisory Professor

---

Peter J. Christie, Ph.D.

---

Kevin A. Morano, Ph.D.

---

Hung Ton-That, Ph.D.

---

Eric J. Wagner, Ph.D.

APPROVED:

---

Dean, The University of Texas  
MD Anderson Cancer Center UTHealth Graduate School of Biomedical Sciences

FUNCTIONAL SIMILARITY OF PRD-CONTAINING VIRULENCE REGULATORS IN  
*BACILLUS ANTHRACIS*

A

DISSERTATION

Presented to the Faculty of

The University of Texas

MD Anderson Cancer Center UTHealth

Graduate School of Biomedical Sciences

in Partial Fulfillment

of the Requirements

for the Degree of

DOCTOR OF PHILOSOPHY

by

Malik Jamaal Raynor, B.S.

Houston, Texas

Date of Graduation (*May, 2018*)

# FUNCTIONAL SIMILARITY OF PRD-CONTAINING VIRULENCE REGULATORS IN

## *BACILLUS ANTHRACIS*

Malik Jamaal Raynor, B.S.

Advisory Professor: Theresa M. Koehler, Ph.D.

*Bacillus anthracis* produces three regulators, AtxA, AcpA, and AcpB, that control virulence gene expression and are members of an emerging class of regulators termed “PCVRs” (Phosphoenolpyruvate-dependent phosphotransferase regulation Domain-Containing Virulence Regulators). AtxA controls expression of the toxin genes; *lef*, *cya*, and *pag*, and is the master virulence regulator and archetype PCVR. AcpA and AcpB are less well studied. AcpA and AcpB independently positively control transcription of the capsule biosynthetic operon *capBCADE*, and culture conditions that enhance AtxA activity result in *capBCADE* transcription in strains lacking *acpA* and *acpB*. RNA-Seq was used to assess the regulons of the paralogs in strains producing individual PCVRs at native levels. Plasmid- and chromosome-borne genes were PCVR-controlled, with AtxA, AcpA, and AcpB having a  $\geq 4$ -fold effect on transcript levels of 145, 130, and 49 genes respectively. Several genes were co-regulated by two or three PCVRs. Results from transcriptional reporters of PCVR-regulated promoters fused to promoterless *lacZ* genes largely mirrored RNA-Seq data showing AtxA alone had activity on *Plef-lacZ*, and AcpA and AcpB had more activity than AtxA on *PcapB-lacZ*. Studies to test the effect of AtxA levels on virulence and sporulation used *atxA* mutants. A mutant that overexpressed *atxA* and exhibited elevated AtxA and toxin levels *in vitro*, was not increased for virulence in a murine anthrax infection model. AtxA levels also affected sporulation efficiency. Culture of *B. anthracis* in medium containing bicarbonate and elevated carbon dioxide increased PCVR activity compared to culture in ambient air in medium lacking bicarbonate. However, neither the solubility nor stability of the regulators was affected by carbon dioxide concentration. AcpA and AcpB form homomultimers and multimerization was dependent on the

EII<sub>B</sub>-like domains, as shown previously for AtxA. Heteromultimers of AtxA-AcpA were detected and in co-expression experiments, AcpA activity was reduced by increased levels of AtxA. An AtxA orthologue in *Bacillus cereus*, AtxA2, had less activity than AtxA from *B. anthracis* potentially due to reduced dimer formation. The results provided in this dissertation increase our knowledge of virulence gene expression in *B. anthracis*, while advancing our understanding of this newly-discovered class of transcriptional regulators.

## Table of Contents

Approval Sheet.....	i
Title Page.....	ii
Abstract.....	iii
Table of Contents.....	v
List of Figures.....	viii
List of Tables.....	x
<b>Chapter I: Introduction.....</b>	<b>1</b>
1.1 Gene expression modulated by environmental conditions.....	2
1.2 PRD-containing virulence regulators.....	5
1.3 <i>Bacillus anthracis</i> and anthrax disease.....	7
1.4 Virulence factors in anthrax pathogenesis.....	9
1.5 AtxA: the most well-characterized PCVR.....	11
1.6 AcpA and AcpB: regulators of capsule expression.....	14
1.7 AtxA2, an AtxA homologue in <i>Bacillus cereus</i> strain G9241.....	14
1.8 Gaps in knowledge and significance of this work.....	15
<b>Chapter II: Materials and Methods.....</b>	<b>17</b>
2.1 Culture conditions.....	18
2.2 Strain construction.....	18
2.3 Native and IPTG-induced PCVR expression.....	21
2.4 RNA isolation for RNA-seq.....	21
2.5 Creation of Next Generation Sequencing (NGS) libraries for RNA-seq and sequencing.....	22
2.6 RNA-seq and bioinformatic analysis.....	23
2.7 Western blotting.....	24
2.8 India ink exclusion assay.....	25

2.9 Co-affinity purification.....	25
2.10 AcpA-His and AcpB-His purification.....	26
2.11 Bis-maleimido-hexane crosslinking.....	26
2.12 Mouse infections.....	27
2.13 Heat-resistant CFU determination.....	27
2.14 Real-time quantitative PCR (RT-qPCR).....	28
<b>Chapter III: Regulons of PRD-containing <i>Bacillus anthracis</i> virulence regulators reveal overlapping but distinct functions.....</b>	<b>35</b>
3.1 Introduction.....	36
3.2 Results.....	38
3.2.1 Amino acid sequence and predicted domain similarity of the <i>B. anthracis</i> PCVRs.....	38
3.2.2 Native PCVR protein and transcript levels.....	41
3.2.3 Overlapping regulons of AtxA, AcpA, and AcpB.....	45
3.2.4 Loci of PCVR-regulated genes.....	49
3.2.5 Effects of individual PCVRs on established virulence genes.....	54
3.3 Discussion.....	58
<b>Chapter IV: Carbon dioxide, protein stability, and PCVR interactions.....</b>	<b>63</b>
4.1 Introduction.....	64
4.2 Results.....	66
4.2.1 Induced expression of <i>acpA</i> and <i>acpB</i> in <i>B. anthracis</i> cultures.....	66
4.2.2 AcpA and AcpB activity in <i>B. anthracis</i> cultures.....	68
4.2.3 Carbon dioxide effect on regulator activity.....	69
4.2.4 Relative activities of the <i>B. anthracis</i> PCVRs on <i>in vivo</i> reporters.....	74
4.2.5 <i>B. anthracis</i> PCVR homomultimerization and the role of the intrinsic functional domains.....	77
4.2.6 Heteromultimerization of PCVRs.....	90

4.3 Discussion.....	93
<b>Chapter V: The roles of AtxA orthologs in an anthrax-like <i>Bacillus cereus</i> strain.....</b>	<b>98</b>
5.1 Introduction.....	99
5.2 Results.....	102
5.2.1 Activity of AtxA and AtxA2.....	102
5.2.2 Multimerization of AtxA proteins.....	102
5.3 Discussion.....	109
<b>Chapter VI: Dual role for AtxA: control of sporulation and anthrax toxin production....</b>	<b>112</b>
6.1 Introduction.....	113
6.2 Results.....	118
6.2.1 AtxA modulates sporulation efficiency through SkiA.....	118
6.2.2 Elevated <i>atxA</i> expression does not result in increased virulence.....	122
6.3 Discussion.....	122
<b>Chapter VII: Discussion.....</b>	<b>127</b>
7.1 Noteworthy results and significance of <i>B. anthracis</i> PCVRs.....	128
7.2 Model for virulence gene regulation in <i>B. anthracis</i> .....	129
7.3 AtxA, AcpA, and AcpB: a case for divergent evolution.....	132
7.4 Evolutionary advantage to cross-talk between genetic elements.....	135
7.5 PCVR paralogues in other organisms may have shared functionality.....	136
7.6 Concluding remarks.....	137
<b>References.....</b>	<b>142</b>
<b>Vita.....</b>	<b>159</b>



## List of Figures

<b>Figure 1-1.</b> The phosphoenolpyruvate-dependent phosphotransferase system.....	4
<b>Figure 1-2.</b> PRD-Containing Virulence Regulators.....	6
<b>Figure 1-3.</b> Model for virulence gene regulation in <i>B. anthracis</i> .....	12
<b>Figure 3-1.</b> Amino acid sequence alignment and structures of <i>Bacillus anthracis</i> PCVRs.....	40
<b>Figure 3-2.</b> <i>In vivo</i> activity of recombinant His-tagged and FLAG-tagged AcpA and AcpB.....	42
<b>Figure 3-3.</b> Native PCVR expression and capsule production.....	44
<b>Figure 3-4.</b> PCVR transcript levels.....	46
<b>Figure 3-5.</b> Venn diagrams of PCVR regulons.....	48
<b>Figure 3-6.</b> Sequencing reads mapping to PCVR-regulated loci.....	51
<b>Figure 3-7.</b> Heat map and dendrogram of hierarchical clustering among PCVR regulons.....	53
<b>Figure 3-8.</b> Edema Factor Production by the individual PCVRs.....	55
<b>Figure 3-9.</b> Capsule production by the individual PCVRs.....	57
<b>Figure 4-1.</b> Induced PCVR expression.....	70
<b>Figure 4-2.</b> <i>In vivo</i> activity of AcpA-His and AcpB-His.....	72
<b>Figure 4-3.</b> AcpA and AcpB CO <sub>2</sub> -dependent activity.....	75
<b>Figure 4-4.</b> Effects on steady state protein levels by culture in CA-Air vs. CACO <sub>3</sub> .....	76
<b>Figure 4-5.</b> Stability of AcpA-FLAG and AtxA-FLAG in CACO <sub>3</sub> and CA-Air.....	78
<b>Figure 4-6.</b> Activities of <i>B. anthracis</i> PCVRs on <i>PcapB-lacZ</i> and <i>Plcf-lacZ</i> .....	79
<b>Figure 4-7.</b> Homomultimerization AcpA and AcpB.....	82
<b>Figure 4-8.</b> Multimerization and activity of AcpA and AcpB EIIB-like domain truncation mutants.....	85
<b>Figure 4-9.</b> AtxA crystal structure and structural models of <i>B. anthracis</i> chimeric PCVRs.....	86
<b>Figure 4-10.</b> Dose-dependent expression and activity of PCVR chimeras.....	87
<b>Figure 4-11.</b> PCVR chimera multimerization.....	89
<b>Figure 4-12.</b> Heteromultimerization by PCVRs.....	91
<b>Figure 4-13.</b> AtxA effect on AcpA and AcpB activity.....	92

<b>Figure 5-1.</b> Amino acid alignment of AtxA homologues.....	103
<b>Figure 5-2.</b> <i>In vivo</i> activity of AtxA-His and AtxA2-His.....	104
<b>Figure 5-3.</b> Dimerization of AtxA2.....	107
<b>Figure 5-4.</b> Specific binding of AtxA2-His to AtxA-FLAG.....	108
<b>Figure 6-1.</b> Schematic representation of the <i>atxA</i> promoter region.....	119
<b>Figure 6-2.</b> Spore quantification and <i>skiA</i> transcript levels in PA-air.....	120
<b>Figure 6-3.</b> Spore quantification and <i>skiA</i> transcript levels in CACO <sub>3</sub> .....	123
<b>Figure 6-4.</b> Virulence of parent and <i>atxA</i> mutants.....	124
<b>Figure 7-1.</b> Comprehensive model of virulence gene regulation in <i>B. anthracis</i> .....	130
<b>Figure 7-2.</b> Phylogram of AtxA, AcpA, and AcpB.....	133
<b>Figure 7-3.</b> PCVR locus-activity relationships.....	140

## List of Tables

<b>Table 2-1.</b> <i>B. anthracis</i> strains and plasmids.....	30
<b>Table 2-2.</b> Primers used in this dissertation.....	33
<b>Table 3-1.</b> Genes most highly regulated by the PCVRs.....	50

# **Chapter I.**

## **Introduction**

## 1.1 Gene expression modulated by environmental conditions

Bacteria occupy diverse habitats and must respond to changing environmental conditions, which may include nutrient availability, cell density, temperature stress, UV radiation, and desiccation, among others. To survive, bacteria may adapt to these conditions by altering their physiology through changes in gene expression. Environmental sensing and gene expression are often linked by specialized mechanisms that include cell surface receptors, phosphorelay pathways, and transcriptional regulators.

In quorum sensing, small molecules released into the extracellular medium by bacteria stimulate cell-surface or intracellular receptors and initiate gene expression changes. The concentration of these small molecules function as a proxy for cell density and modulate gene expression networks that produce phenotypes that could be beneficial when produced by many cells (1, 2). Quorum sensing coordinates processes related to biofilm formation, virulence, and antibiotic resistance in response to the local density of the bacterial population (3).

While quorum sensing enables bacterial communities to coordinate changes in gene expression, two-component systems allow bacteria to sense and respond to changes in the environment in a manner largely independent of other bacteria. These systems typically consist of a membrane-bound histidine kinase that responds to a specific environmental signal such as a nutrient, and a cognate response regulator that confers a cellular response, typically through regulation of target gene expression (4). Upon stimulation by an environmental signal the histidine kinase autophosphorylates a specific histidine and the cognate response regulator transfers the phosphate to a specific aspartate residue on the response regulator. The phosphorylated response regulator undergoes a conformational change that allows for activation (or repression) of target genes (5). Two-component systems have been adapted to sense and respond to changes in osmolarity, antibiotics, temperature, chemo attractants, and pH, in addition to other environmental conditions and stresses (6).

A third system, the phosphoenolpyruvate (PEP)-dependent phosphotransferase system (PTS), functions specifically as a carbohydrate sensor and is responsible for expression of

genes involved in both the uptake and catabolism of certain sugars (**Figure 1-1**). Glucose, mannose, fructose, and cellobiose are some of the sugars imported into bacteria by the PTS (7). The PTS has two general cytoplasmic components: Enzyme I (EI) and Histidine Protein (HPr) (**Figure 1-1**). EI autophosphorylates at a specific histidine in the presence of PEP aiding in the conversion of phosphoenolpyruvate to pyruvate (8). Phosphorylated EI transfers the phosphate to HPr at a specific histidine. HPr can then phosphotransfer to a carbohydrate-specific Enzyme II (EII) complex which consists of one or two integral membrane domains (domains C and D) and two cytoplasmic domains (domains A and B). The multiple EII domains work together to transport and phosphorylate carbohydrates across the bacterial membrane to be used in catabolic pathways such as glycolysis (7).

In response to the availability of carbohydrates in the environment the PTS regulates the expression of catabolic genes. Phosphorylated HPr and several phosphorylated EIIBs, in addition to their role as phosphocarriers to phosphorylate imported carbohydrates, can phosphorylate transcriptional regulators to control their activity (**Figure 1-1**). These transcriptional regulators control expression of operons encoding carbohydrate-specific PTS components. Many of these PTS-controlled transcriptional regulators have similar domain organization. The amino termini contain motifs for nucleic acid binding, followed by two PTS regulation domains (PRD). The carboxy termini of these regulators generally contain motifs with homology to components of the EII complex (EIIA or EIIB). The homologous EII region of the transcriptional regulators often contain residues that can act as phosphoryl acceptors. In the absence of a cognate sugar to import some regulators are phosphorylated by membrane-bound EII components sequestering them to the membrane where they remain inactive (9). The PRDs are unique domains with the specific function of controlling transcriptional activity of these proteins. PRDs are generally found in tandem pairs with each domain containing two histidine residues that can be phosphorylated by HPr or EIIB.

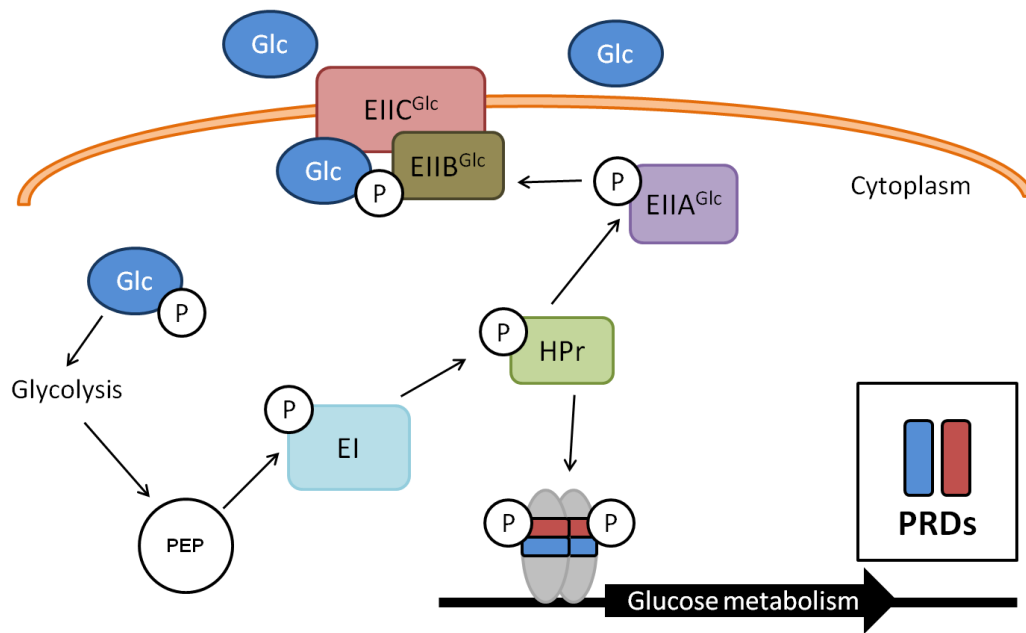


**Figure 1-1.** The phosphoenolpyruvate-dependent phosphotransferase system  
 The phosphotransferase system is responsible for import and metabolism of many carbohydrates in both Gram + and Gram – bacteria. The system consists of two general proteins, Enzyme I (EI) and HPr and an Enzyme II complex usually consisting of 3 components, EIIA, B, & C which are specific for each sugar imported. This cartoon depicts the glucose-specific EII. To begin the cycle, EI autophosphorylates using a phosphate from phosphoenolpyruvate or PEP, which is a product of glycolysis. The phosphate is transferred from EI to HPr. HPr transfers the phosphate to the sugar-specific EIIA. EIIA then transfers the phosphate to the sugar specific EIIB. EIIC is membrane spanning and translocates glucose inside the cell at which point EIIB phosphorylates the sugar leading to glucose-6-phosphate. G-6-P can then enter glycolysis continuing the cycle. HPr can also phosphorylate transcriptional regulators that control the expression of genes needed for cognate carbohydrate metabolism. Phosphorylation of these regulators occurs at conserved histidines within phosphotransferase regulatory domains, or PRDs.

Phosphorylation within PRDs can either be stimulatory or inhibitory with regard to transcriptional activity (7).

The PTS, in addition to two-component and quorum sensing systems, together represent some of the multitude of environmental sensing networks that are coupled with manipulation of gene expression, and underscore the importance of these networks for survival of bacteria in the environment. For pathogenic bacteria, the host environment represents a harsh environment lacking readily available nutrients such as iron. Many of these environmental sensing networks have evolved to function within the host environment. Moreover, in pathogens such as group A *Streptococcus* and uropathogenic *Escherichia coli*, the PTS has been associated with virulence.

## 1.2 PRD-containing virulence regulators

Within the last several years a subset of PRD-containing transcriptional regulators has been associated with virulence (**Figure 1-2**). These PRD-Containing Virulence Regulators (PCVR) are present primarily in Gram-positive pathogens. In *Streptococcus pyogenes*, a group A Streptococci, the transcriptional activator Mga is required for adhesion, internalization, and immune evasion (10). The amino acid sequence of Mga is predictive of an amino terminal conserved Mga domain (CMD) and DNA-binding region, followed by two PRDs, and finally a carboxy-terminal domain with homology to EII of the PTS. Phosphorylation of Mga by the PTS has been demonstrated, and phosphomimetic mutations affect DNA-binding affinities of Mga-regulated promoters (11). The RivR regulator, also in GAS, has two putative DNA-binding domains at the amino terminus followed by two PRDs. Expression of the protein-G-related  $\alpha_2$ -macroglobulin-binding protein (GRAB), a cell wall-anchored virulence factor involved in inhibition of proteases in human plasma, and hyaluronic acid capsule are negatively regulated by RivR (12). The amino acid sequence of RivR has 22% identity and 49% similarity to that of Mga in *S. pyogenes*, and predicts two amino terminal helix-turn-helix domains in addition to a PRD (13). In *Streptococcus pneumoniae*, the MgaSpn transcriptional regulator plays a



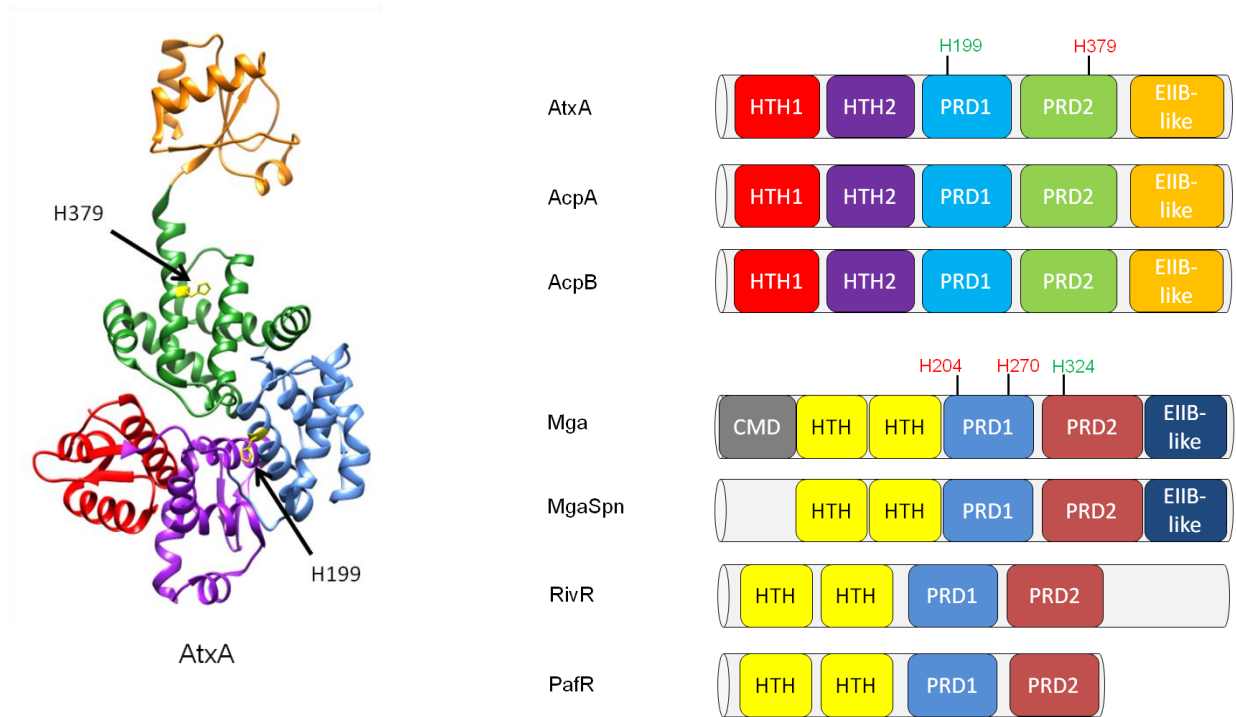


**Figure 1-2.** PRD-Containing Virulence Regulators

The AtxA crystal structure contains five domains: a winged helix-turn-helix (**WH**) motif, a helix-turn-helix (**HTH**) motif, two PTS regulation domains (**PRD1** & **PRD2**), and an Enzyme IIB-like (**EIIB-like**) motif. Cartoons of other PCVRs are shown for comparison to AtxA and many show similar domain organization. Mga contains a conserved Mga domain (CMD) that plays a role in target specificity. Phosphorylated histidines are indicated for PCVRs in which the phosphorylation state is known. A green label indicates a positive effect on activity, whereas a red label denotes a negative effect on activity.

significant role in both nasopharyngeal colonization and progression to pneumonia in murine infection models (14). The amino acid sequence of MgaSpn has 21.4% identity and 42.6% similarity to that of Mga produced by *S. pyogenes*. A putative domain search using the amino acid sequence of MgaSpn also predicts similar domains to Mga, including two PRDs. In uropathogenic *Escherichia coli* (UPEC), PafR is a transcriptional regulator with antiterminator activity, and is required for optimal urinary tract colonization in a murine infection model. PafR also inhibits biofilm formation and motility in UPEC (15). *In silico* analysis of the PafR amino acid sequence reveals at least one PRD.

*Bacillus anthracis*, the etiologic agent of anthrax, possesses three such PCVRs; AtxA, AcpA, and AcpB, that control expression of the major virulence determinants. The presence of three PCVRs in *B. anthracis* presents a unique opportunity to study the activity and interactions of multiple similar regulators that are native to a single organism. The work I present in this dissertation specifically examines PCVR activity, providing a global and specific analysis of the role of each *B. anthracis* PCVR homologue in virulence gene expression.

### **1.3 *Bacillus anthracis* and anthrax disease**

*B. anthracis* is a Gram-positive spore-forming bacterium that is commonly found in the soil. The genome consists of a 5.23-Mb chromosome and two large plasmids, pXO1 (182 kb) and pXO2 (96 KB) (16). Genes encoding the major virulence factors are located on the plasmids. The anthrax toxin structural genes; *pagA* (Protective Antigen, PA), *cya* (Edema Factor, EF), and *lef* (Lethal Factor, LF) are located on pXO1. The genes required for capsule biosynthesis (*capBCADE*) are encoded in an operon on pXO2 (17).

Plasmids with similarity to pXO1 and pXO2 have been found in other closely related *Bacillus* species. *B. anthracis* is a member of the *Bacillus cereus* group species which includes *Bacillus cereus*, a causative agent of food poisoning and opportunistic infections, and *Bacillus thuringiensis*, an insect pathogen. Plasmids similar to pXO1 and pXO2 have been identified in *B. cereus* strains (18–20). Given that all three species share DNA sequence similarity and gene

synteny, it is likely that horizontal gene transfer is a mechanism for sharing plasmids among closely related soil pathogens (21).

The soil habitat presents challenges such as temperature variation, desiccation, UV irradiation, and nutrient deprivation. *B. anthracis* forms spores to survive adverse environmental conditions. Spores exhibit minimal metabolic activity and retain viability when faced with multiple environmental challenges (22). In the soil environment, alkaline pH, high organic content, moisture, temperatures above 15°C, and exudates from plant roots have been reported to promote spore germination (23, 24).

The *B. anthracis* spore is the infectious form of the bacterium. Spores can enter the body through cuts or scrapes on the skin, inhalation, or ingestion with each route of entry leading to a specific anthrax disease pathology. Regardless of the route of infection, *B. anthracis* spores are thought to be transported by macrophages to regional draining lymph nodes and then enter the blood stream, resulting in systemic dissemination (25). Cutaneous anthrax results from spore entry through skin abrasions and accounts for 95% of all anthrax cases (26). Patients with cutaneous anthrax present with a small blister surrounded by swollen tissue that develops into a painless black ulcer called an eschar (25). Gastrointestinal and inhalational anthrax result from ingestion or inhalation of spores, respectively. Gastrointestinal anthrax results in gastrointestinal pain, vomiting of blood, severe diarrhea, acute inflammation of the digestive tract, and loss of appetite (27). Inhalational anthrax symptoms are very similar to cold and flu symptoms and include fever, shortness of breath, cough, fatigue, and chills. Inhalational anthrax is distinguished by a characteristic widening of the mediastinum. Inhalational anthrax has the highest mortality rate of all forms of the disease, 45% with antibiotic therapy and more than 97% without treatment. Gastrointestinal has a similar mortality rate to inhalational anthrax, and cutaneous anthrax has the lowest mortality rate, 1% with antibiotic treatment and 20% with no treatment (28).

#### 1.4 Virulence factors in anthrax pathogenesis

Following germination in the host, *B. anthracis* vegetative cells synthesize several factors associated with pathogenesis. Two of the most studied virulence factors are a tripartite toxin and a poly- $\gamma$ -D-glutamic acid (PDGA) capsule. Capsule-negative or toxin-deficient mutants are highly attenuated in some animal models for anthrax (29, 30).

The anthrax toxins are classified as A/B-type bacterial toxins, with LF or EF comprising the enzymatic activity, or (A) moiety, and PA representing the binding component (B) (31). Initially, PA binds either of two proteinaceous cellular receptors; ANTXR1 and ANTXR2 (32), and is cleaved by a furin protease. PA is cleaved into two fragments, PA<sub>20</sub> (20 kDa) and PA<sub>63</sub> (63 kDa) (33). PA<sub>63</sub> remains bound to the cellular receptor and spontaneously heptamerizes on the cell surface (34). EF and LF bind to heptameric PA<sub>63</sub> and the complex enters the cell by endocytosis (35–37). Once the endosome matures, the pH drops following the reversal of proton pumps in the endosomal membrane. Low pH triggers a conformational change in the PA complex resulting in the formation of a pore and escape of EF and LF from the endosome (38, 39). Lethal factor is a Zn<sup>2+</sup> metalloprotease that cleaves mitogen-activated protein kinase kinases which results in suppression of pro-inflammatory cytokines and may induce apoptosis (40). Edema factor is a calmodulin- and Ca<sup>2+</sup>-dependent adenylate cyclase that elevates the intracellular cAMP concentration (41). Edema factor has been shown to inhibit phagocytosis of spores by human polymorphonuclear leukocytes in an *in vitro* infection model (42).

The proteinaceous PDGA capsule of *B. anthracis* is uncommon in bacteria, but is essential for establishing infection leading to anthrax. *In vitro* experiments show that the PDGA capsule is antiphagocytic, similar to capsule function in other bacteria (43, 44). The *capBCADE* operon on pXO2 encodes proteins required for capsule synthesis. CapB is an ATP-dependent ligase and functions with CapC to synthesize PDGA (45). Polymers of  $\gamma$ -linked D-glutamic acid residues can reach up to 216 kDa (46). Polymers of PDGA are transported across the cell membrane by CapA and CapE (47). CapD is a  $\gamma$ -glutamyl transpeptidase (GGT)-family protein

that cleaves the  $\gamma$ -linked peptide bond of the polyglutamate capsule which is thought to serve two roles; anchoring capsule polymers to the cell wall, and the release of small PDGA polymers into the extracellular environment; the latter function is required for full virulence (47–49). The release of small PDGA polymers may contribute to pathogenesis by suppressing the responses of immune cells and disrupting the maturation of immature dendritic cells (50).

Although toxin and capsule are considered the primary virulence factors required for *B. anthracis* pathogenesis, several other factors may contribute to overall disease progression. The secreted chaperone/protease HtrA, for High temperature requirement A, is thought to aide in survival during heat, oxidative, ethanol, and osmotic stress. *htrA* mutants exhibit delayed growth in a macrophage infection assay, in addition to a  $\geq 6$ -fold decrease in virulence relative to the parent strain in a guinea pig model of anthrax (51). MntA is the solute-binding component of a  $Mn^{2+}$  ATP-binding cassette transporter and is involved in optimal growth and survival of *B. anthracis* when incubated with cultured macrophages, or when the bacteria are exposed to oxidative stress. Moreover, the lethal dose ( $LD_{50}$ ) of *mntA*-null mutants was reported to be  $10^4$ -fold higher than that of the parent strain in a guinea pig model for anthrax in which spores were injected subcutaneously (52). The regulatory ATPase subunit of the ClpXP protease, ClpX, is required for hemolytic and proteolytic phenotypes observed when *B. anthracis* is cultured on blood and casein solid agar media, respectively. Strains lacking ClpX are attenuated in murine and guinea pig models of anthrax. Host substrates for extracellular proteolytic activity requiring ClpX functionality include cathelicidin and alpha-defensin antimicrobial peptides, in addition to lysozyme (53). Additionally, *B. anthracis* produces two siderophores, bacillibactin and petrobactin, but only petrobactin has been shown to be required for full virulence in a murine infection model (54). Lastly, the surface adhesin BslA, a protein found in the S-layer, a paracrystalline matrix distal to the peptidoglycan, is required for sufficient adhesion to host cells. Deletion of *bslA* results in a substantial increase in  $LD_{50}$ , mean time-to-death, and decreased bacterial burden in host organs (55). So while the toxin and capsule may be the

major contributors to anthrax pathogenesis, other virulence determinants play smaller roles that contribute to overall disease progression.

### 1.5 AtxA: The most well-characterized PCVR

The Anthrax Toxin Activator AtxA (56 kDa) is the master virulence regulator in *B. anthracis*, and controls expression of the anthrax toxin genes *lef*, *cya*, and *pagA* (49, 56, 57) (**Figure 1-3**). In addition to positive regulation of toxin gene expression, microarray studies to determine the AtxA regulon indicate that expression of the capsule biosynthesis operon and at least 38 other genes are affected by AtxA (56). How AtxA initiates transcription is unknown and a consensus sequence within AtxA-regulated promoters has not been identified. However, intrinsic curvature in AtxA-regulated promoters may play a role in AtxA-mediated gene expression (58). In agreement with positive regulation of toxin and capsule, an *atxA*-null mutant exhibits attenuated virulence in a murine model of anthrax (30).

Expression of *atxA* is governed by environmental signals and other *trans*-acting factors. Cultures of *B. anthracis* cultivated at 37°C produce more *atxA* transcripts and higher AtxA protein levels than cultures incubated at 28°C (59). Two small c-type cytochromes, which influence cellular redox state, were found to affect expression of *atxA*. Deletion of genes encoding c-type cytochromes and other constituents in the cytochrome c biogenesis pathway cause *atxA* expression to be dysregulated, and transcripts of *atxA* and toxin components were produced earlier in growth phase relative to the parent strain (60). Similar growth phase-dependent dysregulation of *atxA* expression is mediated by AbrB. A well-characterized homolog of AbrB in *Bacillus subtilis* governs the timing of expression of multiple genes by binding to DNA sequences near the transcriptional start site and occluding RNA polymerase (61). In *B. anthracis*, AbrB is the only *trans*-acting factor known to interact directly with the *atxA* promoter to affect transcription. In batch culture, AbrB represses *atxA* during exponential growth and repression is relieved in transition-to-stationary phase (62). Nutrient conditions also influence *atxA* expression. In batch culture the presence of glucose

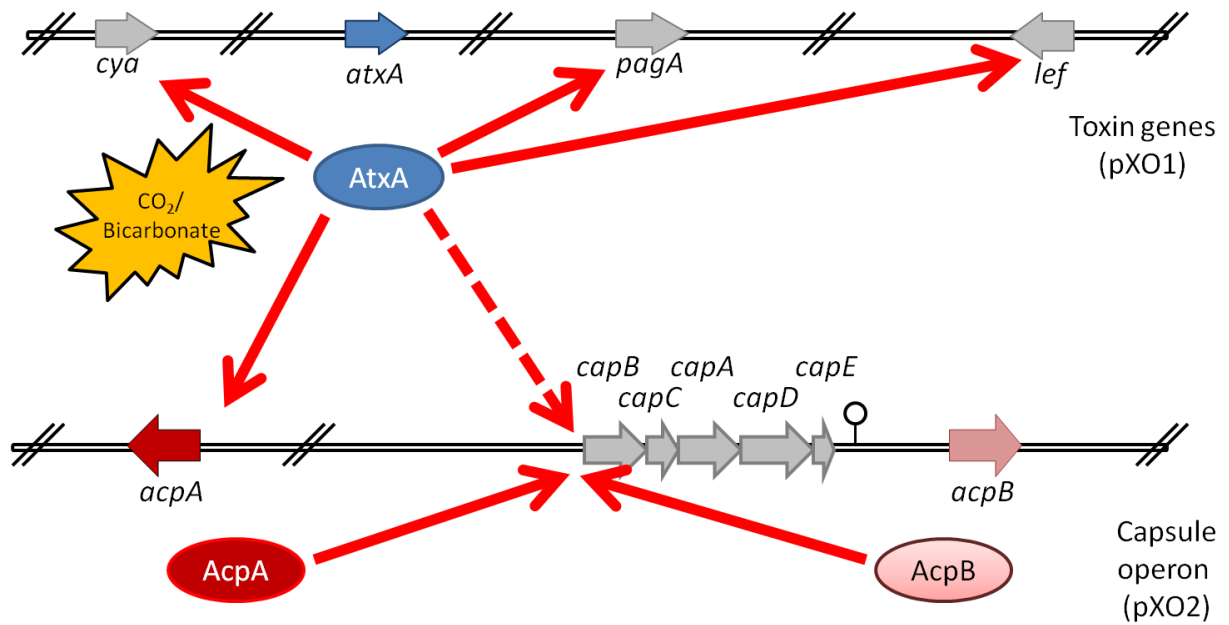


**Figure 1-3.** Model for virulence gene regulation in *B. anthracis*

AtxA is the master virulence regulator and controls expression of the anthrax toxin genes in addition to the capsule biosynthetic operon via transcriptional control of *atxA*. The *atxA* gene is located on plasmid pXO1. Culture in elevated CO<sub>2</sub> atmosphere in medium containing dissolved bicarbonate increases AtxA activity and AtxA positively regulates expression of the anthrax toxin genes *cya*, *pagA*, and *lef* located on pXO1. In these culture conditions AtxA also positively affects expression of *acpA* located on pXO2. AcpA positively affects expression of *capBCADE*. There is a weak transcriptional terminator downstream of *capE*, but ~10% of transcripts include *acpB*. AcpB also promotes *capBCADE* expression resulting in a positive feedback loop. The overexpression of AtxA has on *capBCADE* expression when cultured in 20% atmospheric CO<sub>2</sub> is represented by the hashed red arrow.

increases *atxA* transcript levels in a catabolite control protein A (CcpA)-dependent manner indicating carbon catabolite activation (CCA) is involved (63).

The crystal structure of AtxA has been solved and functional roles for each of the five domains have been defined (**Figure 1-2**). A winged helix-turn-helix motif and a helix-turn-helix motif are present near the amino terminus indicative of a DNA-binding domain. The central region of the protein has two adjacent PRDs that govern AtxA activity. A domain with homology to Enzyme IIB of the PTS is located near the carboxy terminus and functions in homodimerization (64, 65).

Post-translational modifications, environmental conditions, and metabolic state affect AtxA activity. Histidines at position 199 in PRD1 and 379 in PRD2 are phosphorylated (**Figure 1-2**). Phosphomimetic and phosphoablative mutations at positions 199 and 379 affect AtxA activity and suggest that phosphorylation at H199 allows AtxA to be active while phosphorylation at H379 functions as a dominant negative, with regard to the phosphorylation state of H199, and abolishes AtxA activity (65, 66). AtxA activity is also affected by *in vitro* culture conditions, specifically elevated carbon dioxide (CO<sub>2</sub>)/bicarbonate. Expression of AtxA-dependent genes, including the anthrax toxin genes, is enhanced when cells are cultured in 5% atmospheric CO<sub>2</sub> in medium containing dissolved bicarbonate, compared to culture in air in medium without bicarbonate added (56, 67). The increase in AtxA activity in response to culture in CO<sub>2</sub>/bicarbonate correlates with an increase in the AtxA dimer-to-monomer ratio. AtxA dimerization is imperative for activity, and mutants of AtxA that cannot dimerize have no activity (64). The elevated CO<sub>2</sub>/bicarbonate signal is thought to mimic the host physiological environment, and could provide a signal to promote virulence gene expression. AtxA steady state levels are affected indirectly by a transcriptional regulator, CodY. Studies in *B. subtilis* have elucidated factors influencing CodY activity as well as CodY-regulated genes. CodY senses the metabolic state of the cell by binding to GTP and branched chain amino acids (BCAA), two effectors that influence CodY DNA binding. CodY regulates expression of genes needed for survival in nutrient limited conditions, such as genes involved in sporulation and



survival in stationary phase (68). Deletion of *codY* in *B. anthracis* results in a decrease in AtxA steady state levels. Transcription and translation efficiency of *atxA* are unaffected in this mutant indicating that CodY affects AtxA post-translationally through an indirect mechanism (69).

### 1.6 AcpA and AcpB: regulators of capsule expression

While regulation of *atxA* and factors that govern AtxA activity have been studied in great detail, less is known about the AtxA paralogues, AcpA and AcpB. The genes encoding AcpA and AcpB flank the *capBCADE* operon and control its expression via an unknown molecular mechanism (**Figure 1-3**). Either regulator can independently increase *capBCADE* transcript levels. AtxA positively regulates capsule gene expression via transcriptional control of *acpA*. Transcriptional read-through of *capBCADE* results in elevated expression of *acpB* and a positive feedback loop (29, 70). Overexpression of *atxA*, in the absence of *acpA* and *acpB*, has also been reported to produce capsular material when *B. anthracis* is cultured in 20% CO<sub>2</sub> (71). Clues to understanding how the capsule regulators function may be gleaned from information obtained from AtxA. AtxA shares 26% amino acid sequence identity and 50% sequence similarity with each of the capsule regulators. Bioinformatic analyses indicate that both AcpA and AcpB possess amino terminal putative DNA-binding domains similar to that of AtxA. Specific DNA binding has not been tested with either capsule regulator. Two putative PRDs exist in the central region of both proteins, but the phosphorylation state of either protein has not been determined. Similar to AtxA, AcpA and AcpB also have carboxy termini with homology to Enzyme IIB.

### 1.7 AtxA2, an AtxA homologue in *Bacillus cereus* strain G9241

*Bacillus cereus*, a pathogenic *Bacillus* species closely related to *B. anthracis*, is a frequent cause of food poisoning and has been associated with various opportunistic and nosocomial infections (72). Within the last 15 years, *B. cereus* strains carrying pXO1- and pXO2-like plasmids have been isolated from non-human primates and humans that succumbed

to an anthrax-like illness (18, 19, 73). *B. cereus* strain G9241 was recovered from a welder in Louisiana who presented with a severe anthrax-like respiratory illness. Strain G9241 contains two virulence plasmids, pBCXO1 that is highly similar to pXO1 and contains the three anthrax toxin genes in addition to a gene with sequence identity to *atxA* called *atxA1*, and pBC210 that encodes a protective antigen paralog, the ADP-ribosyltransferase Certhrax, and an AtxA homolog AtxA2. Plasmid pBC210 bears little sequence homology to pXO2 from *B. anthracis*. pBCXO1-encoded AtxA is identical in sequence to that from *B. anthracis*, and *atxA2* 79% identical and 91% similar compared to *B. anthracis* AtxA (73). Finally, the *B. cereus* G9240 genome does not code for AcpA and AcpB homologs, and no proteins with homology to AcpA and AcpB have been identified in the *B. cereus* G9241 genome. It is unclear how AtxA1 and AtxA2 function in regulation of *B. cereus* virulence genes.

### **1.8 Gaps in knowledge and significance of this work**

AtxA, AcpA, and AcpB have some functional and amino acid sequence similarities, yet the regulons of these *trans*-acting factors are dissimilar. AtxA regulates 38 genes located on the virulence plasmids and the chromosome, while AcpA and AcpB are thought to affect expression of only a few genes. Previous PCVR regulon studies used PCVR-null mutants to detect global changes in gene expression (56). Given the interdependency of PCVR expression, it is difficult to discern the effects individual PCVRs have on global gene expression. Moreover, the relationship between PCVR loci and linkage of regulated genes has yet to be determined. Each regulator shares high amino acid identity and putative domains with homology to PTS components. AcpA and AcpB share more amino acid identity with each other than either does with AtxA. Whether greater sequence identity correlates with regulon similarity is unknown. Furthermore, it is unclear whether the DNA-binding regions alone are sufficient to provide target specificity to these regulators, or whether input from other intrinsic domains are required.

*B. anthracis* is a model candidate for studying PCVRs because it presents a unique opportunity to study three of these regulators in the same organism. For my thesis work I have determined the regulons of each PCVR and identified relationships between PCVR amino acid sequence similarity and PCVR-controlled gene expression, including discernment of specific and co-regulated gene targets. I assessed PCVR multimerization states and determined how multimerization affects activity. These studies define PCVR roles in culture conditions that mimic the host environment, and provide data suggesting how these regulators may function.

# Chapter II.

## Materials and Methods

*NOTE: A portion of this chapter is derived from works published in 2012, 2016, and 2018 which are cited below. I am an author on all three papers. I have received permission by the publisher of Molecular Microbiology, John Wiley and Sons, to reproduce all of the manuscript in print or electronically for the purposes of my dissertation (License Numbers: 4284271503886 & 4342040215509).*

Dale, J.L., Raynor, M.J., Dwivedi, P., and Koehler, T.M. (2012) *cis*-acting Elements Controlling Expression of the Master Virulence Regulatory Gene *atxA* in *Bacillus anthracis*. *Journal of Bacteriology*. doi:10.1128/JB.00776-12

Scarff, J.M., Raynor, M.J., Seldina, Y., Ventura, C.L., Koehler, T.M., O'Brien, A.D. (2016) The Roles of AtxA Orthologs in Virulence of Anthrax-like *Bacillus cereus* G9241. *Molecular Microbiology*. doi: 10.1111/mmi.13478

Raynor, M.J., Roh, JH., Widen, S.G., Wood, T.G., Koehler, T.M. (2018) Regulons and protein-protein interactions of PRD-containing *Bacillus anthracis* virulence regulators reveal overlapping but distinct functions. *Molecular Microbiology*. doi: 10.1111/mmi.13961.

## 2.1 Culture conditions

*B. anthracis* strains were cultivated at 37°C in Brain Heart Infusion (BHI) (Becton, Dickson and Company, Franklin Lakes, NJ) or Casamino Acid medium containing 0.8% sodium bicarbonate (CA CO<sub>3</sub>) (74, 75). BHI broth cultures were incubated with agitation (200 r.p.m.) in air. CA broth cultures were shaken in 5% atmospheric CO<sub>2</sub>. Cells from stationary phase BHI cultures were sub-cultured into fresh CACO<sub>3</sub> to an optical density at 600 nm (OD<sub>600</sub>) of 0.08. For strains harboring *atxA*, *acpA*, and *acpB* alleles under control of the hyper-spank promoter (*Phyper-spank*) (76), expression was induced with isopropyl β-D-thiogalactoside (IPTG) during early exponential phase at 2 h and harvested at early stationary phase at 4 h. Optical densities for early exponential phase cultures ranged from OD<sub>600</sub> 0.25-0.35, and early stationary phase cultures ranged from 1.2 to 1.7.

Cultures were supplemented with antibiotics when appropriate at the following concentrations: spectinomycin (MP Biomedicals, Solon, OH) (50 µg ml<sup>-1</sup> for *E. coli* and 100 µg ml<sup>-1</sup> for *B. anthracis*), erythromycin (Fisher Bioreagents, Fair Lawn, NJ) (150 µg ml<sup>-1</sup> for *E. coli* and 10 µg ml<sup>-1</sup> for *B. anthracis*), and carbenicillin (Research Products International Corp, Mt. Prospect, IL) (100 µg ml<sup>-1</sup> for *E. coli*).

## 2.2 Strain construction

*B. anthracis* strains and plasmids are shown in **Table 2-1**. The virulent Ames strain (pXO1<sup>+</sup> pXO2<sup>+</sup>) (77) and isogenic mutants were used for RNA-Seq experiments and the assessment of capsule and edema factor production. The attenuated ANR-1 strain (Ames nonreverting) (pXO1<sup>+</sup> pXO2<sup>-</sup>) and isogenic mutants were used for all other experiments. *Escherichia coli* strains TG1 (78), GM2163 (79), and SCS110 (Stratagene, San Diego, CA) were employed for cloning plasmids. General laboratory practices were used for amplification, manipulation, and purification of plasmid DNA. Non-methylated plasmid DNA was isolated from *E. coli* GM2163 or SCS110 for electroporation into *B. anthracis* (57, 79), (Stratagene).

The Ames *atxA**acpA**acpB*-null mutant (UTA40) was created by sequential deletion of each gene using a markerless temperature-sensitive integration system described previously (80). Initially, the *atxA* coding sequence was removed using pUTE937. Details regarding pUTE937 construction can be found in Hammerstrom et al. (64). Subsequently, to remove *acpA* from the *atxA*-null strain Ames genomic DNA was amplified using the polymerase chain reaction (PCR) and primers MJR014-JR175a to produce a 990-bp DNA fragment corresponding to sequence -1 to -991 relative to the *acpA* translational start site. Primers MJR017-JR176s were used to amplify a 1021-bp DNA fragment corresponding to sequence +1452 to +2473 relative to the *acpA* translational start site. The two DNA fragments were fused via splicing by overlapping extension PCR (SOE-PCR) (81) and inserted into pHY304 using a *Sac*II restriction enzyme site. pHY304 is a temperature-sensitive *E. coli* - *B. anthracis* shuttle vector that encodes an erythromycin-resistance cassette (80). *B. anthracis* containing the pHY304-derived construct was cultivated at 41°C (the non-permissive replication temperature) in medium supplemented with erythromycin to select for isolates in which the plasmid incorporated into one of the *acpA* flanking regions via homologous recombination. Cultures were passaged successive times at 30°C or 37°C in medium lacking antibiotic to allow excision of the pHY304 derivative from the *acpA* locus. Individual colonies were tested using the PCR and sequencing to confirm removal of the *acpA* coding sequence. Finally, removal of the *acpB* coding sequence from the *atxA**acpA*-null strain was accomplished in a manner similar to deletion of *acpA*. Primers MJR002-MT06 were used to amplify a 1008-bp DNA sequence -1 to -1009 relative to the *acpB* translational start. A 1006-bp DNA sequence corresponding to sequences +1445 to +2441 from the *acpB* translational start site was amplified using primers MJR003-MT09. DNA fragments were joined by SOE-PCR, cloned into pHY304, and used to remove *acpB* as described above.

UT423 harbors the *capB* promoter sequence fused to a promoterless  $\beta$ -galactosidase gene (*lacZ*) incorporated into the *plcR* locus, a nonfunctional gene in *B. anthracis*. To construct UT423, a DNA fragment corresponding to approximately 1.2 kb upstream of the *capB*

translational start (-1 to -1249) was amplified using primers AB142 and AB143 and inserted into pHT304-18z (82) using BamHI and SacI restriction enzyme sites upstream of a plasmid-borne *lacZ*. The DNA sequence inclusive of the upstream *capB* region and *lacZ* gene was excised using XhoI and EcoRI restriction enzymes and cloned into an *E. coli* - *B. anthracis* shuttle vector pUTE744 which contains an  $\Omega$ kanamycin cassette that is flanked by two 1.2 kb *plcR* flanking regions. pUTE744 confers chloramphenicol resistance and is unstable when *B. anthracis* strains are grown without selection. The *capB-lacZ* fusion was inserted upstream of the  $\Omega$ kanamycin cassette adjacent to the *plcR* flanking region creating pUTE1067 and electroporated into UT374, a markerless *atxA*-deletion mutant in the ANR-1 (pXO1<sup>+</sup> pXO2<sup>-</sup>) background, with chloramphenicol selection. Electroporants were passaged in medium without selection and screened for kanamycin-resistance and chloramphenicol-sensitivity. Appropriate isolates were confirmed by PCR.

*B. anthracis* Ames strain derivatives (UTA35, UTA36, UTA37) were constructed carrying recombinant alleles of *atxA*, *acpA*, or *acpB* engineered to express carboxy-terminal FLAG-tagged proteins from the respective native loci. To construct these strains, PCR was used to amplify regions flanking the 3' end of each PCVR open reading frame with primers engineered to attach the FLAG-tag coding sequence to the 3' end of each coding sequence, and to incorporate 5' and 3' restriction enzyme sites. Amplicons for *atxA*, *acpA*, or *acpB* were joined by SOE-PCR and ligated into pPHY304. Flanking regions for *acpA* corresponded to +443 to +1452 and +1453 to +2473, relative to the translational start codon. The *acpB* flanking regions were comprised of sequences +441 to +1444 and +1445 to +2474 relative to the start codon. Flanking regions for *atxA* included sequences +462 to +1424 and +1428 to +2481 from the start codon. The resulting plasmids containing the PCVR allele and respective flanking regions were individually electroporated into the *B. anthracis* Ames strain. Isolates in which the native PCVR allele was replaced with an allele encoding a FLAG-tagged PCVR were obtained as described above for the creation of UTA40.

### 2.3 Native and IPTG-induced PCVR expression

Steady state levels of the PCVR proteins were determined using strains expressing FLAG-tagged proteins from native PCVR loci. Strains UTA35, UTA36, and UTA37 were cultivated in CACO<sub>3</sub> for 7 h. Cell lysates were prepared as described previously (64). Sample volumes for SDS-PAGE were normalized by OD<sub>600</sub> readings at sample collection and loaded on 12.5% poly-acrylamide gels. Samples were separated by PAGE and transferred to an Immobilon-P membrane (Millipore, Billerica, MA, USA) and subsequently blotted with  $\alpha$ -FLAG antibody (Genscript, Piscataway, NJ, USA).

The IPTG concentrations necessary to express plasmid-borne  $P_{hyper-spank}$  - controlled recombinant PCVR alleles at protein levels comparable to those found in strains producing PCVRs from native promoters were determined. *B. anthracis* strains harboring recombinant *atxA*, *acpA*, or *acpB* alleles encoding FLAG-tagged proteins under the control of  $P_{hyper-spank}$  in pUTE657 were cultured in CACO<sub>3</sub>. Cultures were induced at early exponential phase with 5  $\mu$ M, 10  $\mu$ M, 20  $\mu$ M, 100  $\mu$ M, 150  $\mu$ M, or 200  $\mu$ M IPTG and harvested at early stationary phase (OD<sub>600</sub>). Cell lysates were prepared and samples containing IPTG-induced FLAG-tagged PCVRs were loaded on 12.5% poly-acrylamide gels adjacent to lysates containing FLAG-tagged PCVRs expressed from the native locus and harvested at early stationary phase. Samples were separated by PAGE, transferred to a membrane, and blotted with anti-FLAG antibody as described previously. IPTG concentrations that yielded PCVR expression similar to native PCVR expression were used for subsequent RNA-Seq experiments (5  $\mu$ M for *atxA*, 5  $\mu$ M for *acpA*, and 150  $\mu$ M for *acpB*).

### 2.4 RNA isolation for RNA-seq

Cultures of *B. anthracis* strains Ames, the Ames-derived *atxAacpAacpB*-null mutant UTA40 containing pUTE657, UTA40 (pUTE1054), UTA40 (pUTE1056), and UTA40 (pUTE992) were grown in CACO<sub>3</sub>. PCVR expression was induced with IPTG (5  $\mu$ M for *atxA* and *acpA* expression and 150  $\mu$ M for *acpB* expression) at early exponential phase and 4-ml samples



were harvested at early stationary phase ( $OD_{600} = 1.2-1.7$ ). Samples were centrifuged at 10,000 *g* at 4°C and resulting pellets were resuspended in 500 µl of  $CaCO_3$ . An equivalent volume of saturated acid phenol (pH 4.3; Fisher Bioreagents, Fair Lawn, NJ) at 65°C was added to each sample and transferred to screw top tubes containing 400 µl of 0.1 mm Zirconia/Silica beads (BioSpec Products Bartlesville, OK). Samples were lysed mechanically for 1 min, incubated for 5 min at 65°C, and subsequently lysed for an additional 1 min followed by centrifugation at 3,000 *g* at 4°C. Supernates were transferred to 500 µl of saturated acid phenol at 65°C. Samples were vortexed, incubated at room temperature (RT) for 5 min, and centrifuged at 16,000 *g* for 3 min at 4°C. One-third volume of chloroform was added to the aqueous phase. Following incubation for 10 min at RT, samples were centrifuged at 16,000 *g* for 15 min at 4°C. The aqueous phase was transferred to a new tube and RNA was precipitated by the addition of one-half volume diethyl-pyrocabonate (DEPC)-treated water and one total volume (aqueous phase + DEPC-treated water) of isopropanol followed by incubation at RT for 10 min. Samples were centrifuged at 16,000 *g* for 15 min at 4°C, and pellets containing precipitated RNA were washed with 75% ethanol. Following removal of ethanol, pellets were air-dried and finally resuspended in DEPC-treated water.

## **2.5 Creation of Next Generation Sequencing (NGS) libraries for RNA-seq and sequencing**

RNA samples were quantified using a Qubit fluorescence assay (Thermo Scientific). Total RNA quality was assessed using an RNA 6000 chip on an Agilent 2100 Bioanalyzer (Agilent Technologies). Creation of libraries for NGS analysis used total RNA (1.0 µg). Samples were treated with Ribo-Zero (Epicentre) to remove ribosomal RNA prior to fragmentation using divalent cations and heat (94°C, 8 minutes). Libraries were created using an Illumina TruSeq sample preparation kit following the protocol as recommended by the manufacturer. Briefly, RNA samples were converted to cDNA by random primed synthesis using Superscript II reverse transcriptase (Invitrogen). Second strand synthesis using DNA polymerase I and RNase H was performed and the double-stranded DNAs were treated with

T4 DNA polymerase, 5' phosphorylated and an adenine residue was added to the 3' ends of the DNA. Adapters were ligated to the ends of these target template DNAs. The adapter structure used by Illumina is a key element in the sequencing strategy. One end of the adapter has a 5' phosphorylation and a 3' "T" overhang that is compatible with ligation to DNA templates. The other end of the adapter has non-complementary ends on each DNA strand, resulting in a "Y"-shaped structure for the adapter. After ligation, the template DNAs were amplified using primers specific to each of the non-complementary sequences in the adapter. All libraries were indexed. The final concentration of all NGS libraries were determined using a Qubit fluorescence assay (Thermo Scientific) and the fragment size of each library was assessed using a DNA 1000 chip and an Agilent 2100 Bioanalyzer. qPCR analysis was used to determine the template concentration of each library prior to clustering. NGS sequencing was performed as a paired-end 50 base sequence using an Illumina HiSeq 1500 following the protocol recommended by the manufacturer. Quality assessment of the sequencing run was assessed using FastQC (<http://www.bioinformatics.bbsrc.ac.uk/projects/fastqc>).

## 2.6 RNA-seq and bioinformatic analysis

The Integrative Genomics Viewer (IGV) (83) (for read mapping), and Cufflinks (84) (for the differential expression analysis) were used to analyze RNA-Seq results. Reads were aligned to the *B. anthracis* strain 'Ames Ancestor', accession AE017334.2, using bowtie2 version 2.2.5 (85) with default parameters. The bedtools genomeCoverageBed command (84) was used to create bedgraph files from the aligned read files in bam format. The IGVtools function of the Integrated Genome Viewer (IGV) (83) was used to convert the bedgraph files to tdf format files for use in the IGV. Read maps from the different strains were fixed to a scale of "0-2000" for comparison. The featureCounts function of the subread software package (86) was used to count reads mapped to each gene with gene as the feature type, using the annotation file GCA\_000008445.1\_ASM844v1\_genomic.gff downloaded from the NCBI website. A table of read counts per gene per sample (3 replicates per condition) was entered into the DESeq2

differential expression analysis program (87) and expression level differences between each condition were determined. For differential gene expression analysis, sequencing files (bam format) were imported into Cufflinks. Triplicate sequencing results of each strain were compared to calculate *Fragments Per Kilobase of transcript per Million fragments mapped* (FPKM) changes using the default setting.

Differentially expressed genes for each complementation strain were subjected to gene set enrichment analysis on annotated KEGG pathways using the PATRIC Comparative Pathway Tool (88). Genes were selected for pathway analysis using a filter of log ratio of 2.0 or greater and a Z-score of 2.0.

## **2.7 Western blotting**

Cell lysates for detection of PCVRs by Western blot were generated as described previously (64). Briefly, 4-ml samples from early stationary phase cultures were centrifuged at 5000 *g* for 5 min at 4°C. Cell pellets were resuspended in KTE-PIC (10 mM Tris-HCl pH 8.0, 100 mM KCl, 10% ethylene glycol, and EDTA-free Complete proteinase inhibitor) to a final volume of 450 µl and transferred to a 1.5 ml screw-cap tube containing 400 µl 0.1 mm Zirconia/Silica Beads (BioSpec Products, Bartlesville, OK). Cells were lysed mechanically using a Mini BeadBeater (BioSpec Products), centrifuged, and resuspended in SDS loading buffer (final concentration of loading buffer was 0.05% bromophenol blue, 0.1M DTT, 10% glycerol, 2% SDS, and 5 mM Tris-Cl pH 6.8). Suspensions were boiled and subjected to SDS-PAGE.

To detect edema factor protein levels, culture supernates were passed through a 0.22-µm nylon filter (Fisher Scientific) and boiled for 10 min. Supernatant volumes to assess edema factor levels were normalized by OD<sub>600</sub> readings at sample collection. Supernates were affixed to a 0.2 µm nitrocellulose membrane (GE Healthcare Life Sciences, Pittsburgh, PA) by vacuum blotting with a slot blot apparatus (Hoefer Scientific, San Francisco, CA). Membranes were blocked at 4°C in TBS-T (20 mM Tris base, 137 mM NaCl, 0.1% Tween 20; pH 7.6) containing

2.5% BSA. Anti-EF (gift of R. J. Collier, ) and goat anti-rabbit-horseradish peroxidase conjugate secondary antibody (Bio-Rad, Hercules, CA, USA) were used for edema factor detection.

## 2.8 India ink exclusion assay

Encapsulated cells were visualized by India ink exclusion. To induce capsule production, *B. anthracis* cells were cultivated in NBY medium supplemented with 0.8% dissolved bicarbonate. Cultures were incubated in 5% atmospheric CO<sub>2</sub> to early stationary phase (89). An equal volume of India ink was added to 1.5 µl of culture on a microscope slide and viewed at 1000x magnification using a Nikon Eclipse TE2000-U microscope (Melville, NY). Images were captured using Metamorph (Imaging Series 6.1) software (Molecular Devices, Sunnyvale, CA).

## 2.9 Co-affinity purification

*B. anthracis* UT423 strains containing plasmids with IPTG-inducible genes encoding affinity-tagged AtxA, AcpA, AcpB, and GFP proteins were cultured individually in 25 ml of CACO<sub>3</sub> at 37°C in 5% atmospheric CO<sub>2</sub>. Protein expression was induced with IPTG (50 µM) during early exponential growth phase and 20 ml of each culture was collected at early stationary phase. Cultures were pooled in pairs as described in Fig. 7 and Fig. 8. Pooled cultures were pelleted and washed with 10 mL Binding Buffer (5 mM imidazole pH 7.9, 0.5 M NaCl, 20 mM Tris, pH 7.15, 5 mM β-mercaptoethanol containing EDTA-free Complete Protease Inhibitor (PIC; Roche, Indianapolis, IN)). Cell pellets were flash frozen and stored at -80°C.

Co-affinity purification was performed as described previously (64). Briefly, soluble cell lysates from pooled *B. anthracis* cultures were incubated 20 min in 5% CO<sub>2</sub> to facilitate CO<sub>2</sub>-dependent interactions. Lysates were mixed with NTA-Ni<sup>2+</sup> resin to bind 6xHis-tagged proteins. The resin was washed to remove any non-specifically bound proteins. 6xHis-tagged proteins, as well as any associated proteins, were eluted from the resin using imidazole and analyzed by Western blot using anti-His and anti-FLAG antibodies.

## 2.10 AcpA-His and AcpB-His purification

Recombinant AcpA-His and AcpB-His were purified from *B. anthracis* using affinity chromatography as described previously (64). Briefly, *B. anthracis* UT423 strains possessing pUTE1090 (AcpA-His) or pUTE1091 (AcpB-His) were cultured in CACO<sub>3</sub> in 5% CO<sub>2</sub>. Cultures were induced with 50 μM IPTG at early exponential phase and cells were collected at early stationary phase by centrifugation. Cells were resuspended in Binding Buffer supplemented with 1x EDTA-free Complete proteinase inhibitor (Roche), 1 mM MgCl<sub>2</sub> and 10 units DNase I (Ambion, Austin, TX). Cell lysis was achieved by three passages through a French Pressure Cell Press (SLM Instruments, Urbana, IL) and soluble lysates were collected following centrifugation. Lysates were incubated with 1 ml NTA-Ni resin (Qiagen, Hilden, Germany) in Binding Buffer (total volume 10 ml) and incubated end-over-end for 2 h at 4°C. The resin was pelleted and washed with Binding Buffer and subsequently washed with Wash Buffer 1 (40 mM imidazole pH 7.9, 1.0 M NaCl, 20 mM Tris pH 7.2, 5 mM β-mercaptoethanol), Wash Buffer High Salt (40 mM imidazole pH 7.9, 1.5 M NaCl, 20 mM Tris pH 7.2, 5 mM β-mercaptoethanol), and Wash Buffer 2 (75 mM imidazole pH 7.9, 1.0 M NaCl, 20 mM Tris pH 7.2, 5 mM β-mercaptoethanol). Proteins were eluted from resin using imidazole. Protein concentration and purity were determined using the Bradford reagent (Bio-Rad) and SDS-PAGE with Coomassie staining.

## 2.11 Bis-maleimido-hexane crosslinking

*B. anthracis* UT423 strains harboring plasmids encoding AcpA-FLAG (pUTE1079) or AcpB-FLAG (pUTE1093) were cultured and induced with IPTG (50 μM) at early exponential phase. After 2 h, 20 ml of each culture was collected by centrifugation at 5000 g for 10 m at 4°C and washed twice with 5 ml PBS-EDTA (1X PBS pH 7.2 containing 10 mM EDTA). Cells were resuspended in PBS-EDTA and lysed by mechanical disruption. Cell lysates were centrifuged at 10,000 g for 5 m at 4°C to pellet insoluble debris. For each experiment, 250 μl of soluble

lysate was mixed with 5  $\mu$ l of 20 mM bis(maleimido)hexane (BMH, Thermo Scientific, prepared freshly in DMSO) and incubated at 4°C with end-over-end mixing for 2 h. Control reactions lacking BMH contained DMSO only. Reactions were quenched by adding cysteine to a final concentration of 40 mM and vortexing for 15 min RT. Samples were boiled in 1X SDS loading buffer (5% glycerol, 100 mM DTT, 2% SDS, 40 mM Tris-Cl pH 6.8) and separated on 12.5% polyacrylamide SDS gels (Bio-Rad). AcpA-FLAG and AcpB-FLAG were detected by Western blotting using  $\alpha$ -FLAG antibody (Genscript).

Preparations of affinity-purified AcpA-His and AcpB-His used for BMH crosslinking experiments were purified using NTA-Ni resin and eluted using imidazole. Equivalent concentrations of purified AcpA-His and AcpB-His were diluted with PBS-EDTA to a final volume of 250  $\mu$ l and BMH crosslinking was performed as described above.

## **2.12 Mouse infections**

All mouse protocols were approved by The University of Texas Health Science Center Institutional Animal Care and Use Committee and performed using accepted veterinary standards. Female 6- to 8-week-old A/J mice were purchased from The Jackson Laboratory (Bar Harbor, ME) and maintained in a pathogen-free vivarium at The University of Texas Health Science Center. Food and water were supplied to the mice ad libitum. The mice were housed three per cage and were allowed to acclimate to their surroundings for 7 days prior to being used in experiments. Mice were infected intravenously by using a 30-gauge needle. The tail vein was injected with 50  $\mu$ l containing between  $10^2$  or  $10^3$  heat-sensitive CFU (vegetative cells).

## **2.13 Determination of heat-resistant CFU**

One-ml samples were obtained from cultures during transition from exponential to stationary (4h), and stationary (7h, 12h) growth phases. Samples were serially diluted and plated on LB agar before and after suspensions were heat-shocked at 65°C for 45 min.

Colonies were counted after overnight incubation at 37°C. The percentage of heat-resistant CFU/ml was calculated by dividing the number of heat-resistant CFU (post heat-shock) by the number of total CFU (pre-heat shock). Total heat-resistant CFU/ml values were determined by calculating the number of CFU/ml following heat-shock.

#### **2.14 Real-time quantitative PCR (RT-qPCR)**

Purified RNA samples (2.5 – 10 µg) were incubated with either 5U of RQ1 DNase enzyme (Promega, Madison, WI) for 30 min or with 2U of DNase I enzyme (New England Biolabs, Ipswich, MA) for 10 min at 37°C. RQ1 DNase reactions were stopped using 0.1 volume or 5 µl (whichever was greater) RQ1 stop buffer (Promega) and incubated at room temperature for 2 min. EDTA was added to a final concentration of 5 mM to stop the DNase I reactions. DNase-treated RNA was precipitated with 0.1 volume of 3 M sodium-acetate pH 5.2 (Ambion, Grand Island, NY) and 2 volumes of ice-cold 100% ethanol for a minimum of 30 min on ice. The mixture was centrifuged at 16,000 x g for 30 min at 4°C. RNA pellets were washed with 1 ml of ice-cold 75% ethanol, dried in an Eppendorf Vacufuge, and resuspended in DEPC-treated water. RNA concentrations were determined using a NanoDrop ND-1000 Spectrophotometer.

RT-qPCR cDNA was synthesized by incubating 5 µg of RNA, 250 ng of random primers, and 10 mM dNTP Mix (final concentration) at 65°C for 5 min followed by incubation on ice. 1X First-Strand Buffer (Invitrogen), 0.1 M DTT, and 200 U of SuperScript III reverse transcriptase (Invitrogen) were added to the mixture and incubated at RT for 5 min. The cDNA synthesis reaction proceeded at 50°C for 60 min. cDNA synthesis for each sample included a reaction lacking reverse transcriptase to test DNA contamination. qPCR consisted of 1X iTaq Universal SYBR Green Supermix (BioRad), 300 nM for both forward and reverse primers (final concentration) (IDT), and 100 ng cDNA template. Each qPCR plate contained a no-template control for each sample to ensure reagents were not contaminated. qPCR plates were covered with Microseal "C" Film (BioRad) and incubated in a CFX96 Real Time PCR Detection System

(BioRad) using the following cycling conditions: 95°C, 2 min; followed by 40 cycles of 95°C, 15 sec and 60°C, 30 sec. Melt curve analysis (65°C-95°C at 0.5°C increments for 2-5 sec/step) was performed at the conclusion of amplification cycles. Data were analyzed by CFX Manager (BioRad) with FAM reporter and ROX as the reference dye. Relative changes in gene expression were determined using the double delta Ct ( $\Delta\Delta Ct$ ) method with *gyrB* as the reference gene.



**Table 2-1.** *B. anthracis* strains and plasmids

<b>Name</b>	<b>Description<sup>a</sup></b>	<b>Reference or source</b>
Strains		
Ames	<i>B. anthracis</i> , Parent strain, pXO1 <sup>+</sup> pXO2 <sup>+</sup>	(90)
UTA40	Ames <i>atxA</i> <i>acpA</i> <i>acpB</i> -null mutant	This work
UTA35	Ames-derived mutant with recombinant AcpA-FLAG expressed from the native locus.	This work
UTA36	Ames-derived mutant with recombinant AcpB-FLAG expressed from the native locus.	This work
UTA37	Ames-derived mutant with recombinant AtxA-FLAG expressed from the native locus.	This work
UTA9	Ames-derived <i>skiA</i> -null <sup>c</sup> ; Sp <sup>r</sup>	This work
UTA22	Ames-derived <i>atxA</i> -null	This work
UTA26	Ames-derived <i>atxA</i> -up mutant (transversion mutation of sequences +14 to +22) <sup>b</sup>	This work
UTA31	Ames-derived <i>skiA</i> -null <sup>c</sup> / <i>atxA</i> -up mutant; Sp <sup>r</sup>	This work
ANR-1	<i>B. anthracis</i> , Parent strain, pXO1 <sup>+</sup> pXO2 <sup>-</sup>	(77)
UT423	ANR-1-derivative, <i>capB</i> promoter - <i>lacZ</i> fusion ( <i>PcapB-lacZ</i> ) incorporated in the <i>plcR</i> locus, <i>atxA</i> -null; Kn <sup>r</sup>	This work
UT374	ANR-1-derivative <i>atxA</i> -null	(91)
UT376	ANR-1-derivative, <i>lef</i> promoter - <i>lacZ</i> fusion ( <i>Plef-lacZ</i> ) at native <i>lef</i> locus, <i>atxA</i> -null	(64)
Plasmids		
pUTE657	Expression vector derived from pDR111 and pBC16 with IPTG-inducible P <sub>hyper-spank</sub> ; Sp <sup>r</sup> Ap <sup>r</sup>	(80)
pUTE1054	pUTE657-derived expression vector for AcpA-FLAG (FLAG-epitope on the C-terminus of AcpA); the <i>acpA</i> ribosome binding site and coding region controlled by P <sub>hyper-spank</sub>	This work
pUTE1079	pUTE657-derived expression vector for AcpA-FLAG (FLAG-epitope on the C-terminus of AcpA) the <i>atxA</i> ribosome binding site and <i>acpA</i> coding region controlled by P <sub>hyper-spank</sub>	This work

pUTE1090	pUTE657-derived expression vector for AcpA-His (6xHis-epitope on the C-terminus of AcpA) the <i>atxA</i> ribosome binding site and <i>acpA</i> coding region controlled by $P_{hyper-spank}$	This work
pUTE1125	pUTE657-derived expression vector for AcpA- $\Delta$ EIIB-His (6xHis-epitope on the C-terminus of AcpA- $\Delta$ EIIB) the <i>acpA</i> ribosome binding site and <i>acpA</i> coding region controlled by $P_{hyper-spank}$	This work
pUTE1056	pUTE657-derived expression vector for AcpB-FLAG (FLAG-epitope on the C-terminus of AcpB) the <i>acpB</i> ribosome binding site and coding region controlled by $P_{hyper-spank}$	This work
pUTE1093	pUTE657-derived expression vector for AcpB-FLAG (FLAG-epitope on the C-terminus of AcpB) the <i>atxA</i> ribosome binding site and <i>acpB</i> coding region controlled by $P_{hyper-spank}$	This work
pUTE1091	pUTE657-derived expression vector for AcpB-His (6xHis-epitope on the C-terminus of AcpB) the <i>atxA</i> ribosome binding site and <i>acpB</i> coding region controlled by $P_{hyper-spank}$	This work
pUTE1126	pUTE657-derived expression vector for AcpB- $\Delta$ EIIB-His (6xHis-epitope on the C-terminus of AcpB- $\Delta$ EIIB) the <i>acpB</i> ribosome binding site and <i>acpB</i> coding region controlled by $P_{hyper-spank}$	This work
pUTE992	pUTE657-derived expression vector for AtxA-FLAG (FLAG-epitope on the C-terminus of AtxA) the <i>atxA</i> ribosome binding site and coding region controlled by $P_{hyper-spank}$	(64)
pUTE991	pUTE657-derived expression vector for AtxA-His (6xHis-epitope on the C-terminus of AtxA) the <i>atxA</i> ribosome binding site and coding region controlled by $P_{hyper-spank}$	(64)
pUTE1013	pUTE657-derived expression vector for GFP-FLAG (FLAG-epitope on the C-terminus of GFP); the <i>gfpmut3a</i> ribosome binding site, coding region, and sequence encoding FLAG controlled by $P_{hyper-spank}$	(64)
pAW285	Xylose-inducible expression vector; Cm <sup>r</sup>	(92)
pUTE1099	pAW285-derived expression vector for AcpA-FLAG (FLAG-epitope on the C-terminus of AcpA) the <i>acpA</i> coding region controlled by $P_{xyIA}$	This work
pUTE1100	pAW285-derived expression vector for AcpB-FLAG (FLAG-epitope on the C-terminus of AcpB) the <i>acpB</i>	This work

coding region controlled by *P<sub>xyIA</sub>*

pUTE1096	pUTE657-derived expression vector for AtxA2-His (6xHis-epitope on the C-terminus of AtxA2) the <i>atxA</i> ribosome binding site and coding region controlled by Phyper-spank	(93)
pUTE1122	pUTE657-derived expression vector for AtxA2-FLAG (FLAG-epitope on the C-terminus of AtxA2) the <i>atxA</i> ribosome binding site and coding region controlled by Phyper-spank	(93)

---

<sup>a</sup> Ap<sup>r</sup>, ampicillin resistant; Cm<sup>r</sup>, chloramphenicol; Kn<sup>r</sup>, kanamycin; Sp<sup>r</sup>, spectinomycin

<sup>b</sup> Numeric values relative to *atxA* P1 transcriptional start site

<sup>c</sup> *skiA* was known previously as *pXO2-0075* and *pXO2-61* (White 2006)

**Table 2-2.** Primers used in this dissertation

Name	Sequence (5' to 3')	Brief Description
MJR014	CCGCGGACAAGTACATAATTGGCATTG	SacII - <i>acpA</i> markerless deletion
JR175a	GCGTATCAAATAAATTATCACCCCTTAGTT ATTTATTTTC	<i>acpA</i> markerless deletion (overlap primer)
MJR017	GGCGCCGTATTTTAGATGCAACAGTG	SacII - <i>acpA</i> markerless deletion & recombinant AcpA-FLAG gene insertion
JR176s	GGGTGATAATTTATTTTGATACGCAATAGC TAGATTG	<i>acpA</i> markerless deletion (overlap primer)
MJR002	ATTGATACTACATATATCGATATCCCTTGC TTTTAAG	<i>acpB</i> markerless deletion (overlap primer)
MJR015	CCGCGGTGTCTTAATTACTGGAAAGTAAC A	SacII - <i>acpB</i> markerless deletion
MJR003	TCGATATATGTAGTATCAATAATATAGAAA AAGCCACTT	<i>acpB</i> markerless deletion (overlap primer)
MT09	GGCGCCTTAATTTTAAGCAATAAAATACAT AG	SacII - <i>acpB</i> markerless deletion
AB142	GGATCCGTCCTTCTCGCACTATCAAGG	BamHI - <i>PcapB</i> insertion
AB143	GAGCTCTTTAGAAACAATTCACCTCGCT	SacI - <i>PcapB</i> insertion
MJR037	CTATTTATCATCATCATCTTTATAATCTTTG CTTGCAAAGATTCTATTTTC	recombinant AcpA-FLAG gene insertion (overlap primer)
MJR038	GGCTCGAGTAGGGGATGAATTTCAAATTA TAC	XhoI - recombinant AcpA-FLAG gene insertion
MJR039	GATTATAAAGATGATGATGATAAATAGTAT TTTGATACGCAATAGCTAGAT	recombinant AcpA-FLAG gene insertion (overlap primer)
MJR040	TACTCGAGAAACCTCTTAGACTTGAGGG	XhoI - recombinant AcpB-FLAG gene insertion
MJR041	CTATTTATCATCATCATCTTTATAATCACCA TCTTGTAATCTAGATAATA	recombinant AcpB-FLAG gene insertion (overlap primer)
MJR042	CCGCGGGAACAATATTTTCATTGCTCCTT CC	SacII - recombinant AcpB-FLAG gene insertion
MJR043	GATTATAAAGATGATGATGATAAATAGTAT CAATAATATAGAAAAGCCAC	recombinant AcpB-FLAG gene insertion (overlap primer)
MJR095	AAAGGCGCCATTTATCTTAAGGTTATATTG CAATATTCC	SacII - recombinant AtxA-FLAG gene insertion
MJR096	CTATTTATCATCATCATCTTTATAATCTATT ATCTTTTTGATTCATGAAAATCTCTTTC	recombinant AtxA-FLAG gene insertion (overlap primer)
MJR097	ATAGATTATAAAGATGATGATGATAAATAG ATGCCCTTTAAATATTTGTTTAATGACAC	recombinant AtxA-FLAG gene insertion (overlap primer)
MJR098	AAACTCGAGCATTAGCCTTAATGTGAGTA GAATC	XhoI - recombinant AtxA-FLAG gene insertion
MT01	GGTAGTCGACAACCTAAGGGTGATAATTAT G	Sall - <i>acpA</i> rbs start codon

MJR056	GTCGACAGGAAAGGAGAATCAATTATAGACATGGAAAAAGATATTAGCCGAAAAATTGATTTG	Sall - <i>atxA</i> rbs <i>acpA</i> open reading frame
MJR005	AAGCATGCTAGTGGTGATGGTGATGATGTTGCTTGCAAAGATTCCTATTTTC	<i>acpA</i> His6 stop codon - SphI
MJR001 1	AAGCATGCTATTTATCATCATCATCTTTATAATCTTTGCTTGCAAAGATTCCTATTTTC	<i>acpA</i> FLAG stop codon - SphI
MT05	AAGCATGCAAGCAAGGGATATCGATATATG	SphI - <i>acpB</i> rbs start codon
MJR057	AACTCGAGAGGAAAGGAGAATCAATTATAGACATGGAAAAAGATATAAAAAGACAAATCCAAATC	XhoI - <i>atxA</i> rbs <i>acpB</i> open reading frame
MJR004	AAGCATGCTAGTGGTGATGGTGATGATGACCATCTTGTAATCTAGATAATA	<i>acpB</i> His6 stop codon - SphI
MJR010	AAGCATGCTATTTATCATCATCATCTTTATAATCACCATCTTGTAATCTAGATAATA	<i>acpB</i> FLAG stop codon - SphI

## Chapter III.

# Regulons of PRD-containing *Bacillus anthracis* virulence regulators reveal overlapping but distinct functions

*NOTE: A portion of this chapter is derived from work published in 2018 which is cited below. I am first author on this publication. I have received permission by the publisher of Molecular Microbiology, John Wiley and Sons, to reproduce all of the manuscript in print or electronically for the purposes of my dissertation (License Numbers: 4284271503886 & 4342040215509).*

Raynor, M.J., Roh, JH., Widen, S.G., Wood, T.G., Koehler, T.M. (2018) Regulons and protein-protein interactions of PRD-containing *Bacillus anthracis* virulence regulators reveal overlapping but distinct functions. *Molecular Microbiology*. doi: 10.1111/mmi.13961.

### 3.1 Introduction

Three PRD-Containing Virulence Regulators (PCVR), AtxA, AcpA, and AcpB, have been identified in *Bacillus anthracis*, the causative agent of anthrax. A defining characteristic of PCVRs is the presence of phosphoenolpyruvate:carbohydrate phosphotransferase system regulatory domains (PRD). The phosphotransferase system, generally involved in the transfer of phosphate to incoming sugar molecules, may also play a role in virulence. AtxA is the master virulence regulator and the most well-studied PCVR. AtxA controls transcription of the anthrax toxin genes, *pagA* (protective antigen), *lef* (lethal factor), and *cya* (edema factor). AtxA also affects expression of the capsule biosynthesis operon *capBCADE* and other genes (29, 30, 57, 59, 64, 67). Expression of *atxA* is subject to complex regulation. Transcription of *atxA*, located on virulence plasmid pXO1 (182 kb), is affected by temperature, carbohydrate availability, redox potential, metabolic state, and growth phase (59–61, 66, 69).

The other two PCVRs in *B. anthracis*, AcpA and AcpB, are encoded by genes on virulence plasmid pXO2 (95 kb). AcpA and AcpB positively regulate *capBCADE* (29, 70). The amino acid sequences of these regulators are similar to that of AtxA, but structure/function studies of AcpA and AcpB are lacking. Initial investigations of AtxA, AcpA, and AcpB employed *atxA*-, *acpA*-, and *acpB*-null mutants in a genetically reconstituted virulent pXO1<sup>+</sup> pXO2<sup>+</sup> strain. The data revealed that the regulons of the three PCVRs are partially overlapping and not limited to expression of the toxin and capsule genes (70). For example, in addition to the toxin and capsule genes, AtxA negatively regulates some chromosomal genes, including genes predicted to be involved in branched chain and aromatic amino acid synthesis (56). AcpA affects expression of pXO1-114, a gene predicted to encode a spore germination protein/permease. Also, AtxA and AcpA have a synergistic effect on expression of *amiA*, a peptidoglycan hydrolase, located on pXO2. AcpB appears to play a larger role in virulence than AcpA. In a murine model of anthrax, an *acpB* mutant exhibited a higher LD<sub>50</sub> and reduced dissemination compared to an *acpA* mutant (70).

Extensive analyses of *capBCADE* regulation support a model in which all three *B. anthracis* PCVRs positively affect *cap* operon transcription. Data from experiments employing null-mutants reveal that expression of the regulators is inter-dependent and suggest functional similarity of AcpA and AcpB. The primary means for AtxA control of *capBCADE* is via positive regulation of *acpA* transcription (70). The *acpA* gene is located upstream of the *cap* locus and in the opposite orientation. AcpA can positively affect transcription of *capBCADE* in the absence of AtxA and AcpB. The *acpB* gene, located downstream of *capBCADE* and in the same orientation, is expressed as a monocistronic transcript initiated from a weak constitutive promoter. AcpB, like AcpA, can positively affect *capBCADE* expression in the absence of the other PCVRs. A weak transcription terminator located between *capE* and *acpB* results in co-transcription of *acpB* with *capBCADE* in roughly 10% of transcripts, thus forming a positive feed-back loop.

It is unknown how AtxA, AcpA, and AcpB affect transcription of target genes or what factors influence target specificity. Clues to determining targets of some transcription factors can often be found in *cis*-acting elements upstream of the gene. Many transcription factors recognize particular DNA sequences, or consensus sequences, in the promoters of genes they regulate (94). A consensus sequence in the control regions of PCVR-regulated genes has not been identified and specific DNA-binding activity by AtxA has not been demonstrated. However, DNA structure has been implicated in AtxA gene regulation. *In silico* modeling of the toxin gene promoters predicts common structural characteristics. A region of high curvature is positioned near the AtxA-dependent transcriptional start sites. Two other AtxA-regulated genes, pXO1-90 and pXO1-91 which are positively regulated 61-fold and 25-fold, respectively, are also predicted to contain promoter regions of high curvature (58). These data suggest that intrinsic DNA curvature of AtxA-regulated promoters may contribute to AtxA-mediated gene expression.

The presence of three paralogous PCVRs in *B. anthracis* presents a unique opportunity to study similarities and differences in PCVR function in a single pathogen. Previously published investigations of the roles of AtxA, AcpA, and AcpB in *B. anthracis* transcription



employed PCVR-null mutants (29, 70). The more recently discerned inter-dependence of PCVR expression complicates interpretation of the data generated using individual null-mutants. In this chapter, I show native protein expression levels of AtxA, AcpA, and AcpB in a fully virulent clinical isolate of *B. anthracis*. I created recombinant strains expressing individual PCVRs and determined the regulons of each factor using RNA-Seq. I identified genes controlled by one or more regulators, and whether PCVRs preferentially controlled genes within pathogenicity islands. I also examined the effects of individual regulators on expression of established virulence genes.

## **3.2 Results**

### **3.2.1 Amino acid sequence and predicted domain similarity of the *B. anthracis* PCVRs**

A comparison of the amino acid sequences of the *B. anthracis* PCVRs is shown in **Figure 3-1A**. Overall, AtxA shares about 27% amino acid sequence identity and close to 50% amino acid sequence similarity with AcpA and AcpB. AcpA and AcpB have 40% amino acid sequence identity and 62% similarity, and are more similar to each other than to AtxA. Structural models of AcpA and AcpB generated using Phyre2 (13) predict similar domain organization to AtxA (**Figure 3-1B**). Sequence homology between the three PCVRs is highest in the predicted DNA-binding domains which are comprised of two helix-turn-helix motifs at the amino termini. Within this region, AcpA and AcpB share 48% amino acid identity, AtxA and AcpA are 33% identical, and there is 29% identity between AtxA and AcpB. At the carboxy-terminal regions of the PCVRs, the predicted EIIB-like domains of AcpA and AcpB are 32% identical to each other, and each share approximately 30% amino acid identity and 50% similarity with the respective domain within AtxA.

Of the five predicted domains associated with each of the AcpA and AcpB amino acid sequences, the PRDs are the most divergent from AtxA. Although the amino acid sequences of the AcpA and AcpB PRD regions share 36% identity, they are 20% and 22% identical to the sequences of the PRDs revealed in the AtxA crystal structure. Phosphorylation of H199 and H379 within AtxA PRD1 and PRD2, respectively affect regulator activity (66). Phosphorylation

of AcpA and AcpB has not been demonstrated and histidine residues within the putative PRDs of AcpA and AcpB do not align with phosphorylated residues of AtxA (**Figure 3-1A**).



### 3.2.2 Native PCVR protein and transcript levels

The importance of AtxA, AcpA, and AcpB in expression of toxin and capsule has been appreciated, but individual contributions by each regulator have not been fully defined. As an initial step I determined the relative level of each PCVR when the parent strain was cultured in optimal conditions for virulence gene expression. To determine native PCVR protein levels, I created strains that expressed AtxA-FLAG, AcpA-FLAG, or AcpB-FLAG from the respective native locus. The FLAG epitope did not affect function of the native protein in *in vivo* reporter strains designed to test AtxA, AcpA, or AcpB activity. (**Figure 3-2 and (64)**). Strains were cultured in either CACO<sub>3</sub> or NBY-CO<sub>3</sub> in atmospheric 5% CO<sub>2</sub>. Culture in CACO<sub>3</sub> and 5% CO<sub>2</sub> is ideal for *atxA*-mediated toxin gene expression (30), and growth in NBY-CO<sub>3</sub> and 5% CO<sub>2</sub> allows optimal capsule production. Strains were harvested at the transition to stationary growth phase and cell lysates prepared. Cell lysates were separated by SDS-PAGE and FLAG-tagged proteins were visualized by western blot using  $\alpha$ -FLAG antibody. In both media, AtxA was the most abundant PCVR detected (**Figure 3-3**). AcpA-FLAG and AcpB-FLAG were detected at levels much lower than AtxA-FLAG in strains cultured in CACO<sub>3</sub> medium. Nevertheless, capsule production was apparent (**Figure 3-3A**). AcpA-FLAG and AcpB-FLAG had higher steady state levels when strains were cultivated in NBY-CO<sub>3</sub> compared to culture in CACO<sub>3</sub> with AcpB-FLAG detected in higher abundance than AcpA-FLAG (**Figure 3-3B**). These results assume equal accessibility of the FLAG epitope by the  $\alpha$ -FLAG antibody for each recombinant protein. Capsule production from cultures grown in NBY-CO<sub>3</sub> was also more robust and resulted in cells with thicker capsule than from CACO<sub>3</sub> cultures. These results indicate that AtxA is the most abundant of the three PCVRs in soluble cell lysates.

I used RNA-Seq to define the regulon of each PCVR and to determine the extent each PCVR plays in expression of genes related to virulence and general metabolism, and to identify co-regulated genes. In order to circumvent the influence of AtxA on *acpA* and *acpB* expression, and to ascertain the significance of each PCVR in a clinical isolate of *B. anthracis*, I created an

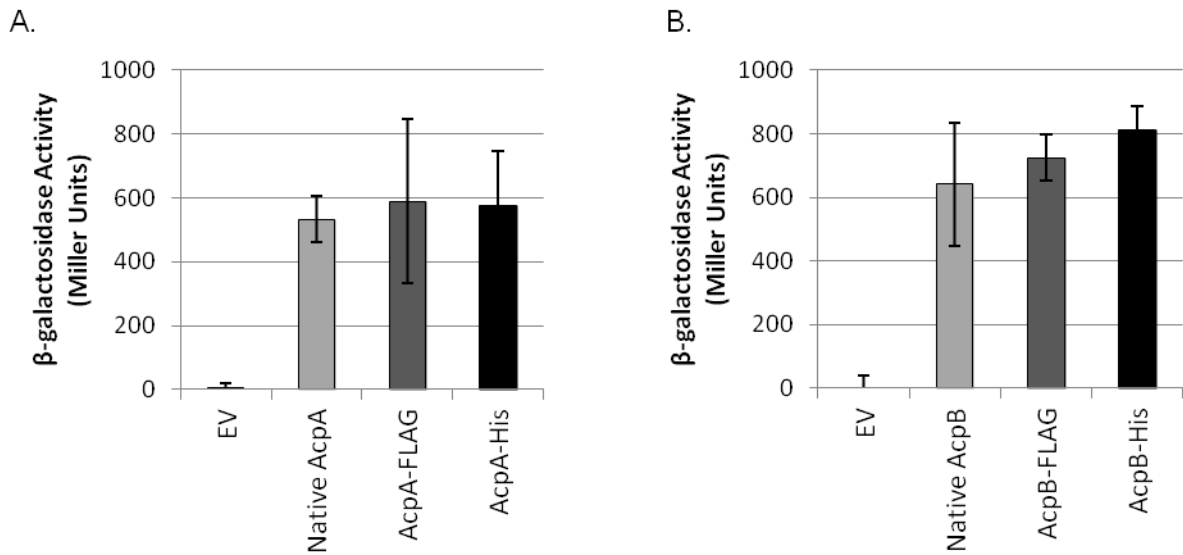


**Figure 3-2.** *In vivo* activity of recombinant His-tagged and FLAG-tagged AcpA and AcpB  
 In an *atxA*-null pXO1+ pXO2- strain (UT423), expression of native, -His<sub>6</sub>, and -FLAG tagged recombinant AcpA and AcpB was induced with IPTG during growth in CACO<sub>3</sub>. The empty vector (EV) lacks both *acpA* and *acpB*. Samples were collected at the transition to stationary phase (4h; OD<sub>600</sub> 1.2-1.8). All strains carried the *PcapB:lacZ* reporter and  $\beta$ -galactosidase activity was measured as described previously (95). Error bars represent standard deviation.

*atxAcpAcpB*-null mutant from the pXO1+ pXO2+ Ames strain (**Table 2-1**) and expressed individual PCVR-encoding genes *in trans* under the control of an IPTG-inducible promoter. PCVR expression was induced with a concentration of IPTG that yielded near-native protein levels.

To determine IPTG concentrations that yield near-native PCVR protein levels, I grew cultures that expressed individual FLAG-tagged PCVRs from the native locus, and cultures of the *atxAcpAcpB*-null strain carrying plasmid-borne *atxA*, *acpA*, or *acpB* under the control of an IPTG inducible promoter. Expression of each PCVR was induced at early exponential growth phase using a range of IPTG concentrations and all cultures were harvested at the transition to stationary phase. Cell lysates from strains that expressed an individual PCVR, either from the native locus or from the IPTG-inducible expression vector, were separated by SDS-PAGE and FLAG-tagged proteins were detected by western blot with anti-FLAG antibody. The IPTG concentration that yielded PCVR expression that most closely mirrored expression from the native locus was used for future experiments.

For RNA-Seq experiments I grew cultures of the parent strain, *atxAcpAcpB*-null strain, and *atxAcpAcpB*-null strains expressing individual PCVR genes from the IPTG-inducible promoter. Cells were grown in toxin-inducing conditions, and expression of each PCVR in the *atxAcpAcpB*-null complementation strains was induced with IPTG. RNA was extracted for sequencing when cultures reached the transition to stationary phase.

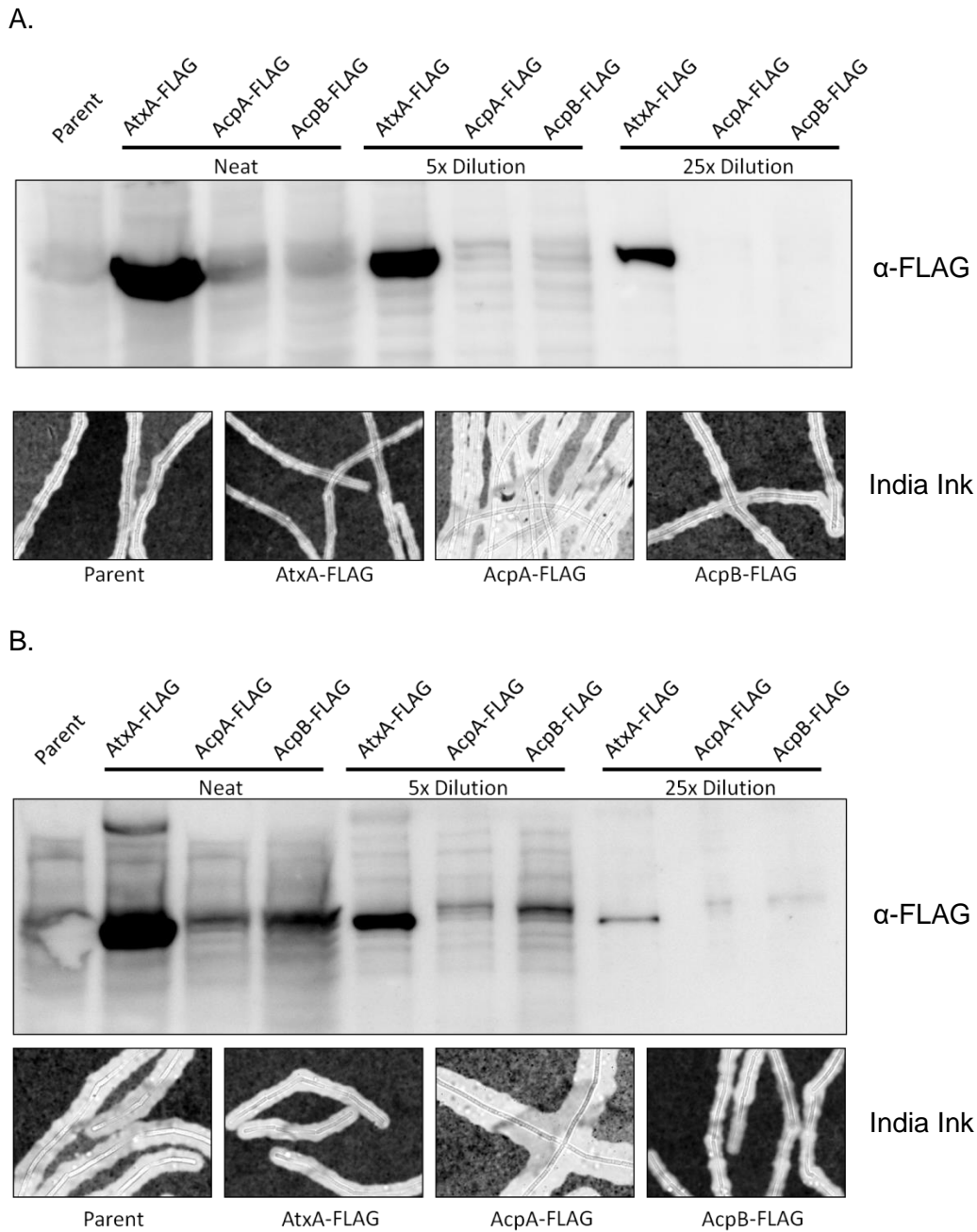


**Figure 3-3. Native PCVR expression and capsule production**

Strains of *B. anthracis* expressing AtxA-FLAG (UTA37), AcpA-FLAG (UTA35), AcpB-FLAG (UTA36) from the respective native locus, and the parent strain Ames were cultivated in either (A) CACO<sub>3</sub> or (B) NBY-CO<sub>3</sub> in 5% atmospheric CO<sub>2</sub> and harvested (8 mLs per culture) at transition to stationary phase (OD<sub>600</sub> 1.2-1.7). Cell lysates were diluted 5-fold or 25-fold in KTE-PIC and load volumes were normalized by OD<sub>600</sub> reading at collection prior to separation by SDS-PAGE. FLAG-tagged proteins were detected by western blot with  $\alpha$ -FLAG antibody. Capsule production was assessed at collection and visualized using Differential Interference Contrast (DIC) microscopy and India Ink staining.

Prior to examining gene expression changes mediated by each PCVR, I assessed the expression levels of *atxA*, *acpA*, and *acpB* in the parent strain and complementation strains to: A) determine the relative abundance of PCVR transcripts, and B) to assess how well PCVR expression in each complementation strain mirrored native expression. I compared the fragments per kilobase of transcript per million reads (FPKM) for each PCVR in the parent, *atxAacpAacpB*-null, and complementation strains (**Figure 3-4**). In the parent strain, *atxA* and *acpA* transcripts were present at similar levels. Transcripts of *acpB* were roughly two-fold more abundant than *atxA* or *acpA* transcripts, potentially due to transcriptional read through from *capBCADE* to *acpB* (**Figure 1-3**). Expression of *atxA*, *acpA*, and *acpB* in the *atxAacpAacpB*-null strain was not detected and complementation with either *atxA* or *acpA* expressed from an IPTG-inducible promoter yielded near-native expression. Expression of *acpB* from the IPTG-inducible promoter yielded *acpB* expression several-fold higher than native *acpB* expression (**Figure 3-4**). Nevertheless, the IPTG concentration used to induce *acpB* expression generated AcpB protein levels commensurate with *acpB* expressed from the native locus. These data suggest that *acpB* transcripts expressed from the IPTG-inducible promoter may be less stable and/or translated less efficiently than *acpB* transcripts expressed from the native locus.

### 3.2.3 Overlapping regulons of AtxA, AcpA, and AcpB

To discern differential effects mediated by each PCVR on global gene expression, I compared RNA sequencing reads obtained using cultures from the different strains. Comparison of the transcriptional profiles of the parent strain and the *atxAacpAacpB*-null mutant revealed vast differences in gene expression. Four-fold or greater differences in transcript levels were found for 716 genes, representing 11.6% of the genome. Gene expression changes of two-fold or greater were observed for 1440 genes representing 23.4% of the genome.

To determine the effects of individual PCVRs on gene expression I compared transcripts from the *atxAacpAacpB*-null mutant to those obtained from mutants expressing one PCVR. Venn diagrams of the PCVR regulons illustrate that *B. anthracis* genes can be



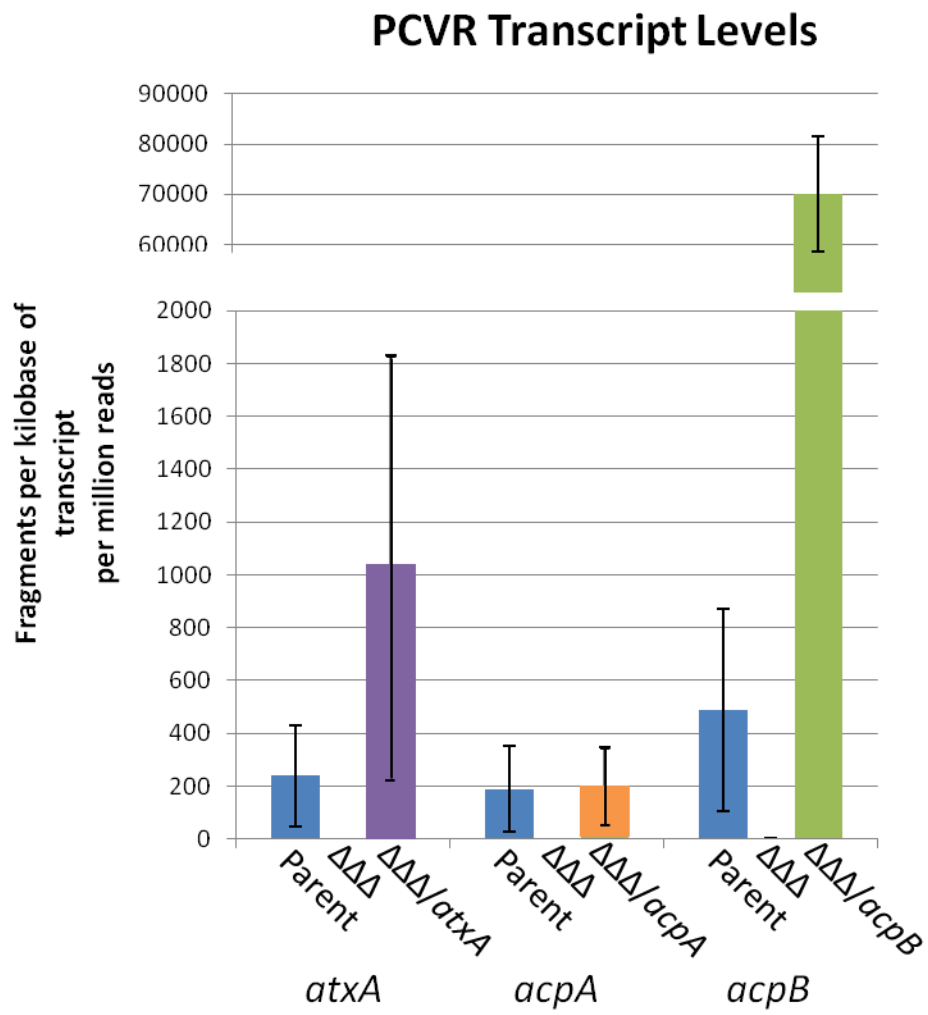


**Figure 3-4.** PCVR transcript levels  
 Transcripts of *atxA*, *acpA*, and *acpB* in the parent, *atxAacpAacpB*-null ( $\Delta\Delta\Delta$ ), and complementation strains expressing *atxA* ( $\Delta\Delta\Delta/atxA$ ), *acpA* ( $\Delta\Delta\Delta/acpA$ ), or *acpB* ( $\Delta\Delta\Delta/acpB$ ) were determined by RNA-Seq following culture in  $CACO_3$  in 5%  $CO_2$ . Error bars represent high and low confidence intervals.

controlled by one, two, or all three regulators (**Figure 3-5**). AtxA had a four-fold or greater effect on expression of 145 genes (**Figure 3-5A**); 80 were positively controlled by AtxA, while 65 were negatively affected by AtxA. **Table 3-1** lists PCVR-regulated genes with a 16-fold or greater change in expression (log<sub>2</sub>-fold change of 4 or greater) in the presence of at least one PCVR, and illustrates specific and co-regulated genes. I found several examples of genes with expression changes that were strongly AtxA-dependent, but unaffected by AcpA or AcpB (**Table 3-1**). For example, expression of *pagAR*, *lef*, and GBAA\_pXO1\_0171 was strongly induced by AtxA, but not affected by the other PCVRs. AtxA regulated independently a greater number of genes ( $\geq 4$ -fold) than either AcpA or AcpB. AcpA affected expression of 130 genes; 83 were positively regulated and 47 were negatively regulated, and AcpB controlled expression of 49 genes; 17 were up-regulated and 32 were down-regulated. AcpA-alone controlled expression of *amiA*, an autolysin encoded by pXO2. AcpB controlled expression of GBAA\_pXO2\_0119, a pseudogene annotated as a truncated transposase. The data set included co-regulated genes that were affected similarly by AcpA and AcpB, but to a different degree by AtxA. Both AcpA and AcpB positively affected expression of GBAA\_pXO2\_0059, but expression of this gene was not affected by AtxA.

Expression of GBAA\_pXO2\_0061 and GBAA\_pXO2\_0122 was strongly affected by AcpA and AcpB, yet weakly controlled by AtxA. For co-regulated genes, there was a predominance of genes controlled by AtxA and AcpA. For genes regulated four-fold or greater, 31 genes were controlled by AtxA and AcpA, 15 genes were co-regulated by AtxA and AcpB, and 5 genes were co-regulated by AcpA and AcpB. Many genes were controlled by all three regulators, and in some cases each PCVR had comparable effects on target genes. The numbers of genes in the regulons increased substantially when I included genes with expression that changed two-fold or greater. These results reveal the vast effects of the PCVRs on *B. anthracis* gene expression and indicate a high degree of functional similarity among the regulators.

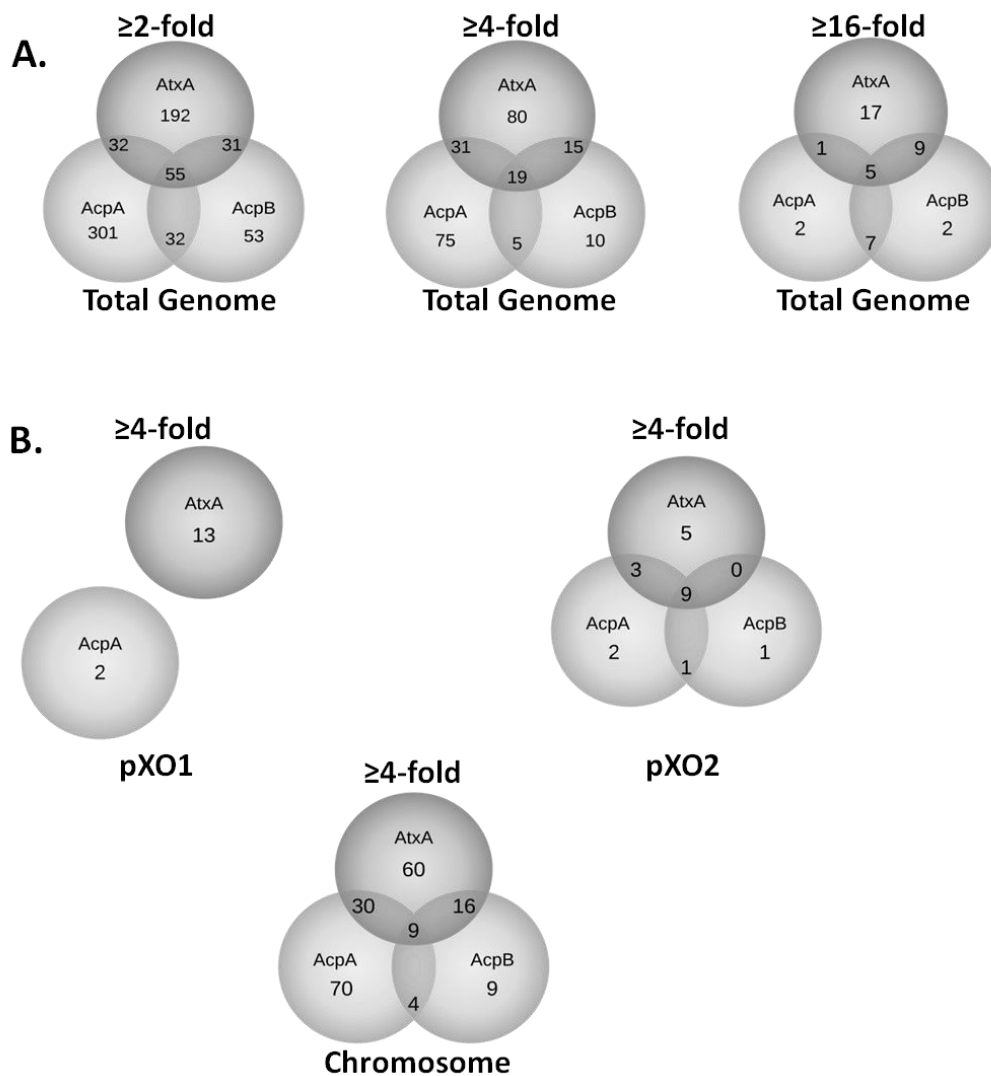


**Figure 3-5.** Venn diagrams of PCVR regulons  
 (A) Gene expression changes of  $\geq 2$ -fold,  $\geq 4$ -fold, and  $\geq 16$ -fold in the *atxAacpAacpB*-null strain (UTA40) complemented with AtxA, AcpA or AcpB. (B) Gene expression changes of  $\geq 4$ -fold organized by genetic element.

### 3.2.4 Loci of PCVR-regulated genes

To determine if genes controlled by AtxA, AcpA, or AcpB are linked, I first determined whether highly-regulated genes mapped to pXO1, pXO2, or the chromosome. **Table 3-1** lists PCVR-regulated genes with a 16-fold or greater change in expression (log<sub>2</sub>-fold change of four or greater) in the presence of at least one PCVR. **Figure 3-5B** shows Venn diagrams of the PCVR regulons associated with each genetic element for genes regulated at least four-fold. Of 203 transcripts associated with pXO1, 15 were altered at least four-fold: 13 by AtxA and 2 by AcpA. No pXO1-derived transcripts were affected four-fold or greater by AcpB. Transcripts regulated by more than one PCVR were not detected, with the exception of *cya* and *bsIA*, which were highly regulated by AtxA and showed a relatively small level of control by AcpA (see **Table 3-1**).

Read maps (**Figure 3-6**) revealed that many of the regulated transcripts from pXO1 were associated with the 35-kb region that lies within a larger 44.8-kb pathogenicity island (96). Of the 47 genes from which I detected transcripts in this region, 12 were AtxA-controlled. These genes included the three toxin genes and the spore germination genes *gerXA*, *gerXB*, and *gerXC*, encoding germination receptors (97). The native *atxA* locus is also within this 35-kb region. The *bsIA* gene, encoding an S-layer protein that mediates adhesion to host cells (55) is the only highly expressed AtxA-regulated gene on pXO1 located outside of the pathogenicity island.

I detected transcripts for 110 genes on pXO2, of which 21 were regulated four-fold or greater by at least one of the three PCVRs (**Figure 3-5B**). The highly-regulated genes clustered within a 35.5-kb region of the plasmid which includes the capsule biosynthetic operon *capBCADE* followed by the weakly co-transcribed *acpB* gene. Other PCVR-controlled genes in this region of pXO2 include *pagR2*, a paralog of the pXO1-encoded transcription factor *pagR1* (98, 99), and multiple genes of unknown function (**Figure 3-6** and **Table 3-1**). The *acpA* and *acpB* genes are also located in the 35.5-kb region.

Genetic Element	Gene Locus Tag	Gene	Log2-fold change		
			AtxA	AcpA	AcpB
pXO1	GBAA_pXO1_0124	<i>bslA</i>	7.02	1.88	-
	GBAA_pXO1_0125		5.05	-	-
	GBAA_pXO1_0142	<i>cya</i>	4.47	1.88	-
	GBAA_pXO1_0220	<i>apt2</i>	4.32	1.45	-
	GBAA_pXO1_0164	<i>pagA</i>	7.10	-	-
	GBAA_pXO1_0166	<i>pagR1</i>	6.60	-	-
	GBAA_pXO1_0171		5.93	-	-
	GBAA_pXO1_0172	<i>lef</i>	6.47	-	-
	GBAA_pXO1_0224		5.64	-	-
pXO2	GBAA_pXO2_0045	<i>amiA</i>	-	4.10	-
	GBAA_pXO2_0059		-	4.28	7.28
	GBAA_pXO2_0061		2.52	7.28	6.30
	GBAA_pXO2_0062	<i>capE</i>	3.54	8.63	7.74
	GBAA_pXO2_0063	<i>capD</i>	3.09	8.11	7.40
	GBAA_pXO2_0064	<i>capA</i>	3.38	8.58	7.90
	GBAA_pXO2_0065	<i>capC</i>	3.92	9.00	8.43
	GBAA_pXO2_0066	<i>capB</i>	3.86	8.73	8.20
	GBAA_pXO2_0069	<i>pagR2</i>	5.21	5.51	6.53
	GBAA_pXO2_0074		6.04	-	-
	GBAA_pXO2_0075	<i>skiA</i>	5.65	-	-
	GBAA_pXO2_0088		3.33	4.25	-
	GBAA_pXO2_0119		-	-	4.13
	GBAA_pXO2_0120		2.36	3.57	6.76
	GBAA_pXO2_0122		4.82	6.04	6.59
Chr.	GBAA_1025	<i>glpF</i>	-4.28	-1.75	-
	GBAA_1416	<i>ilvE1</i>	-5.46	-1.87	-4.42
	GBAA_1417	<i>ilvB</i>	-6.17	-	-5.26
	GBAA_1419	<i>ilvC1</i>	-6.38	-	-6.03
	GBAA_1420	<i>leuA</i>	-6.74	-2.23	-6.26
	GBAA_1421	<i>leuB</i>	-7.05	-	-6.67
	GBAA_1459	<i>brnQ3</i>	-5.09	-	-5.08
	GBAA_1849	<i>ilvE2</i>	-6.06	-	-5.00
	GBAA_1850	<i>ilvB2</i>	-5.67	-	-4.48
	GBAA_1852	<i>ilvC2</i>	-5.10	-	-3.88
	GBAA_1853	<i>ilvD</i>	-5.51	-	-4.17
	GBAA_1854	<i>ilvA</i>	-4.84	-	-
	GBAA_1969	<i>thrC</i>	-5.87	-4.84	-5.27
	GBAA_1970	<i>thrB</i>	-5.78	-4.76	-5.10
	GBAA_2363		-4.19	-	-
	GBAA_2388	<i>thrS1</i>	-7.22	-6.5	-7.02
	GBAA_4790	<i>brnQ6</i>	-4.43	-4.17	-3.39
	GBAA_5273		-4.26	-	-
	GBAA_5274		-4.27	-	-

**Table 3-1.** Genes most highly regulated by the PCVRs

Genes listed showed a Log2-fold change of  $\geq 4$  ( $\geq 16$ -fold) in at least one complementation strain; AcpA (UTA35), AcpB (UTA36), and AtxA (UTA37) when compared to the *atxAacpAacpB*-null strain (UTA40). Genes that appear to be co-transcribed indicated by bracket.

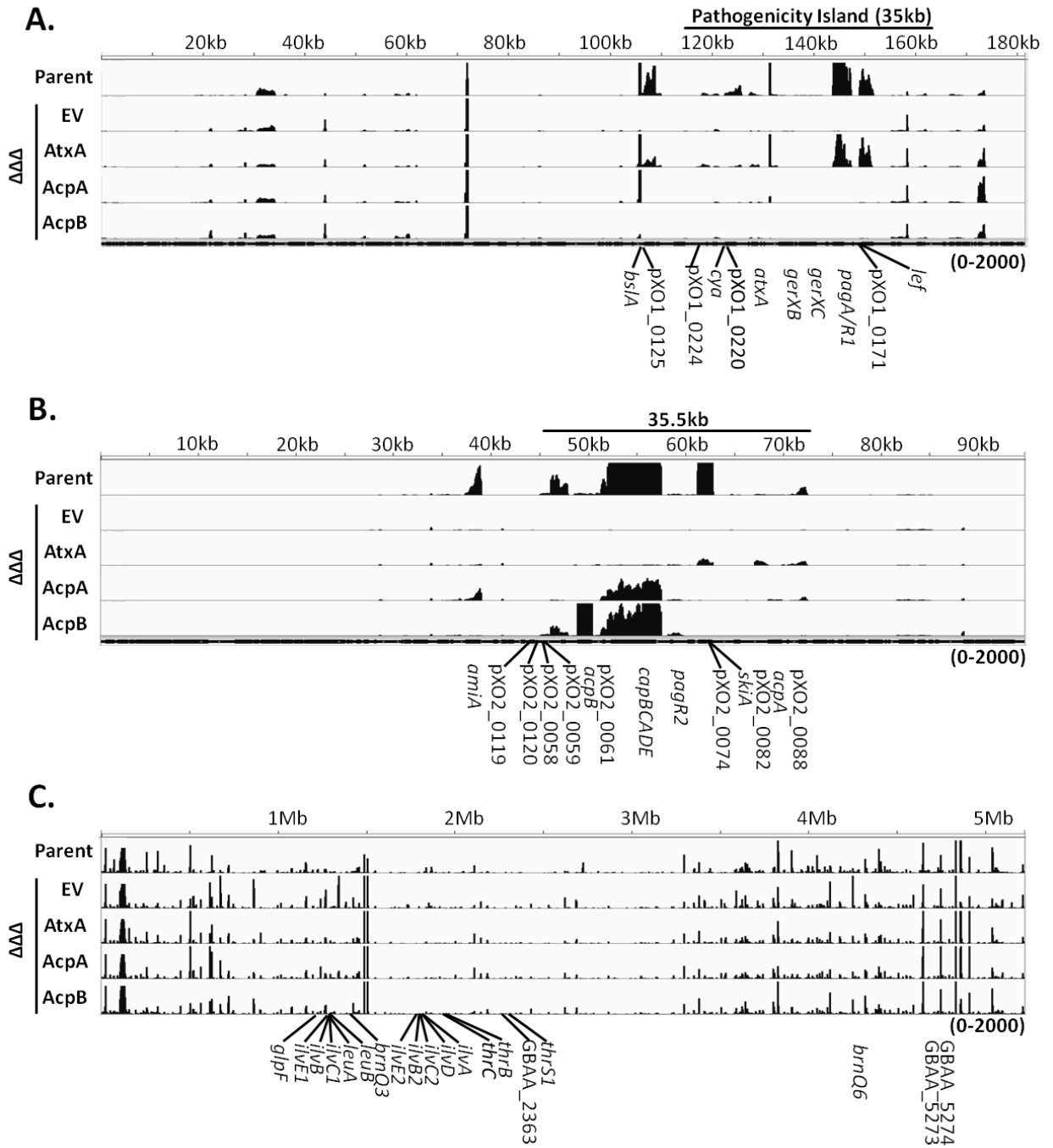


**Figure 3-6.** Sequencing reads mapping to PCVR-regulated loci  
Bedgraphs show normalized sequencing reads mapped to pXO1 (A), pXO2 (B), and the chromosome (C). Regions enriched for PCVR-regulated genes indicated above graph in kilobases.

With the exception of *pagR2*, for pXO2 genes controlled by all three PCVRs, AcpA and AcpB exerted comparable effects, while AtxA had a lower level of control (**Table 3-1**). Other highly-regulated genes on pXO2 included the surface-layer N-acetylmuramoyl-L-alanine amidase gene, *amiA*, controlled solely by AcpA, and a gene of unknown function pXO2\_0119, which was only affected by AcpB.

A significantly smaller proportion of PCVR-regulated genes mapped to the chromosome. Of 5593 transcripts, 198 were altered four-fold or greater by one or more PCVRs. Clustering of PCVR-regulated chromosome genes was not apparent, however transcript reads suggested some operons (**Table 3-1**) and functional relationships. PCVR-controlled chromosomal genes included multiple genes predicted to be associated with metabolic networks. Among the most highly-regulated chromosomal genes were many genes associated with branched chain amino acid (BCAA) synthesis and uptake (**Table 3-1**). Previous reports show that AtxA negatively affected expression of genes involved in branched chain amino acid synthesis (56). My analysis identified AcpB as an additional negative regulator of these genes. Of the 17 genes implicated in BCAA biosynthesis, expression of 13 of these genes is repressed by AtxA and AcpB.

I examined the read maps for evidence of autogenous control of the PCVR genes. For each of the PCVR genes, levels of transcripts mapping to sequences directly upstream of the native open reading frame did not differ in the null mutant, parent strain, and complemented strain, indicating no autogenous control. However, in agreement with previously published studies (29), AtxA positively affected *acpA* transcript levels and AcpA positively increased *acpB* transcripts. Notably, the level of *acpB* transcripts originating from the IPTG-inducible expression vector in the *acpB* complementation strain was higher than that generated by the native locus in the parent strain. Yet, both strains produced comparable amounts of AcpB (data not shown), suggesting that *acpB* transcripts expressed from the inducible promoter have reduced stability or are not translated as efficiently as transcripts expressed from the native locus.

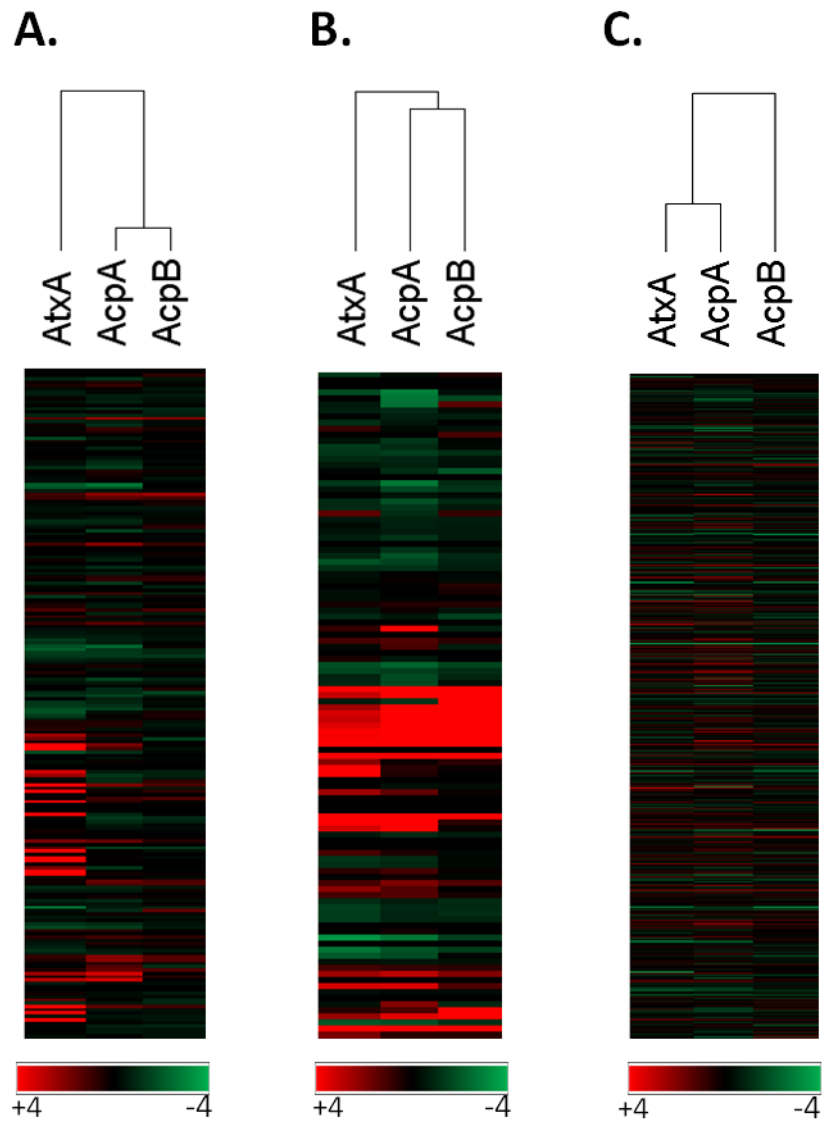


**Figure 3-7.** Heat map and dendrogram of hierarchical clustering among PCVR regulons. Gene expression on pXO1 (A), pXO2 (B), and the chromosome (C) in each complementation strain; AcpA (UTA35), AcpB (UTA36), and AtpA (UTA37) relative to the *atxAacpAacpB*-null strain (UTA40). Relative fold changes in expression are presented in Log<sub>2</sub> scale with up-regulated genes in red and down-regulated genes in green. Hierarchical clustering analysis of completed by GENE-E.



Overall, with the exception of the large number of highly AtxA-regulated genes on pXO1, I did not observe notable relationships between specific PCVRs and genetic elements (plasmids and chromosome loci). Moreover, hierarchical clustering of the PCVRs and their regulons did not reveal a correlation between relative PCVR similarity and co-regulated genes (**Figure 3-7**). The data indicate that AcpA and AcpB elicit similar gene expression patterns for regulated genes on pXO1 and pXO2 genes, whereas the AtxA effect is more distinct. Interestingly, for regulated genes on the chromosome AtxA and AcpA caused similar expression changes, while AcpB elicited more distinct changes in gene expression. I also noted that highly-regulated genes on the plasmids were affected positively by the PCVRs, while chromosomal genes displaying 16-fold or greater regulation were affected negatively.

### **3.2.5 Effects of individual PCVRs on established virulence genes**

The genes most highly-regulated (log<sub>2</sub>-fold change of 4-fold or greater) by at least one PCVR are listed in **Table 3-1**. In agreement with previous reports of AtxA control of toxin gene transcription (30, 49, 57, 71, 100–103), transcripts of *lef*, *cya*, and the *pagAR* operon exhibited a log<sub>2</sub>-fold change of 4.47 or higher in the presence of AtxA. AcpB did not affect toxin gene expression, while AcpA had a modest, yet statistically significant effect on expression of *cya*, encoding EF. In other studies, AcpA was found to have no effect on toxin expression (56, 101). To further investigate AcpA control of *cya*, I tested culture supernates for EF using western blotting (**Figure 3-8**). EF production by the *atxAacpAacpB*-null mutant was markedly less than that of the parent strain. Cultures of the null mutant harboring individual PCVR genes were induced with varying concentrations of IPTG to approximate native levels of PCVR expression, or over-expression of the PCVRs. At both levels of induction, EF was detected in supernates of the null mutant complemented with *atxA*. Interestingly, EF was not detected in culture supernates when either AcpA or AcpB were induced to native or high levels. These results support my RNA-Seq data that AtxA is the major regulator of *cya* expression. Despite a small effect on *cya* transcript levels by AcpA, edema factor was not

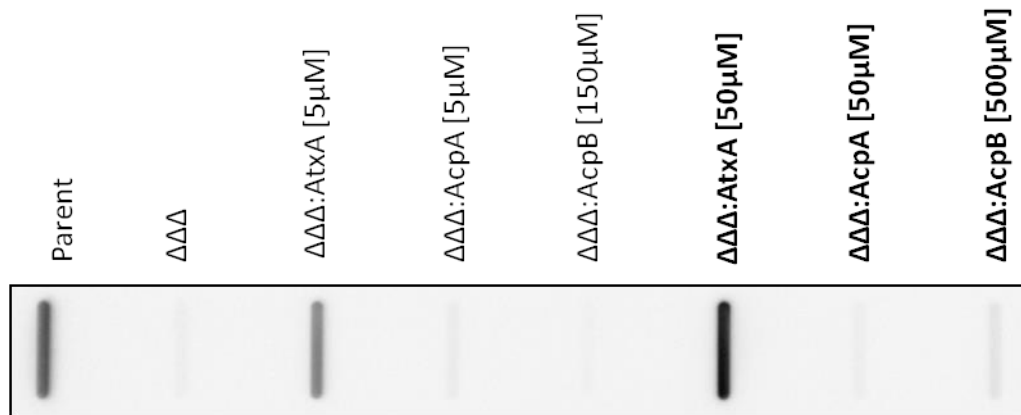


**Figure 3-8.** Edema Factor Production by the individual PCVRs

Expression of recombinant *atxA*, *acpA*, and *acpB* was induced with IPTG to yield either native or overexpressed steady state protein levels (Native - 5  $\mu$ M, 5  $\mu$ M, 150  $\mu$ M respectively; Overexpressed - 50  $\mu$ M, 50  $\mu$ M, 500  $\mu$ M respectively) during growth in  $\text{CACO}_3$  in 5%  $\text{CO}_2$ . Samples of culture supernatants were subjected to slot blot Western analysis using rabbit anti-EF serum raised against *B. anthracis* edema factor.

detected in culture supernates of the null mutant complemented with *acpA*. Further, the increase in edema factor production resulting from overexpression of *AtxA* indicates *AtxA* levels are limiting for *cya* expression.

Expression of the capsule biosynthetic operon was positively affected by all three PCVRs, with *AcpA* and *AcpB* having the strongest effect. The influence of *AtxA* on capsule operon expression was surprising because it was shown previously that native *atxA* transcription in pXO1<sup>+</sup> pXO2<sup>+</sup> strain UT500 deleted for *acpA* and *acpB*, did not produce capsulated bacilli (29). However, another study demonstrated that in a Pasteur II derivative lacking pXO2 (thus missing *acpA* and *acpB*) and harboring plasmid-encoded *capBCA* under the control of the native promoter, overexpression of *atxA* results in the production of capsule material by cultures incubated on LB agar supplemented with bicarbonate in 20% atmospheric CO<sub>2</sub> (71). Typically, to induce capsule synthesis *B. anthracis* is cultured in 5% CO<sub>2</sub>, which is thought to model the host environment (104, 105). I cultured the *atxAacpAacpB*-null mutant and PCVR-complemented strains in 5% CO<sub>2</sub> and 20% CO<sub>2</sub> to test for encapsulated bacilli (**Figure 3-9A, B**). In both CO<sub>2</sub> environments, robust capsule production was observed in strains complemented with *acpA* or *acpB*, but not in the strain expressing only *atxA*. Moreover, overexpression of *atxA* did not result in visible capsule formation (**Figure 3-9**). Combined with the RNA-Seq data, these results indicate that although *AtxA* can elevate *capBCADE* transcript levels, either transcription is not high enough to detect capsule microscopically or robust cell-associated capsule formation by the virulent Ames strain requires additional factors that are regulated by *AcpA* and *AcpB*, but not *AtxA*.

Other genes related to virulence were affected by *AtxA*, *AcpA*, and *AcpB*. The pXO2 *pagR2* gene, which has been implicated in the attenuation of virulence in the Pasteur II vaccine strain (99), was positively regulated 32- to 64-fold by all three PCVRs (**Table 3-1**). In addition, transcription of the  $\beta$ -lactamase gene *bla2*, reported previously to be controlled by the extracytoplasmic function sigma factor–anti-sigma factor gene pair, *sigP-rsiP* (106), was

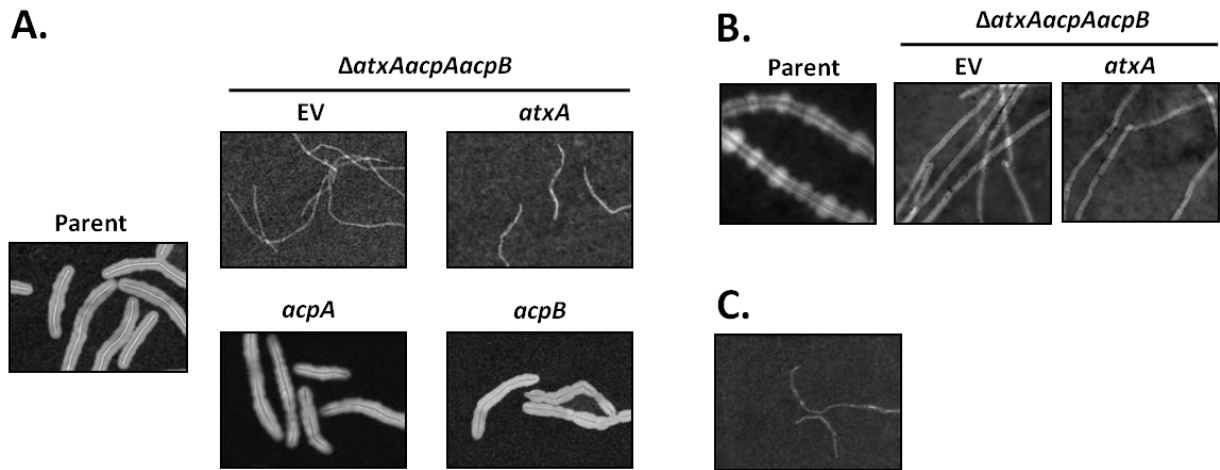


**Figure 3-9.** Capsule production by the individual PCVRs  
 Expression of recombinant *atxA*, *acpA*, and *acpB* was induced with IPTG to yield native steady state protein levels (5  $\mu$ M, 5  $\mu$ M, 150  $\mu$ M respectively) during growth in CACO<sub>3</sub> in 5% CO<sub>2</sub> (A). (B) Expression of recombinant *atxA* induced with 30  $\mu$ M IPTG in UTA40 during growth in CACO<sub>3</sub> in 20% CO<sub>2</sub>. (C) Overexpression of *atxA* with 50  $\mu$ M IPTG during culture in CACO<sub>3</sub> in 5% CO<sub>2</sub>. The UTA40 derivatives were induced at early exponential phase (2h; OD<sub>600</sub> 0.25-0.35) in during growth in CACO<sub>3</sub>. Samples were collected at the transition to stationary phase (4h; OD<sub>600</sub> 1.2-1.8), stained with India Ink, and visualized using DIC microscopy.

also increased 5- to 7-fold in the *AtxA*, *AcpA*, and *AcpB* complementation strains compared to the *atxAacpAacpB*-null mutant.

### 3.3 Discussion

In this chapter, I have reported similarities and differences of the *B. anthracis* PCVRs at the amino acid level, determined the regulon of each PCVR using RNA-Seq, examined linkage relationships between PCVRs and their targets, and studied the specific activity of each PCVR on toxin and capsule expression.

Native transcript levels of *atxA*, *acpA*, and *acpB* from *B. anthracis* cultured in  $\text{CACO}_3$  as determined using RNA-Seq show that transcripts of *atxA* and *acpA* are present at roughly equivalent levels, while transcripts of *acpB* are two-fold more abundant. These data are consistent with previous qRT-PCR data which examined *atxA*, *acpA*, and *acpB* transcript levels in a genetically reconstituted strain of *B. anthracis* (70). However, relative levels of *atxA*, *acpA*, and *acpB* transcripts do not correlate with protein abundance (**Figures 3-3 & 3-4**). Despite having transcript amounts equivalent to that of *acpA*, *AtxA* is far more abundant in soluble cell lysates than *AcpA*. Transcripts of *acpB* are expressed two-fold more highly than *atxA* or *acpA*, but *AcpB* is still less prevalent than *AtxA* in cell lysates. The ribosomal binding site (RBS) among the three genes is not conserved and is likely the cause for the non-linear relationship between PCVR transcripts and protein levels. The ribosomal binding sequence, as well as spacing to the ATG start codon, differs for each of the three genes. Production of *AcpA* and *AcpB* increases when the *atxA* RBS and 5' untranslated sequence are used to drive translation of *acpA* and *acpB* (See Chapter IV and **Figure 4-1**). Differences in the RBS among PCVR genes demonstrate post-transcriptional regulation of PCVR protein levels. It may be advantageous for *B. anthracis* to keep *AcpA* and *AcpB* protein levels at levels much lower than *AtxA* during infection. Both *AcpA* and *AcpB* are limiting for capsule production and overexpression of either *acpA* or *acpB* in the *atxAacpAacpB*-null strain produced cells with capsule radii much thicker than the wild-type strain. An *acpAacpB* mutant is avirulent in a

murine model of anthrax, and single deletions of either *acpA* or *acpB* result in decreased capsule thickness or virulence relative to the parent strain. Reduced dissemination is observed in an *acpB*-null mutant, but not in an *acpA*-null mutant indicating that other factors controlled by these two regulators are important for infection (107). The virulence of *B. anthracis* strains overexpressing *acpA* or *acpB* has not been tested, but it is likely that increased capsule thickness or other factors regulated by either regulator would not attenuate virulence.

One of the overarching questions with regard to PCVR function is what features of the proteins mediate target specificity. Hierarchical clustering shows there is little to no correlation between amino acid conservation among regulators and what genes they control. AcpA and AcpB generated similar expression patterns for genes located on pXO1, which were distinct from AtxA-mediated gene expression on pXO1. Gene expression profiles for all three regulators were very similar for genes located on pXO2. For chromosome-encoded genes, the expression profiles for AtxA and AcpA were most similar. These data suggest that other factors aside from amino acid sequence similarity are involved in PCVR target specificity.

The Koehler lab published previously that phosphorylation at H199 within AtxA is thought to reposition the linker between PRD1 and HTH2 of AtxA thereby affecting the HTH2-DNA interaction (65). The phosphorylation state of AcpA and AcpB has not been determined. The putative PRDs of AcpA and AcpB are the most dissimilar domains when compared to the AtxA amino acid sequence. Histidine residues within the PRDs of AcpA and AcpB do not align with phosphorylated histidines at position 199 nor 379 within AtxA (**Figure 3-1**, (66)). Differential positioning of histidine residues within the PRDs of AcpA and AcpB relative to AtxA may be cause for differences in target specificities between these three PCVRs. It is possible that if phosphorylated histidine residues exist within PRD1 of AcpA and AcpB, differences in the location of these residues relative to the HTH2 of the DNA-binding domain may account for differences in target specificities observed among AtxA, AcpA, and AcpB.

Metal binding might also play a role in PCVR target specificity, as was demonstrated for Mga, the PCVR of Group A Streptococcus. Mga DNA-binding specificity is influenced by Zn<sup>2+</sup>

and Ni<sup>2+</sup> (108). The involvement of metal ions in AtxA, AcpA, and AcpB DNA-binding has not been tested. However, if metal ions play a similar role in *B. anthracis* PCVR function, amino acid differences between AtxA, AcpA, and AcpB could influence the DNA-binding specificity of these regulators.

My data show that PCVR-regulated genes on pXO1 and pXO2 cluster within defined loci. On pXO1, PCVR-controlled genes clustered within a 35-kb region identified previously as a pathogenicity island. The pathogenicity island is flanked by IS1627 insertion elements (ISs) with near identical sequence similarity. This region harbors loci for several other putative ISs, transposases, and integrases (109) and inversions of this pathogenicity island have been observed in other *B. anthracis* strains (96). Similarly, the 35.5-kb region on pXO2 that contains a cluster of PCVR-regulated genes has also been suggested as a pathogenicity island (110). In line with PCVR control of genes within pathogenicity islands, MgaSpn, a PCVR expressed in *S. pneumoniae*, represses expression of the 12-kb *rlr* pathogenicity islet. This region encodes three sortases and a cognate transcriptional regulator which mediate bacterial colonization in the host pulmonary and nasopharyngeal environments (14, 111). In GAS, Mga controls expression of genes localized to a 47-kb region that is inclusive of *emm* which encodes M-protein, as well as other Mga-regulated virulence factors. In addition to genes related to virulence, features associated with mobile elements, such as transposases and multiple short direct repeats, are also within this region (112). To my knowledge, RivR and PafR have not been associated with regulation of any pathogenicity islands in their respective host organisms.

The capsule biosynthetic operon is located within an apparent pathogenicity island on pXO2. The *capBCA* genes are not unique to *B. anthracis* as homologs are present in other members of the *Bacillus* genus (113). In other species *capBCA* homologues are regulated by factors other than AcpA and AcpB homologues. In *B. subtilis* IFO 16449, which harbors chromosome-encoded *capBCA* homologues and produces large quantities of  $\gamma$ -polyglutamic acid, activity of a *PcapB-lacZ* reporter increases five-fold with the addition of L-glutamic acid to cultures of Spizizen minimal medium (114). Homologs of AtxA, AcpA, or AcpB have not been

identified in this strain of *B. subtilis*. In *B. anthracis*, culture in medium supplemented with bicarbonate in 5% atmospheric CO<sub>2</sub> is required for capsule formation (105). Other *Bacillus* species that produce a cell-associated poly-γ-D-glutamic acid capsule harbor pXO2-like plasmids that include the *capD* and *capE* genes at the 3' end of the *capBCA* operon. CapD is required for cell-wall anchoring of polyglutamate to the cell wall, and CapE has been proposed to form a complex with CapA to transport D-glutamic acid polymers across the cell membrane (47–49). The presence of pathogenicity islands on pXO1 and pXO2 provide evidence for horizontal gene acquisition in *Bacillus anthracis*. Considering that many virulence factors are acquired by horizontal gene transfer and plasmid acquisition, it is reasonable to postulate that these factors are added gradually over time and that transcriptional regulators associated with these factors both gain and lose functionality. Given that *atxA*, *acpA*, and *acpB* are located in apparent pathogenicity islands, over the course of evolution they may have gained functionality to control expression of genes outside of their original/initial targets providing a fitness advantage.

Perhaps the most interesting disparity between the *B. anthracis* PCVR regulons and the PCVR regulons of other species is within the collection of target genes that do not encode classic virulence factors. Prior to my results, metabolic gene targets of PCVRs have frequently included genes associated with carbohydrate utilization. The *S. pyogenes* Mga regulon includes genes involved in fermentation, the mannose PTS, fructose PTS, and maltose utilization (115). RivR of *S. pyogenes* positively regulates genes required for metabolism of sucrose (116). In uropathogenic *E. coli*, PafR represses expression of genes required for maltose utilization (15). My data indicate that the *B. anthracis* PCVRs do not play a significant role in carbohydrate utilization. Rather, AtxA, AcpB, and to a lesser extent AcpA negatively regulate operons and genes associated with branched chain amino acid biosynthesis and transport. The physiological significance of PCVR control of metabolic genes has been purported to be related to diverse microenvironments of pathogens during infection. *S. pyogenes* can colonize the skin, pharynx, soft tissues, and cause invasive infections (117,



118). Uropathogenic *E. coli* can colonize both the colon and urinary tract (119). Like these bacteria, *B. anthracis* can thrive in diverse host environments, including the dermis, blood, cerebral spinal fluid, and many organs (120, 121). However, the significance of branched chain amino acid (BCAA) metabolism in these environments is not clear.

Although minimal media for culture of *B. anthracis* have been described, there are few reports of nutritional requirements of the bacterium during infection. *B. anthracis* mutants deficient in synthesis of aromatic amino acids were less virulent than a wild-type Sterne strain in models of anthrax infection (90). Also, a recent study suggested that *B. anthracis* requires exogenous valine to grow in a medium that mimics serum (122). There are few reported links between BCAA metabolism and virulence in other pathogens. In *Staphylococcus aureus*, single deletions of *brnQ* alleles, predicted to encode BCAA transporters, have affected virulence. A *brnQ1* mutant was attenuated compared to the parent strain in a murine infection model. In contrast, a *brnQ2* mutant had a significant increase in virulence relative to parent (123). In *Listeria monocytogenes* CodY, a BCAA-responsive transcriptional regulator that has been well characterized in *B. subtilis* (68, 124), binds the coding sequence of the master virulence regulator, *prfA*, resulting in up-regulation of *prfA* transcription in low BCAA conditions. Mutation of the CodY binding sequence in *prfA* attenuated bacterial virulence in a murine infection model (125). I determined that AtxA and AcpB down-regulate expression of *brnQ3* and *brnQ6*, which are annotated as BCAA transport system II carrier proteins (126). AtxA and AcpB also repress expression of BCAA synthetic operons. Interestingly, CodY has been implicated in AtxA protein stability in *B. anthracis* (69).

# Chapter IV

## Carbon dioxide, protein stability, and PCVR interactions

*NOTE: A portion of this chapter is derived from work published in 2018 which is cited below. I am first author on this publication. I have received permission by the publisher of Molecular Microbiology, John Wiley and Sons, to reproduce all of the manuscript in print or electronically for the purposes of my dissertation (License Number: 4342040215509)*

Raynor, M.J., Roh, JH., Widen, S.G., Wood, T.G., Koehler, T.M. (2018) Regulons and protein-protein interactions of PRD-containing *Bacillus anthracis* virulence regulators reveal overlapping but distinct functions. *Molecular Microbiology*. doi: 10.1111/mmi.13961.

## 4.1 Introduction

Based on *in vitro* experiments designed to study virulence gene expression in response to culture conditions, it is surmised that when *B. anthracis* enters a host at least two important cues, temperature and bicarbonate/carbon dioxide ( $\text{HCO}_3^-/\text{CO}_2$ , abbreviated as  $\text{CO}_2$ ), induce expression of toxin and capsule. When *B. anthracis* is cultured *in vitro*, expression of *atxA* is greater when cells are grown at 37°C relative to 30°C. (59). The effect of carbon dioxide on virulence gene expression by *B. anthracis* in culture has been well documented, and the production of toxin and capsule is highly dependent on growth in elevated  $\text{CO}_2$  relative to air. Cultures incubated in 5% atmospheric  $\text{CO}_2$  show a 10-fold increase in transcription of the three toxin genes and an increase of more than 20-fold in expression of the capsule operon (67, 100). Carbon dioxide and bicarbonate are in dynamic equilibrium within the cell and concentrations of each are regulated by carbonic anhydrase and other factors. *B. anthracis* has two putative carbonic anhydrases but these enzymes do not appear to be associated with  $\text{CO}_2$ /bicarbonate-induced toxin production because toxin gene expression is unaffected in a mutant in which both carbonic anhydrase genes are deleted (Koehler lab, unpublished data). The  $\text{CO}_2$ /bicarbonate effect on virulence gene expression is specific and not simply a matter of the buffering capacity of dissolved bicarbonate during bacterial culture. Elevated toxin and capsule synthesis is not observed when cultures are grown in highly buffered media in air (41, 105). Carbon dioxide concentrations are often higher in mammalian tissues compared to other environments which may be a reason why  $\text{CO}_2$  functions as a signal to promote virulence gene expression (16). Carbon dioxide is present at a concentration of 5.5% in human blood (127) which is very close to the concentration required for optimal toxin and capsule synthesis in *B. anthracis*. The mechanism for the  $\text{CO}_2$  effect has not been discerned, but the effect of bicarbonate in culture medium may be comparable with its physiological role. Bicarbonate is used by animals to guard against pH fluctuations in the blood where it is at equilibrium with  $\text{CO}_2$  and buffers extracellular fluids (128). This functionality marks bicarbonate concentration as a

good indicator for the host environment, and potentially acts as a signal to modulate the activity of proteins involved in virulence factor expression.

AtxA is required for the CO<sub>2</sub> effect on toxin and capsule induction. The effect of CO<sub>2</sub> on AtxA-mediated virulence gene expression is not at the level of *atxA* expression because transcripts of *atxA* are unchanged in cultures incubated in ambient air, 5% CO<sub>2</sub>, or 20% CO<sub>2</sub> (59). Roles for CO<sub>2</sub> in AtxA activity have been defined as described in Chapter 1 (1.5). Briefly, AtxA activity on the lethal factor promoter fused to *lacZ* increases when strains are incubated in medium containing dissolved bicarbonate and 5% atmospheric CO<sub>2</sub> compared to strains grown in ambient air in medium lacking bicarbonate. Growth in 5% CO<sub>2</sub> also increases the AtxA dimer-to-monomer ratio compared to growth in ambient air (64). Whether CO<sub>2</sub> affects AcpA and AcpB activity has not been determined.

Multimerization by transcription factors increases the specificity of these proteins for their DNA target sequences and provides a mechanism to control the activity of these proteins. Dimerization allows for the proper orientation of DNA-binding regions of each monomer to facilitate efficient DNA-binding. This is especially relevant when the transcription factor must recognize a palindromic DNA sequence (129). The activity of many transcription factors is also governed by multimerization in response to cofactor/ligand binding, phosphorylation, or other signals that convey the physiological state of the cell. In actinomycete bacteria, dimerization of the BldD transcription factor, which controls multicellular differentiation progression in sporulating bacteria, is mediated by tetramers of c-di-GMP (130). Finally, multimerization of Mga, is controlled by phosphorylation (11).

In *B. anthracis*, the ability of AtxA to form dimers is essential for activity, such that mutants of AtxA that cannot dimerize are inactive (described in detail in Chapter 1 (1.5)). The EIIB-like domain at the carboxy terminus of AtxA is required for dimer formation (**Figure 1-2**). AtxA crystallized as a dimer with each monomer in an anti-parallel arrangement. The dimer interface occurred mainly between PRD2 of monomer one and the EIIB-like domain of monomer two (64, 65). The importance of dimerization for AtxA activity provides rationale to

study the multimerization states of AcpA and AcpB. Moreover, if AcpA and AcpB are able to form homomultimers, the amino acid conservation among the regulators may allow heteromultimers to form.

Phosphorylation of PRD-containing proteins can control multimerization, as well as interactions with other PTS components. There are several cases where the phosphorylation state of the PEP-dependent phosphotransferase system (PTS) EIIB component can mediate interactions with PRD-containing transcriptional regulators (9). In at least one system, the transcriptional regulator interacts with a membrane-bound EIIB component thereby sequestering the regulator to the membrane. In *B. subtilis* the transcriptional activator of the mannitol operon, MtlR, interacts with the nonphosphorylated EIIB<sup>Mtl</sup> domain of the membrane-bound mannitol-specific PTS permease. The interaction of MtlR with the EIIB<sup>Mtl</sup> domain occurs via the carboxy-terminal EIIB-EIIA region of MtlR and is required for MtlR activation (131).

In *B. anthracis*, phosphorylation of histidines within AtxA at positions 199 and 379 in PRD1 and PRD2, respectively has been demonstrated. Additionally, phosphomimetic and phosphoablative mutations at positions 199 and 379 affect AtxA activity and dimerization (65, 66). It has yet to be determine what factor(s) phosphorylate AtxA, and experiments to identify any proteins that interact with AtxA were largely restricted to soluble proteins. It is unknown whether AtxA interacts with any membrane components.

In this chapter I show that like AtxA, the activity of AcpA and AcpB is CO<sub>2</sub>-responsive, but that CO<sub>2</sub> does not affect protein stability or solubility. I also present data that answer questions about homomeric and heteromeric interactions among the PCVRs and how these interactions influence activity.

## **4.2 Results**

### **4.2.1 Induced expression of *acpA* and *acpB* in *B. anthracis* cultures**

I determined previously that native protein levels of AtxA, AcpA, and AcpB in the fully virulent Ames strain were not equivalent and AtxA was detected in far greater quantity than

AcpA or AcpB (**Figure 3-3**). To directly compare the activities of the three regulators *in vivo*, I wanted to express the individual regulators at comparable levels. In order to overcome differences in PCVR steady state levels and to uncouple PCVR gene expression for differing transcriptional control elements, I used an inducible expression system to study PCVR function. Each PCVR open reading frame with the respective native ribosomal binding site (RBS) and 5' leader sequence was cloned downstream of an IPTG-inducible *hyper-spank* promoter encoded by a low-copy plasmid. Each PCVR was engineered to express a carboxy-terminal 6xHis or FLAG epitope to facilitate detection by western blot. IPTG-inducible expression constructs were introduced into an *atxA*-null mutant of the ANR-1 strain (pXO1<sup>+</sup> pXO2<sup>-</sup>) to alleviate the need to work in the fully virulent Ames strain (pXO1<sup>+</sup> pXO2<sup>+</sup>). Strains were cultured in CA medium supplemented with 0.8% bicarbonate in 5% CO<sub>2</sub> atmosphere (CACO<sub>3</sub>) and protein expression was induced with the indicated IPTG concentrations at early exponential growth phase (**Figure 4-1A, B, C**). Samples for western blots were collected at the transition to stationary phase. PCVR protein levels increased following IPTG addition. AtxA-His was detected with IPTG concentrations of 40μM and 400μM. AcpA-His and AcpB-His were only detectable when cultures were induced with 400 μM IPTG, and both proteins were less abundant than AtxA-His induced with the same IPTG concentration.

The RBS among the three genes is not conserved and is likely the cause for the differences in protein levels (**Figure 4-1D**). The ribosomal binding sequences, as well as distances from the ATG, differ for each of the three genes, likely affecting translation efficiency. To improve *acpA* and *acpB* translation efficiency and increase protein expression I created IPTG-inducible expression constructs in which the native RBS and 5' leader sequence was replaced with the complementary sequence from *atxA*. Production of AcpA-His and AcpB-His increased when the *atxA* RBS and 5' leader sequence is used to drive translation of *acpA* and *acpB* (**Figure 4-1E, F**). These data show that in addition to several factors affecting transcription of these regulators, regulation occurs at the level of translation.

#### 4.2.2 AcpA and AcpB activity in *B. anthracis* cultures

I developed a system to quantitatively assess AcpA and AcpB activity in *B. anthracis*. Transcriptional analyses indicate AcpA and AcpB strongly regulate expression of the *capBCADE* operon, which encodes genes required for synthesis of the poly- $\gamma$ -D-glutamic acid capsule. A region inclusive of 1 kb upstream from the *capB* translational start codon was fused to a promoter-less *lacZ* gene and incorporated into the nonfunctional *plcR* locus on the chromosome of an *atxA*-null *B. anthracis* strain to create the *PcapB-lacZ* transcriptional reporter strain UT423. Activity assays were performed in the ANR-1 strain background (pXO1+ pXO2-) (**Table 2-1**). Plasmids bearing IPTG-inducible alleles of *acpA* or *acpB* engineered to express a carboxy-terminal 6xHis tag were introduced into UT423.

I first tested whether AcpA and AcpB had dose-dependent activity on *PcapB-lacZ* and determined the linear range for activity (**Figure 4-2A-D**). Expression of *acpA* and *acpB* was induced using IPTG and translation occurred via the respective native ribosomal binding site and 5' leader sequence (**Figure 4-2A, B**), or the *atxA* ribosomal binding site and 5' leader sequence (**Figure 4-2C, D**) which increases protein production. Dose-dependent production of AcpA-His and AcpB-His was observed for all expression constructs, and AcpB-His translated using the *atxA* RBS and 5' leader sequence was more abundant in cell lysates than AcpB-His translated from the native RBS and 5' leader sequence (**Figure 4-2B, D**). However, dose-dependent  $\beta$ -galactosidase activity was not observed when the *atxA* RBS and 5' leader sequence was used for translation (**Figure 4-2C, D**). It is unclear how the *atxA* RBS and 5' leader sequence disrupts the link between protein abundance in cell lysates and AcpA and AcpB activity on the *PcapB-lacZ* reporter. Only AcpB-His that was translated from the native RBS and 5' leader sequence yielded dose-dependent  $\beta$ -galactosidase activity. Given that the *acpB* RBS and 5' leader sequence yielded dose-dependent AcpB activity on *PcapB-lacZ*, I tested whether expression of *acpA* with the *acpB* RBS and 5' leader sequence would result in dose-dependent AcpA activity (**Figure 4-2E, F**). Expression of *acpA* with the *acpB* RBS and 5'

leader sequence yielded dose-dependent AcpA-His expression as well as dose-dependent activity.

#### 4.2.3 Carbon dioxide effect on regulator activity

AtxA, AcpA, and AcpB are paralogous transcriptional regulators that share a high degree of amino acid sequence similarity, and the regulons of these proteins indicate some functional similarity. The molecular mechanism by which these proteins promote transcription is unknown, but AtxA activity has been shown to increase when *B. anthracis* strains are cultivated in medium containing dissolved bicarbonate and 5% CO<sub>2</sub> (64). Given that the *B. anthracis* PCVRs are paralogues and that CO<sub>2</sub> concentration is an important host-related signal that promotes expression of virulence genes in *B. anthracis* and some other mammalian pathogens, I wanted to investigate whether AcpA and AcpB were also CO<sub>2</sub>-responsive. Initially, I compared β-galactosidase activity from strains producing AcpA-His or AcpB-His cultivated in CACO<sub>3</sub> in 5% CO<sub>2</sub> (**Figure 4-2B, F**) or CA-Air (CA medium lacking bicarbonate in ambient air) (**Figure 4-2G, H**). Production of His-tagged proteins was variable, including when the same amount of IPTG was used to induce the same protein in CACO<sub>3</sub> or CA-Air. However, a comparison of activity from CACO<sub>3</sub> and CA-Air samples with proteins present at similar levels regardless of the amount of IPTG shows that AcpA-His activity on *PcapB-lacZ* is higher when cells are cultured in CACO<sub>3</sub>. The same was true for AcpB-His. To more definitively test the effects of culture in elevated CO<sub>2</sub> versus culture in ambient air on AcpA and AcpB activity, I cultured strains separately in three growth conditions: 1) CA-Air, 2) CACO<sub>3</sub> in 5% atmospheric CO<sub>2</sub>, and 3) CACO<sub>3</sub> in 20% atmospheric CO<sub>2</sub>. In an attempt to have consistent protein levels in all growth conditions, different amounts of IPTG dependent on the protein being expressed and



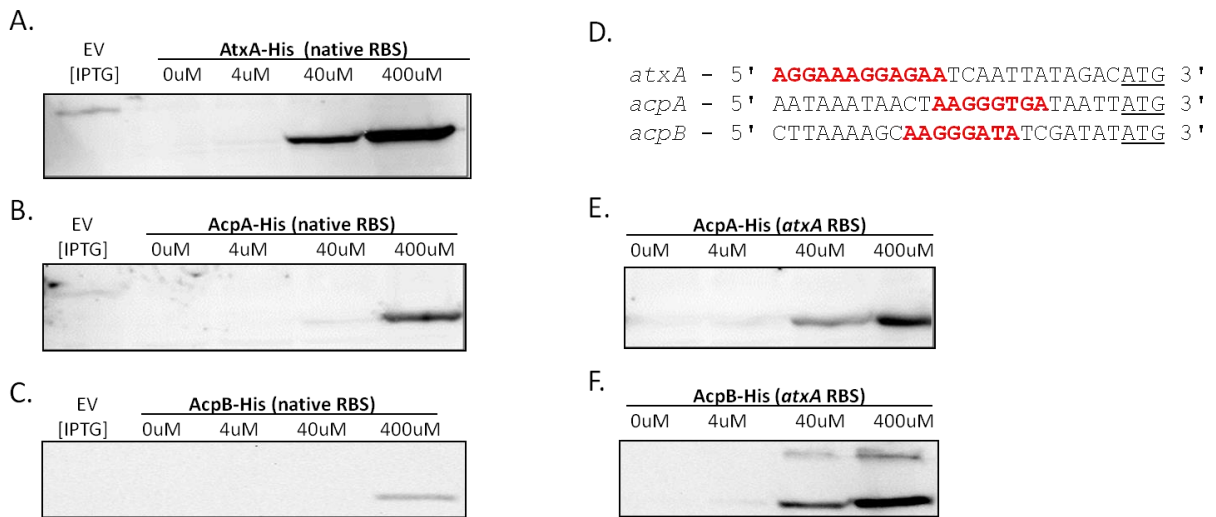


**Figure 4-1.** Induced PCVR expression

*B. anthracis* strains containing PCVR proteins translated from the native ribosomal binding site; AtxA-His (pUTE991), AcpA-His (pUTE1055), or AcpB-His (pUTE1092), or the *atxA* ribosomal binding site AcpA-His (pUTE1090), AcpB-His (pUTE1091) were cultivated in CACO<sub>3</sub>. Protein expression was induced at indicated IPTG concentrations during early exponential growth phase and samples were collected at the transition to stationary phase. Cell lysate load volumes were normalized to the OD<sub>600</sub> reading at collection. AcpA-His and AcpB-His proteins were detected by immunoblotting with α-His antibody.

growth medium were used to induce expression. Cultures were induced at early exponential growth phase and samples were harvested for protein detection and measurement of  $\beta$ -galactosidase activity at the transition to stationary phase. **Figure 4-3** shows AcpA-His and AcpB-His levels in the different growth media and corresponding  $\beta$ -galactosidase activity. AcpA-His activity increased 8- to 10-fold when cells were cultured in CO<sub>2</sub> compared to culture in ambient air. AcpB-His appeared to follow the same trend, but inconsistent protein levels complicate data interpretation. Interestingly, both AcpA-His and AcpB-His required much more IPTG to yield detectable amounts of protein when cultures were cultivated in CA-Air compared to CACO<sub>3</sub>.

To determine whether culture in CA-Air reproducibly results in diminished steady state PCVR levels, and to test whether AtxA levels are also affected, I grew cultures of UT423 harboring IPTG-inducible plasmids engineered to express *acpA*, *acpB*, or *atxA* in CA-Air, CACO<sub>3</sub> in 5% CO<sub>2</sub>, and CACO<sub>3</sub> in 20% CO<sub>2</sub>. Expression of *acpA*, *acpB*, and *atxA* was induced with 40  $\mu$ M IPTG in all media to observe medium-dependent changes in protein abundance. Indeed, levels of AcpA-FLAG, AcpB-FLAG, and AtxA-FLAG were all severely diminished when strains were cultured in CA-Air compared to culture in either concentration of atmospheric CO<sub>2</sub> in CACO<sub>3</sub> (**Figure 4-4**).

The *B. anthracis* PCVRs are soluble proteins and my experiments examining how CO<sub>2</sub> affects the activity of these regulators have focused on the soluble fraction of cell lysates. However, some PRD-containing proteins are sequestered to the membrane as a means of modulating activity (131). Therefore, I tested whether AcpA-FLAG and AcpB-FLAG were being sequestered to the insoluble fraction during culture in CA-Air. I grew strains containing AcpA-FLAG or AcpB-FLAG in CA-Air, CACO<sub>3</sub> in 5% CO<sub>2</sub>, and CACO<sub>3</sub> in 20% CO<sub>2</sub>. Cell lysates were generated and the soluble and insoluble fractions were separated by centrifugation. The insoluble fraction was washed and resuspended in 8M urea to increase solubility. Lysates were separated by SDS-PAGE and proteins were detected by western blot.

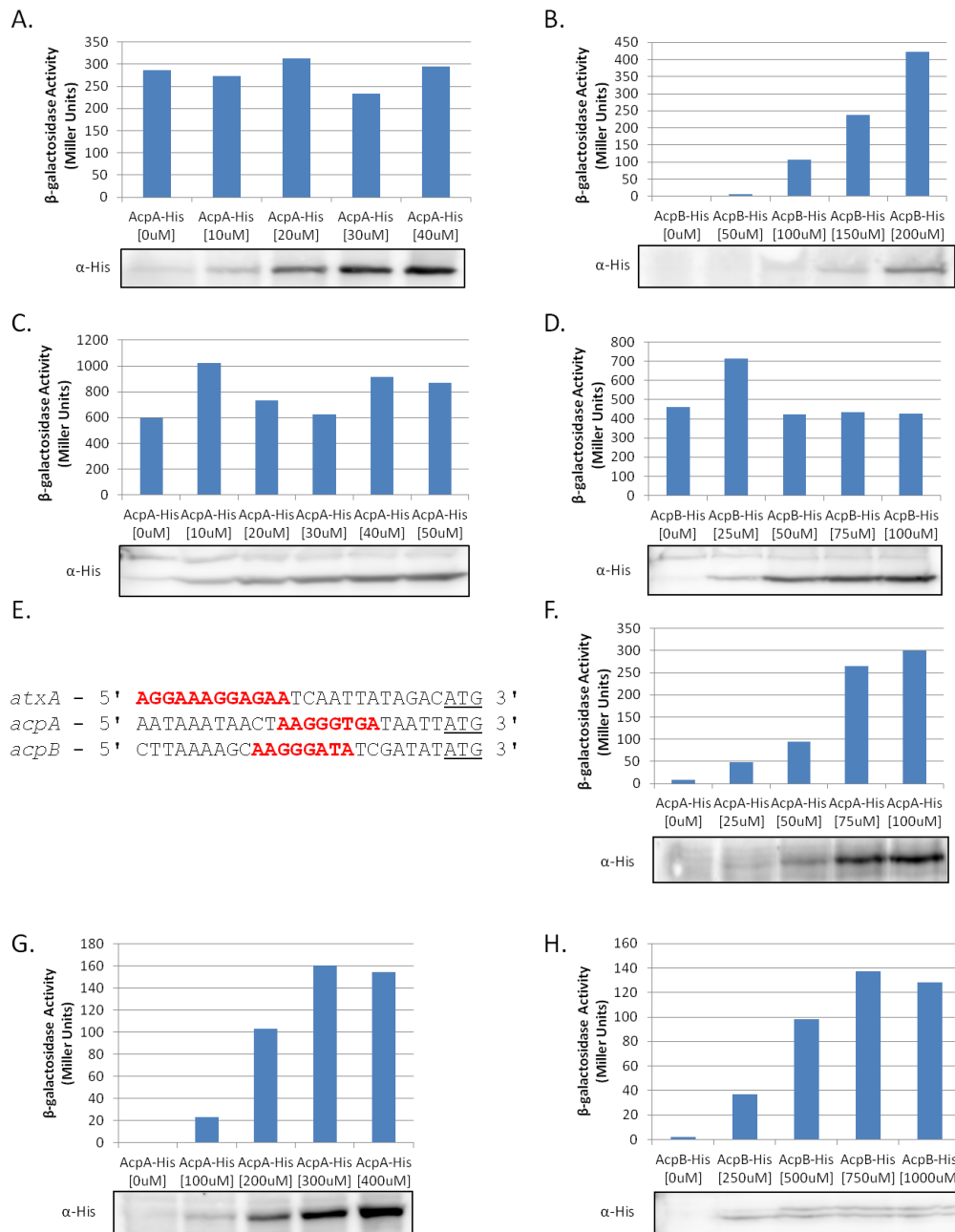


**Figure 4-2.** *In vivo* activity of AcpA-His and AcpB-His

The  $\beta$ -galactosidase activity of AcpA-His and AcpB-His was measured in an *atxA*-null strain harboring a *PcapB-lacZ* reporter (pXO1<sup>+</sup> pXO2<sup>-</sup>) (UT423) during culture in CACO<sub>3</sub> (A-D, F) or CA-Air (G, H). Translation of *acpA* and *acpB* occurred from the native RBS (A) pUTE1055, (B) pUTE1092, the *atxA* RBS (C) pUTE1090, (D) pUTE1091, or the *acpB* RBS (G) pUTE1103, (H) pUTE1092. Putative RBS (in red) and 5' leader sequences (sequence between RBS and ATG) used to drive translation of PCVRs (E). Protein expression was induced at indicated IPTG concentrations during early exponential growth phase and samples were collected at the transition to stationary phase.  $\beta$ -galactosidase activity of *B. anthracis* strains was determined as described previously (95). Cell lysate load volumes were normalized to the OD<sub>600</sub>. Neither AcpA-FLAG nor AcpB-FLAG were detected in the soluble or insoluble fractions following culture in CA-Air. reading at collection. AcpA-His and AcpB-His proteins were detected by immunoblotting with  $\alpha$ -His antibody.

To ensure that the IPTG-inducible promoter,  $P_{hyperspank}$ , used to express *atxA*, *acpA*, and *acpB* was not sensitive to culture in CA-Air or  $\text{CACO}_3$  I grew *B. anthracis* strains containing an IPTG-inducible GFP-FLAG expression plasmid. Individual cultures were incubated in both media and GFP-FLAG expression was induced with IPTG. Western blots of cell lysates showed that GFP-FLAG was present at equivalent levels when *B. anthracis* was cultured in either CA-Air or  $\text{CACO}_3$ . In summary, I have shown that culture in CA-Air dramatically decreases steady state levels of the *B. anthracis* PCVRs when expressed from an IPTG-inducible promoter, these proteins were not detected in either the soluble or insoluble fraction of cell lysates when cultured in CA-Air, and that the IPTG-inducible  $P_{hyperspank}$  promoter used to express the PCVRs functioned equivalently in CA-Air and  $\text{CACO}_3$ .

One possibility for the significant reduction in steady state levels of the *B. anthracis* PCVRs during culture in CA-Air is that the proteins were degraded in these growth conditions. Transcriptional regulators are a part of the main regulatory proteins in the cell and their activity, as well as their concentration, are often tightly regulated. The half-lives of some bacterial transcription factors can be as short as one minute, as is the case with *cII* in *Escherichia coli* (132). It is therefore possible that the stability of the *B. anthracis* PCVRs is affected by growth conditions.

To test PCVR protein stability I performed a modified pulse-chase experiment in which I grew cultures induced for expression of AcpA-FLAG or AtxA-FLAG in  $\text{CACO}_3$ . One hour after induction with IPTG I pelleted, washed, and resuspended the cells in an equivalent volume of either spent CA-Air or spent  $\text{CACO}_3$  medium, both lacking IPTG and containing a sub-inhibitory concentration of chloramphenicol to inhibit nascent protein synthesis. Spent media consisted of filter sterilized media from separate same-age cultures that were harvested at the time of media change. Cultures were incubated for five hours following media change. Samples were collected for western blot analysis at hourly time points. I compared FLAG-tagged protein levels from the  $\text{CACO}_3 \rightarrow$  CA-Air cultures to cultures never shifted from  $\text{CACO}_3$  (**Figure 4-5**). AcpA-FLAG and AtxA-FLAG levels in cultures cultivated entirely in  $\text{CACO}_3$  were not significantly

diminished following removal of IPTG and the addition of chloramphenicol. This result suggests that AcpA-FLAG and AtxA-FLAG are stable proteins in these growth conditions. Interestingly, shifting CACO<sub>3</sub> cultures to CA-Air did not dramatically affect AcpA-FLAG or AtxA-FLAG protein levels indicating culture CA-Air does not negatively affect protein abundance. My inability to detect the *B. anthracis* PCVRs expressed from the IPTG-inducible promoter when strains are cultivated in CA-Air does not seem to be physiologically relevant, and may be an artifact of using the *atxA* RBS and 5' leader sequence to drive translation. Moreover, experiments designed to examine AtxA production from the native promoter in CA-Air, and CACO<sub>3</sub> in 5% and 20% CO<sub>2</sub> indicate that AtxA is present at the same level in all growth conditions (59).

#### **4.2.4 Relative activities of the *B. anthracis* PCVRs on *in vivo* reporters**

The *Plef-lacZ* reporter (UT376) has been used to measure *in vivo* activity of AtxA (64). With the creation of the *PcapB-lacZ* reporter (UT423) I was able to measure the *in vivo* activities of AtxA, AcpA and AcpB. My RNA-Seq data indicate AtxA alone positively regulates lethal factor expression. AcpA and AcpB were the major regulators of capsule expression, with AtxA having a smaller effect. In the RNA-Seq experiment, the genes encoding AtxA, AcpA, and AcpB were induced with IPTG to produce near-native protein levels. Given the relatedness of the PCVRs I tested whether PCVR overexpression would reveal functional similarity among the regulators with regard to activity on *Plef* and *PcapB*. I grew cultures of UT376 and UT423 harboring IPTG-inducible expression plasmids for AcpA-FLAG, AcpB-FLAG, and AtxA-FLAG in CACO<sub>3</sub> and overexpressed each regulator with a concentration of IPTG that induced higher than native protein expression levels. I harvested cells and measured  $\beta$ -galactosidase activity in each strain. **Figure 4-6** shows the  $\beta$ -galactosidase activity mediated by each regulator from the two reporters. Importantly, there is no  $\beta$ -galactosidase activity in strains harboring only the empty vector indicating no other factors have activity on either reporter. As expected, AtxA-FLAG alone controlled expression of *Plef*; neither AcpA-FLAG nor AcpB-FLAG had activity on this promoter (**Figure 4-6A**). These results

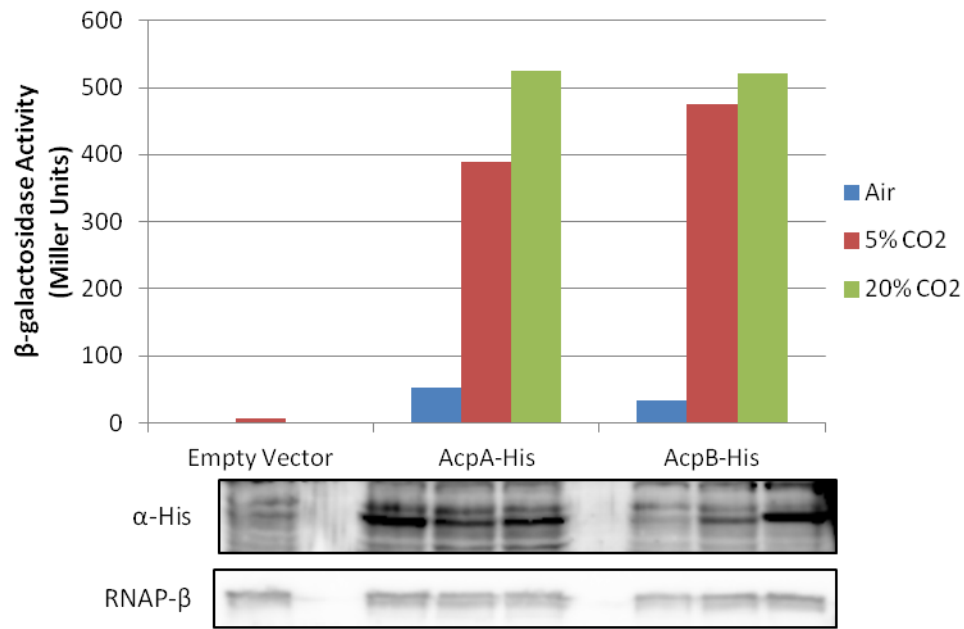


**Figure 4-3.** AcpA and AcpB CO<sub>2</sub>-dependent activity

Cultures of UT423, containing expression plasmids for AcpA-His (pUTE1103) and AcpB-FLAG (pUTE1092) were cultivated in CA-Air, CACO<sub>3</sub> in 5% CO<sub>2</sub> atmosphere, and CACO<sub>3</sub> in 20% CO<sub>2</sub> atmosphere. Protein expression was induced by varying concentrations of IPTG (pUTE1103-Air [200  $\mu$ M], -CO<sub>2</sub> [50  $\mu$ M]; pUTE1092-Air [300  $\mu$ M], -CO<sub>2</sub> [150  $\mu$ M]) at early exponential growth phase and cells were harvested two hours after induction at the transition to stationary phase. Empty vector represents the expression plasmid.  $\beta$ -galactosidase activities resulted from expression of the *PcapB-lacZ* reporter. Cell lysate load volumes were normalized for OD<sub>600</sub> reading at collection, and proteins were detected via immunoblot with  $\alpha$ -His antibody or an antibody for the  $\beta$  subunit of RNA polymerase; a load control.

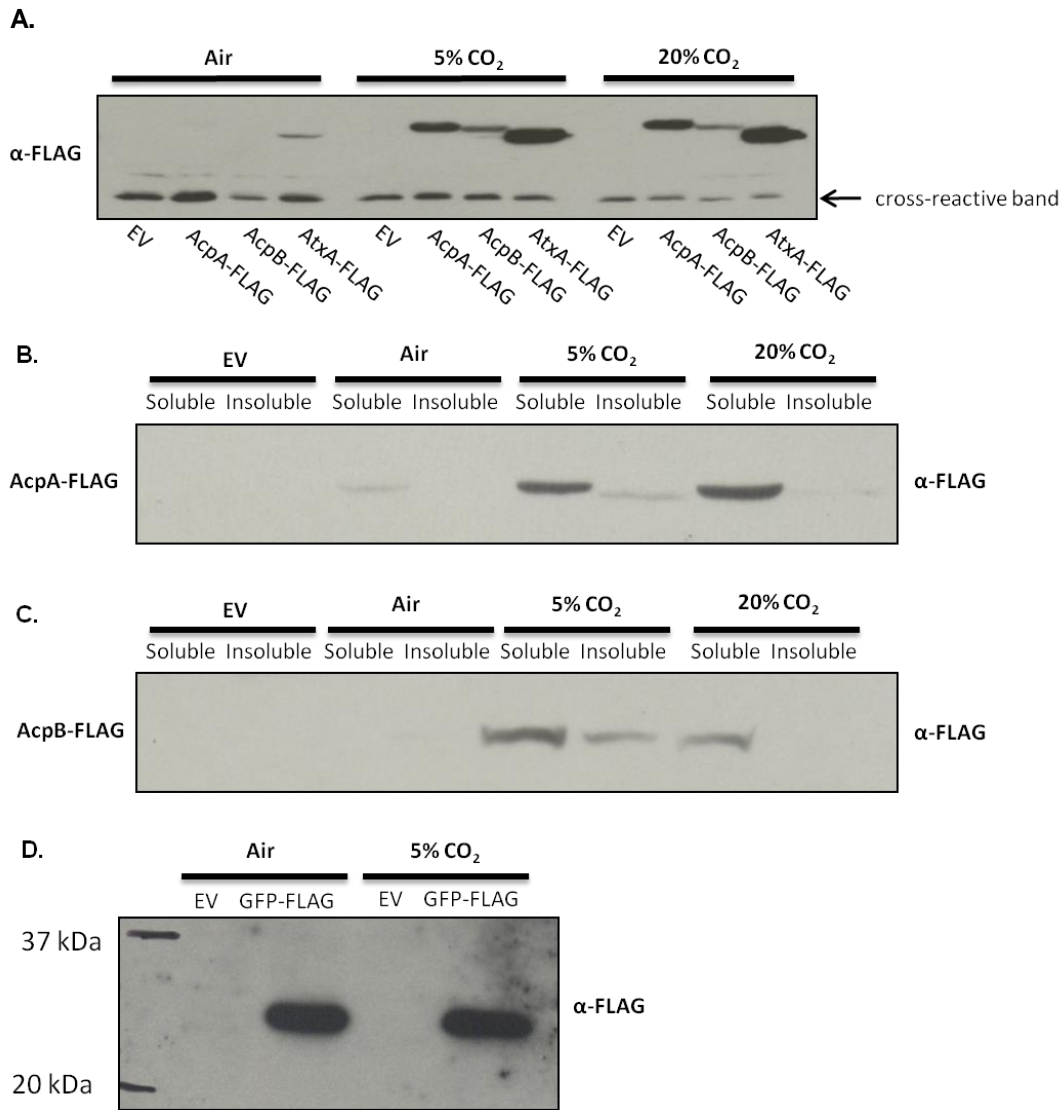


**Figure 4-4.** Effects on steady state protein levels by culture in CA-Air vs. CACO<sub>3</sub> (A) Cultures of UT423 containing expression plasmids for AcpA-FLAG (pUTE1090), AcpB-FLAG (pUTE1091), or AtxA-FLAG (pUTE992) were cultivated in CA-Air, CACO<sub>3</sub> in 5% CO<sub>2</sub>, or CACO<sub>3</sub> in 20% CO<sub>2</sub>. Expression of FLAG-tagged proteins was induced with 40  $\mu$ M IPTG at early exponential growth phase and cells were harvested at the transition to stationary phase. Cell lysate load volumes were normalized to OD<sub>600</sub> reading at collection and proteins were detected by immunoblotting with  $\alpha$ -FLAG antibody. UT423 cultures expressing AcpA-FLAG (pUTE1090) (B) or AcpB-FLAG (pUTE1091) (C) were induced with IPTG and harvested as indicated above; EV = Empty Vector (pUTE657). Cell lysates were centrifuged to pellet the insoluble fraction. The soluble fraction was removed and the insoluble fraction was then washed and resuspended in 8M urea for one hour to increase solubility. Proteins were then separated by SDS-PAGE and visualized by immunoblotting with  $\alpha$ -FLAG antibody. (D) UT423 cultures harboring an IPTG-inducible GFP-FLAG expression plasmid (pUTE1013) were cultivated in either CA-Air or CACO<sub>3</sub> in 5% CO<sub>2</sub>. Protein expression was induced with 30  $\mu$ M IPTG at early exponential growth phase and cells were harvested at the transition to stationary phase. Cell lysates were used for immunoblotting with  $\alpha$ -FLAG antibody as stated above.

are consistent with my RNA-Seq data. Both AcpA-FLAG and AcpB-FLAG had activity on the *PcapB-lacZ* reporter (**Figure 4-6B**). These data are also consistent with my dose-dependent activity experiments using the *PcapB-lacZ* reporter, as well as my RNA-Seq results. However, AtxA-FLAG did not have activity on *PcapB-lacZ*. My RNA-Seq data indicate AtxA increased expression of *capB* by a log<sub>2</sub>-fold change of 3.86 (~14 fold). To ensure that the DNA sequence necessary for AtxA-mediated control of *capB* expression was present in the reporter construct I compared the DNA sequence at which *capBCADE* transcripts initiated using transcript read maps generated by my RNA-Seq experiment. Transcripts of *capBCADE* generated by complementation with *acpA*, *acpB*, and *atxA* start ~500 bp upstream of the *capB* translational start codon. Our lab and others published previously that PCVR control of *capBCADE* occurs primarily from two transcriptional start sites, 530 bps and 424 bps upstream of the *capB* translational start site, and a third less active start site 595 bps upstream of *capB* (70, 71). The *PcapB-lacZ* reporter included 1 kb upstream of the *capB* translational start codon indicating the DNA sequence required for AtxA control of *capB* is present in the reporter. It is possible that an unknown pXO2-encoded factor is required for AtxA activity on *PcapB*.

Taken together, these results indicate that PCVR control of *Plef* is in agreement with RNA-Seq results such that AtxA positively regulates *Plef*, and that overexpression of *acpA* or *acpB* does not result in activity of this promoter. Moreover, my results suggest that additional factors may be required for AtxA activity on *PcapB*.

#### **4.2.5 *B. anthracis* PCVR homomultimerization and the role of the intrinsic functional domains**

The importance of AtxA multimerization with regard to activity has been explained in detail in Chapter 1 (1.5) and above (4.1). The significance of AcpA or AcpB multimerization has



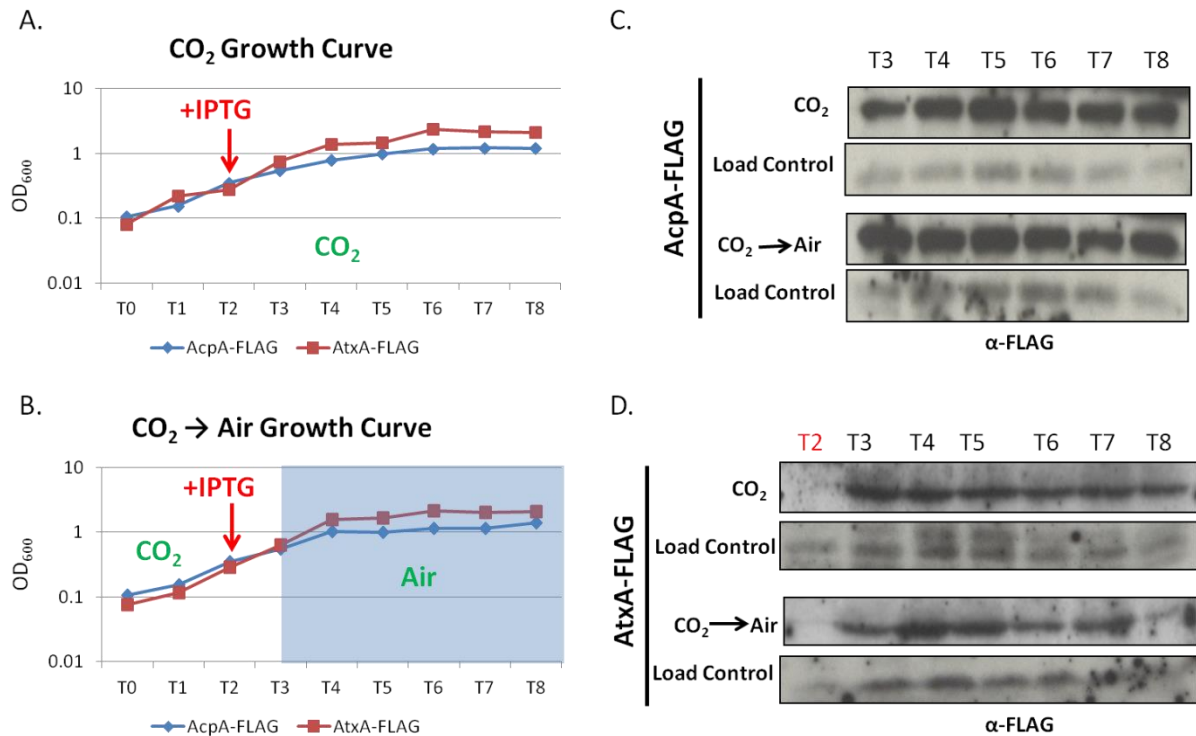


**Figure 4-5. Stability of AcpA-FLAG and AtxA-FLAG in CACO<sub>3</sub> and CA-Air**  
*B. anthracis* cultures containing IPTG-inducible expression plasmids for AcpA-FLAG and AtxA-FLAG were cultivated in CACO<sub>3</sub> medium. Protein expression was induced with 30 μM IPTG at early exponential growth phase. One hour after induction, cells were pelleted, washed, and resuspended in an equivalent volume of either spent CACO<sub>3</sub> or spent CA-Air medium, both containing a sub-inhibitory concentration of chloramphenicol (15 μg/ml) and no IPTG. Cultures were incubated in spent medium for five hours and samples were taken for western blot analysis at hourly time points. (A & B) OD<sub>600</sub> readings throughout the growth curve. Western blots of samples taken hourly of AcpA-FLAG (pUTE1090) (C) or AcpB-FLAG (pUTE1091) (D) blotted with α-FLAG antibody.

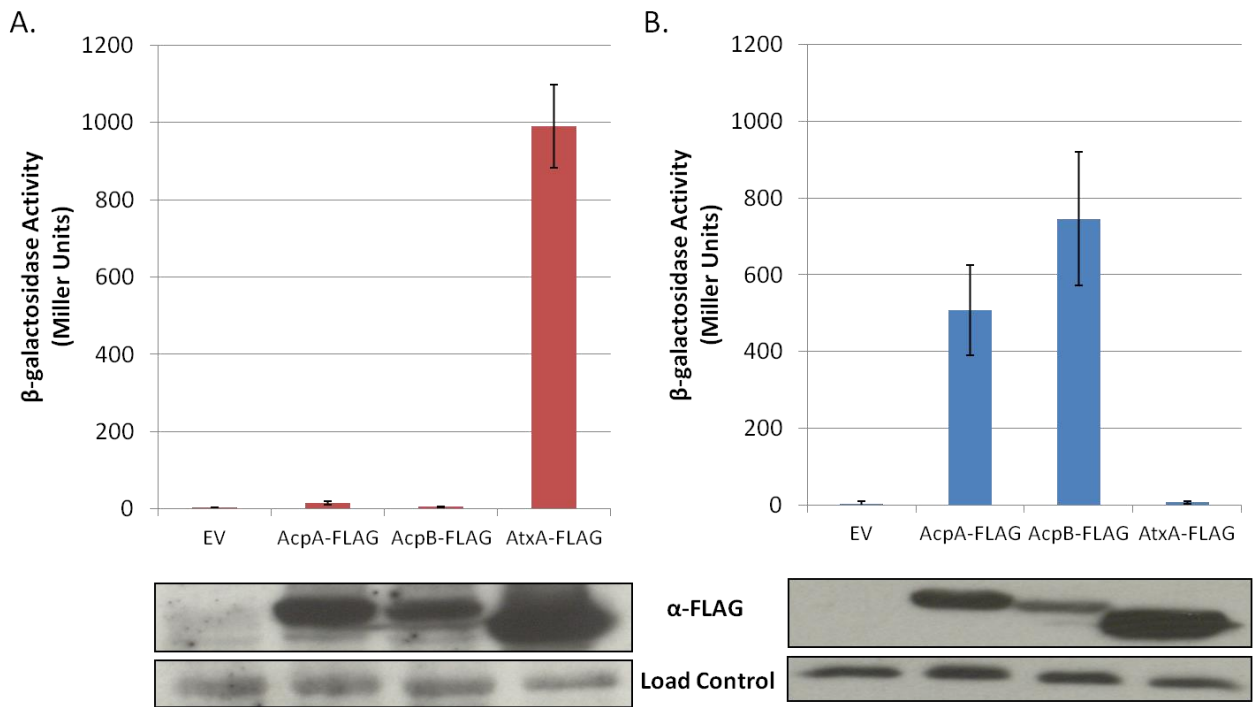


**Figure 4-6.** Activities of *B. anthracis* PCVRs on *PcapB-lacZ* and *Plef-lacZ*

Cultures of UT376 (*Plef-lacZ*) (A) and UT423 (*PcapB-lacZ*) (B), harboring genes encoding AcpA-FLAG (pUTE1090), AcpB-FLAG (pUTE1091), and AtxA-FLAG (pUTE992) driven by an IPTG-inducible promoter were cultured in CACO<sub>3</sub>. EV = empty vector (pUTE657). Cells were collected 2 h after induction with IPTG.

not been tested. AcpA and AcpB have been shown to: 1) have amino acid sequence similarity to AtxA, 2) co-regulate a subset of genes in the AtxA regulon, and 3) have increased activity when cultures of *B. anthracis* are cultivated in 5% CO<sub>2</sub> in medium containing bicarbonate. To explore protein-protein interactions involving AcpA or AcpB I first tested whether these proteins self-associate.

To determine if AcpA and AcpB multimerize, I employed co-affinity purification and chemical crosslinking methods. First, I tested whether FLAG-tagged AcpA and AcpB were able to co-purify with 6xHis-tagged counterparts via nickel affinity purification. I grew individual cultures in CACO<sub>3</sub> expressing recombinant AcpA or AcpB with either a carboxy terminal 6xHis or a FLAG epitope. Strains expressing FLAG-tagged GFP served as controls. Recombinant proteins were expressed from a plasmid-borne IPTG-inducible promoter in an *atxA*-null *B. anthracis* strain lacking pXO<sub>2</sub>, the native plasmid carrying the *acpA* and *acpB* genes. Cultures were pooled in the following pairs: (1) AcpA-His and AcpA-FLAG, (2) AcpA-His and GFP-FLAG, and (3) AcpA-FLAG and GFP-FLAG, (4) AcpB-His and AcpB-FLAG, (5) AcpB-His and GFP-FLAG, and (6) AcpB-FLAG and GFP-FLAG. Lysates generated from pooled cultures were subjected to affinity purification using NTA-Ni resin and proteins were detected using western blotting. In **Figure 4-7A, B** lanes 1-3 show that prior to affinity purification all tagged proteins were present in the appropriate pool. Lanes 4-6 show eluates from the NTA-Ni resin. AcpA-FLAG coeluted with AcpA-His and AcpB-FLAG coeluted with AcpB-His (**Figure 4-7A, B**). GFP-FLAG functioned as a negative control for non-specific interactions. These results demonstrate that AcpA and AcpB form homomultimers *in vitro*.

I also used chemical crosslinking to test for multimerization of the tagged proteins. Bis-maleimido-hexane (BMH) crosslinks free cysteine residues irreversibly within 13 Å and was employed previously to demonstrate AtxA multimerization (64). AcpA has cysteine residues at positions 33, 321, 342. Cysteine residues of AcpB are at positions 33, 34, 332, and 465. Cell lysates containing either AcpA-FLAG or AcpB-FLAG were treated with BMH, and proteins were separated by SDS-PAGE and visualized using western blotting with α-FLAG antibody (**Figure**

**4-7C**). For each protein, a single band was detected slightly above the 50-kDa marker in BMH-treated and untreated lysates. A band near the 100-kDa marker was detected only in lysates treated with BMH. The predicted molecular weight for each PCVR is 57 kDa; therefore the approximate 100-kDa bands suggested dimers of AcpA or AcpB crosslinked by BMH. To confirm that the observed complexes were indeed homomeric, I affinity-purified AcpA-His and AcpB-His using NTA-Ni resin and crosslinked using BMH. The migration pattern of crosslinked purified AcpA-His was similar to that of AcpA-FLAG present in crosslinked cell lysates with bands near 50 kDa (monomer) and 100 kDa (dimer) (**Figure 4-7D**). The comparable experiment using AcpB was not possible because affinity-purified AcpB-His became insoluble following treatment with BMH. These data provide further evidence that like AtxA, AcpA and AcpB form homomultimers and crosslink as dimers.

To determine if the EIIB-like domains of AcpA and AcpB are required for dimerization and activity, as is true for AtxA (64), I created carboxy-terminal truncation mutants lacking the EIIB-like domain. The EIIB-like domain of AtxA is defined by amino acids 385-475. Structural modeling using the amino acid sequence of AcpA and AcpB predict the EIIB-like domain to be amino acids 390 - 483 for AcpA and 391 - 482 for AcpB. I deleted the respective domain in AcpA and AcpB and engineered the recombinant truncated proteins to have a carboxy-terminal 6xHis tag. Cell lysates containing either full-length or truncated His-tagged AcpA or AcpB were subjected to BMH crosslinking. The full-length proteins displayed the typical dimer bands (~100 kDa). The migration of AcpA- $\Delta$ EIIB-His and AcpB- $\Delta$ EIIB-His was unaffected after crosslinking; only a ~40 kDa band was present (**Figure 4-8A**), indicating lack of dimer formation in the absence of the C-terminal domains.

To test the activity of the AcpA and AcpB truncation mutants I used the *PcapB-lacZ* reporter strain UT423. Plasmids encoding full-length and truncation mutants of AcpA-His and AcpB-His, were expressed individually in the reporter strain via an IPTG-inducible promoter. Activity of the full-length and truncation mutants was quantified by measuring  $\beta$ -galactosidase activity in cell lysates following IPTG induction of each gene. **Figure 4-8B** shows relative

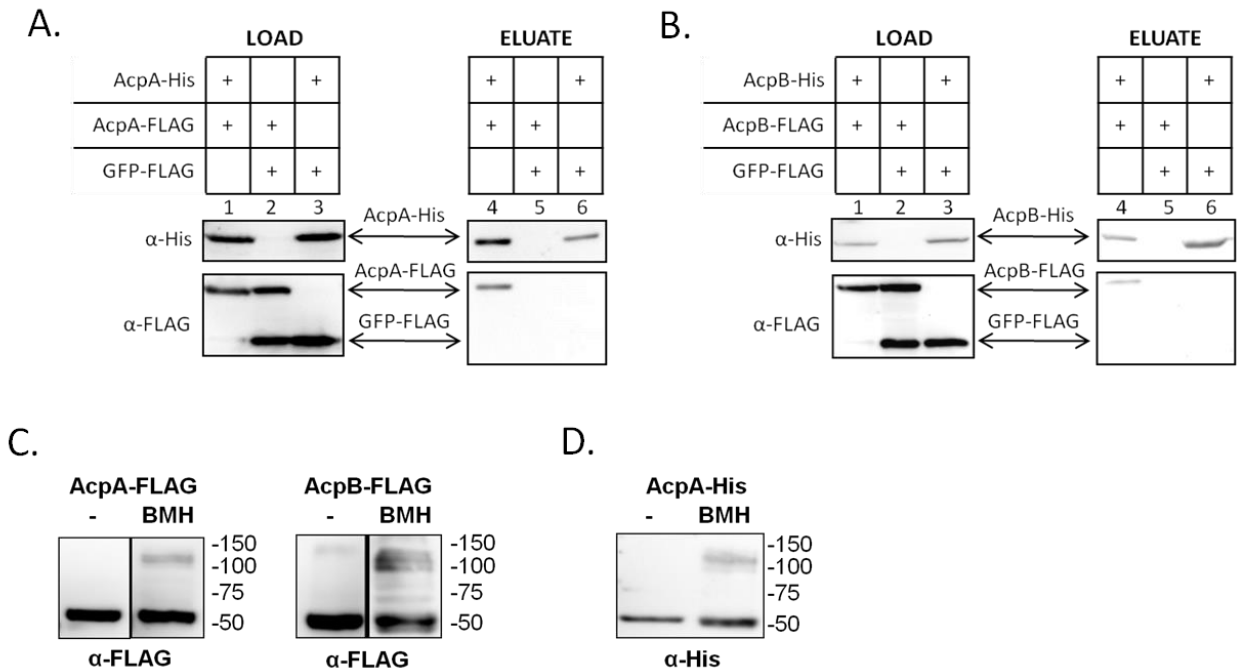


**Figure 4-7. Homomultimerization AcpA and AcpB**

Lysates from *B. anthracis* *atxA*-null pXO1+ pXO2- strains (UT423) containing plasmids that encode IPTG-inducible (A) AcpA-His (pUTE1090), AcpA-FLAG (pUTE1079), or GFP-FLAG (pUTE1013); (B) AcpB-His (pUTE1091), AcpB-FLAG (pUTE1093), or GFP-FLAG (pUTE1013) were co-incubated as indicated, then co-affinity purified with Ni<sup>2+</sup>-NTA resin. Proteins present in the mixed lysates prior to (Load, lanes 1-3) and after purification (Eluate, lanes 4-6) were subjected to SDS-PAGE and Western blot with  $\alpha$ -His and  $\alpha$ -FLAG antibodies as indicated. Arrows indicate the predicted sizes of AcpA-His, AcpA-FLAG, AcpB-His, AcpB-FLAG, and GFP-FLAG; (C) FLAG-tagged AcpA (pUTE1079) and AcpB (pUTE1093) were induced by IPTG in a *B. anthracis* *atxA*-null pXO1+ pXO2- strain. Lysates were incubated with or without the crosslinking agent BMH and subjected to SDS-PAGE and Western blot. Proteins were detected with  $\alpha$ -FLAG antibody. (D) Affinity purified AcpA-His from *B. anthracis* ANR-1 (pUTE1090) incubated with or without BMH and subjected to SDS-PAGE and Western blot. Proteins were detected with  $\alpha$ -His antibody.

activities of both full-length and truncated AcpA-His and AcpB-His.  $\beta$ -galactosidase activity was observed for full-length AcpA-His and AcpB-His, but neither EIIB truncation mutant showed activity. This indicates that, like AtxA, AcpA and AcpB require the EIIB-like domain for multimerization and activity.

After confirming that the EIIB-like domain has similar function among the three regulators, I designed experiments to determine how the other PCVR functional domains contribute to regulator activity. The DNA-binding domains of the three *B. anthracis* PCVRs have the highest sequence similarity with AcpA and AcpB sharing 48% amino acid identity, 33% identity between AtxA and AcpA, and 29% identity between AtxA and AcpB. It is unclear whether the DNA-binding domain alone confers target specificity for PCVR-regulated genes, or whether input from other domains is required. Analysis of the AtxA crystal structure suggest that phosphorylation at H199 within PRD1 may influence positioning of the DNA-binding domain, thereby affecting target specificity (65).

To test whether the DNA-binding domains alone are sufficient for target specificity I created chimeric proteins in which I exchanged DNA-binding domains (DBD) among the PCVRs. In total I created four chimeras, AtxA<sup>DBD</sup>AcpA<sup>PRD+EIIB</sup>, AtxA<sup>DBD</sup>AcpB<sup>PRD+EIIB</sup>, AcpA<sup>DBD</sup>AtxA<sup>PRD+EIIB</sup>, AcpB<sup>DBD</sup>AtxA<sup>PRD+EIIB</sup>. To make the AtxA<sup>DBD</sup>AcpA<sup>PRD+EIIB</sup> and AtxA<sup>DBD</sup>AcpB<sup>PRD+EIIB</sup> chimeras I used the AtxA crystal structure to identify an unstructured linker region between the DBD and PRDs (**Figure 4-9**), consisting of amino acids 164 to 176 (13 amino acids). Genes encoding chimeric proteins were engineered to express a carboxy-terminal 6xHis epitope to facilitate detection, and were under transcriptional control of an IPTG-inducible promoter. Strains of the *PcapB-lacZ* reporter and the *Plef-lacZ* reporter harboring individual chimera expression plasmids, were cultured in CACO<sub>3</sub> and cells were harvested at the transition to stationary phase to assess  $\beta$ -galactosidase activity (**Figure 4-10**). Both the AtxA<sup>DBD</sup>AcpA<sup>PRD+EIIB</sup> and AtxA<sup>DBD</sup>AcpB<sup>PRD+EIIB</sup> chimeras were detected in soluble cell lysates following induction with IPTG (**Figure 4-10A-D**). However, neither chimera had activity on *Plef-*

*lacZ* nor *PcapB-lacZ*. Neither the AcpA<sup>DBD</sup>AtxA<sup>PRD+EIIB</sup> nor AcpB<sup>DBD</sup>AtxA<sup>PRD+EIIB</sup> chimeras were stably produced (**Figure 4-10E, F**).

A possible reason for the lack of activity by the two chimeras is that they were folded improperly. One way to measure PCVR activity, and by extension activity of the chimeras, is to test their ability to multimerize. Multimerization is required for activity of all three *B. anthracis* PCVRs, and at least for AtxA, contact between two monomers occurs between the EIIB-like domain of one monomer and PRD2 of the other monomer (65). As an indirect method of measuring proper protein folding by each chimera, I tested whether full-length AcpA-FLAG could interact with AtxA<sup>DBD</sup>AcpA<sup>PRD+EIIB</sup>-His using co-affinity purification. I tested AtxA<sup>DBD</sup>AcpA<sup>PRD+EIIB</sup>-His for interaction with AcpA-FLAG because it was the most stable of the two chimeras. I combined culture lysates of *B. anthracis* strains containing full-length AcpA-FLAG and AtxA<sup>DBD</sup>AcpA<sup>PRD+EIIB</sup>-His. AcpA-His and GFP-FLAG were used as controls. Lysates were pooled in the pairs as shown in **Figure 4-11**. Pooled lysates were incubated with a NTA-Ni resin, washed, eluted with imidazole, and detected by western blot. Lanes 1-5 show that all proteins are present in lysates prior to incubation with the NTA-Ni resin. Eluates from the NTA-Ni resin are shown in lanes 6-10. Lane 6 shows that AcpA-FLAG did not co-elute with AtxA<sup>DBD</sup>AcpA<sup>PRD+EIIB</sup>-His, however AcpA-FLAG co-eluted with the positive control AcpA-His (lane 7). The model for AtxA multimerization is that the EIIB-like domain of one monomer interacts with PRD2 of the other monomer. If this holds true for AcpA, then the domains required for AcpA-AcpA interaction remain intact in the AtxA<sup>DBD</sup>AcpA<sup>PRD+EIIB</sup>-His chimera and theoretically should not disrupt multimerization. These data suggest that although the AtxA<sup>DBD</sup>AcpA<sup>PRD+EIIB</sup>-His chimera is stably produced, it is not properly folded.

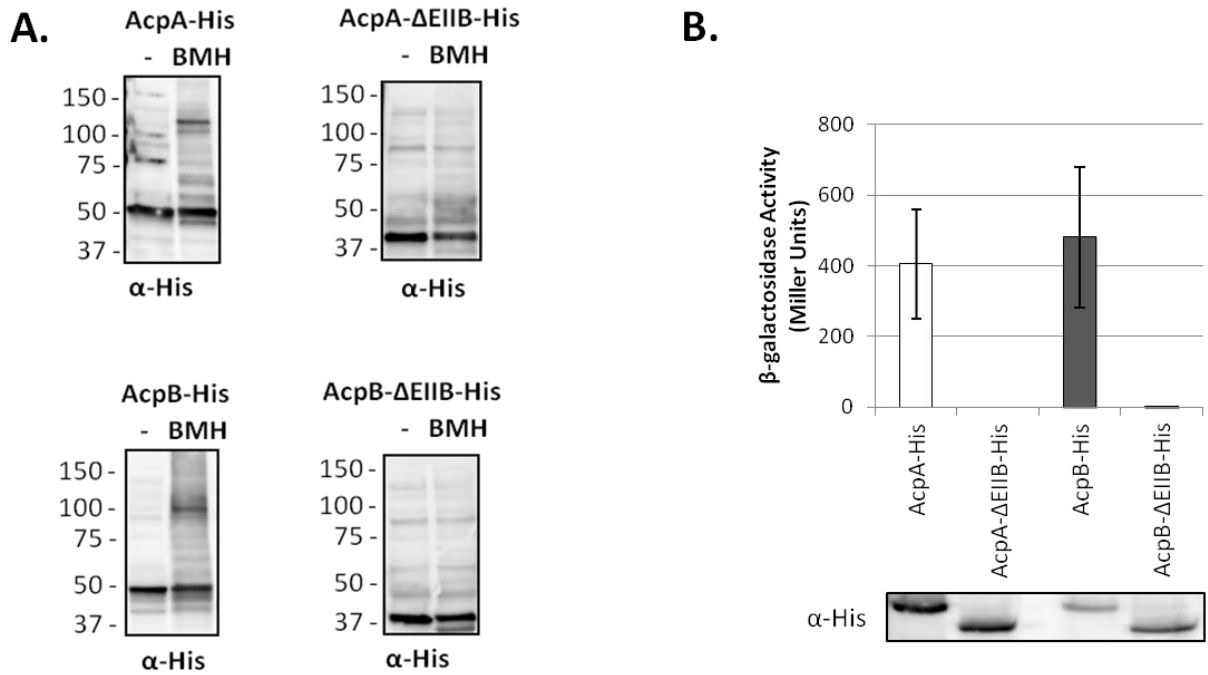


**Figure 4-8.** Multimerization and activity of AcpA and AcpB EIIB-like domain truncation mutants UT423 strains expressing AcpA-ΔEIIB-His (pUTE1125), AcpA-FLAG (pUTE1079), AcpB-ΔEIIB-His (pUTE1126), or AcpB-FLAG (pUTE1093) were cultured in CACO<sub>3</sub> in 5% CO<sub>2</sub> atmosphere and induced with 30-50 μM IPTG. (A) Cell lysates containing IPTG-induced proteins were treated with crosslinking agent BMH or vehicle alone (DMSO). Molecular weights of protein standards are listed. (B) The β-galactosidase activity of *B. anthracis* strains harboring the *PcapB-lacZ* reporter and IPTG-induced AcpA and AcpB variants was determined as previously described (95). Errors represent ±1 SD.



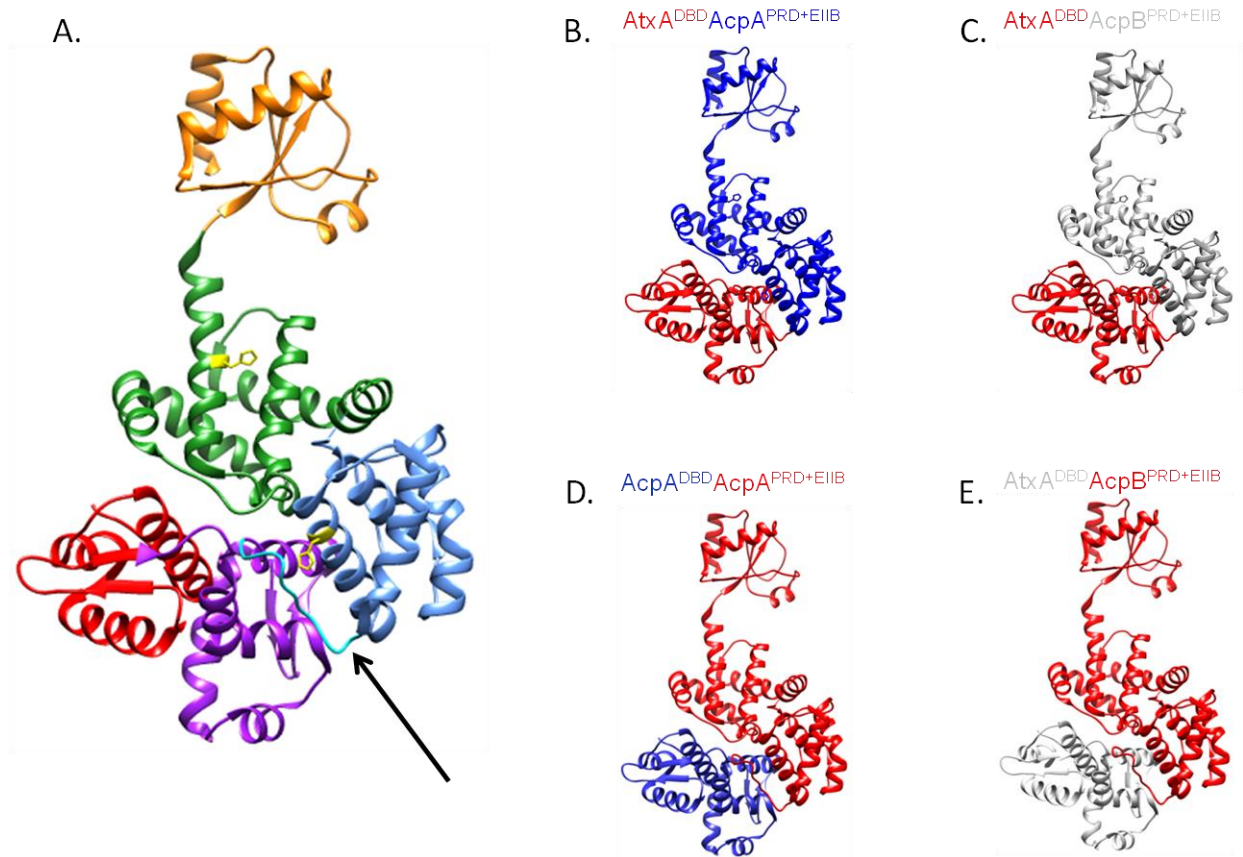


**Figure 4-9.** AtxA crystal structure and structural models of *B. anthracis* chimeric PCVRs (A) Crystal structure of AtxA with the five domains indicated by color: winged helix-turn-helix (WH) motif, a helix-turn-helix (HTH) motif, two PTS regulation domains (PRD1 & PRD2), and an Enzyme IIB-like (EIIB-like) motif. Black arrow points to the unstructured region of AtxA (cyan) that was used to link the AtxA DBD to PRD1 of either AcpA or AcpB, and to link AtxA PRD1 to the DBD of AcpA or AcpB. (B) pUTE1123, (C) pUTE1114, (D-E) Structural models of chimeric PCVRs, domain color indicates the donor protein.

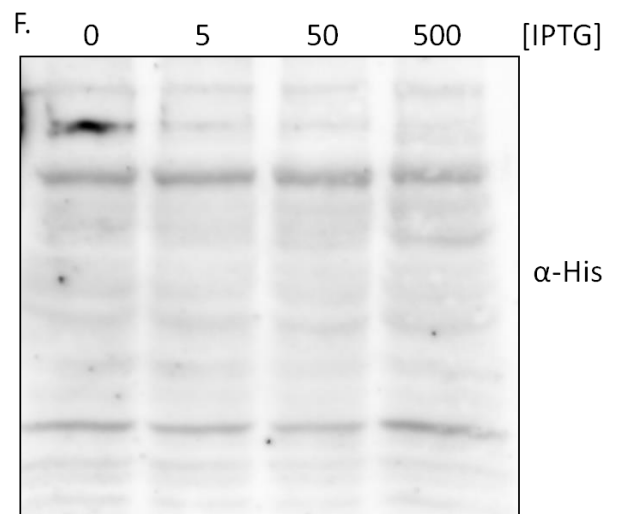
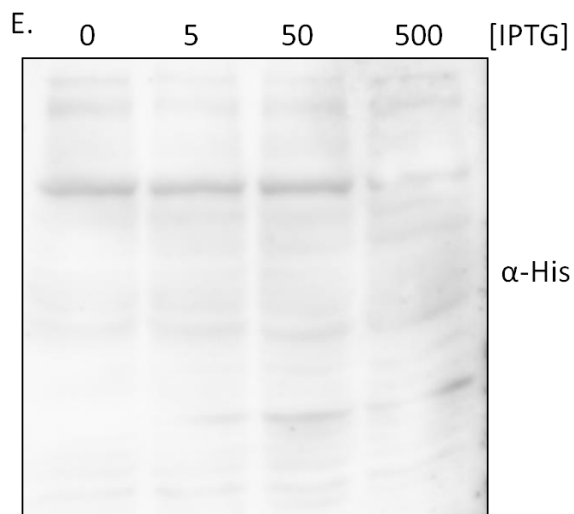
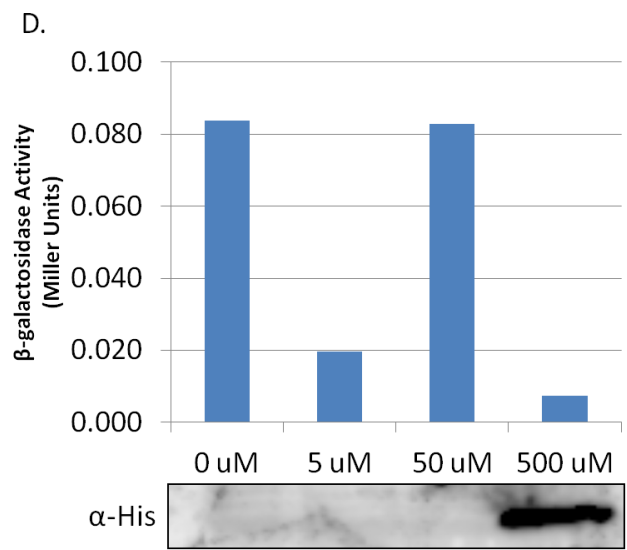
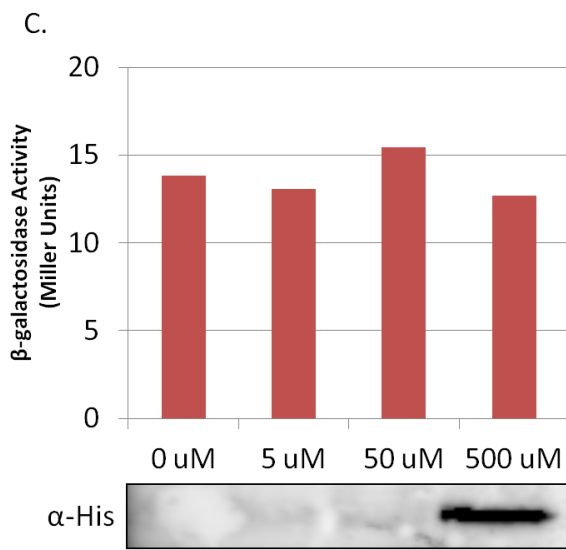
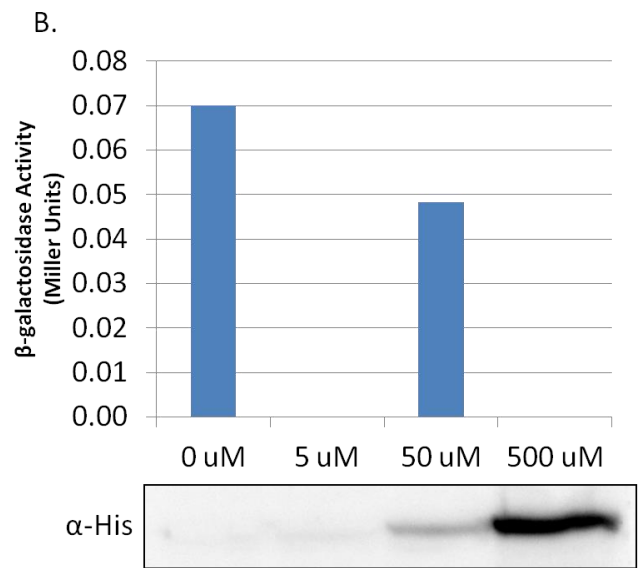
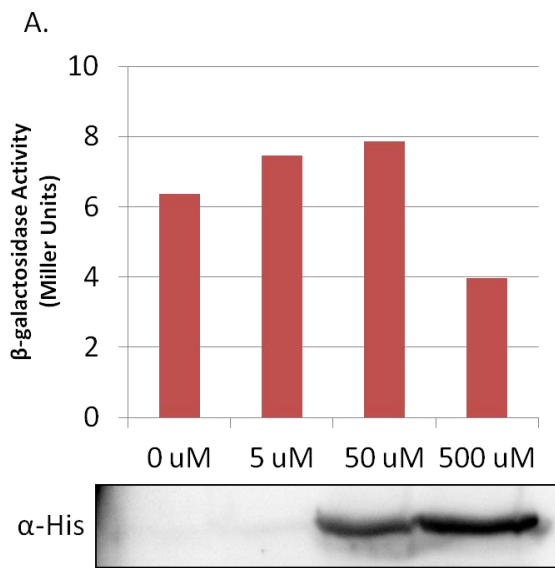


**Figure 4-10.** Dose-dependent expression and activity of PCVR chimeras

Cultures of *B. anthracis* reporter strains UT376 (*P<sub>lef-lacZ</sub>*) (A, C) and UT423 (*P<sub>capB-lacZ</sub>*) (B, D, E, F) containing expression plasmids for AtxA<sup>DBD</sup>AcpA<sup>PRD+EIIB</sup> (pUTE1123) (A, B), AtxA<sup>DBD</sup>AcpB<sup>PRD+EIIB</sup> (pUTE1114) (C, D), AcpA<sup>DBD</sup>AtxA<sup>PRD+EIIB</sup> (E), AcpB<sup>DBD</sup>AtxA<sup>PRD+EIIB</sup> were induced with IPTG. Cells were collected in the transition to stationary phase for chimera activity assays and western blotting with  $\alpha$ -His antibody. Chimera activity was measured as  $\beta$ -galactosidase activity from either *P<sub>lef-lacZ</sub>* or *P<sub>capB-lacZ</sub>*. Cell lysate load volumes for western blots were normalized to OD<sub>600</sub> reading at time of collection.

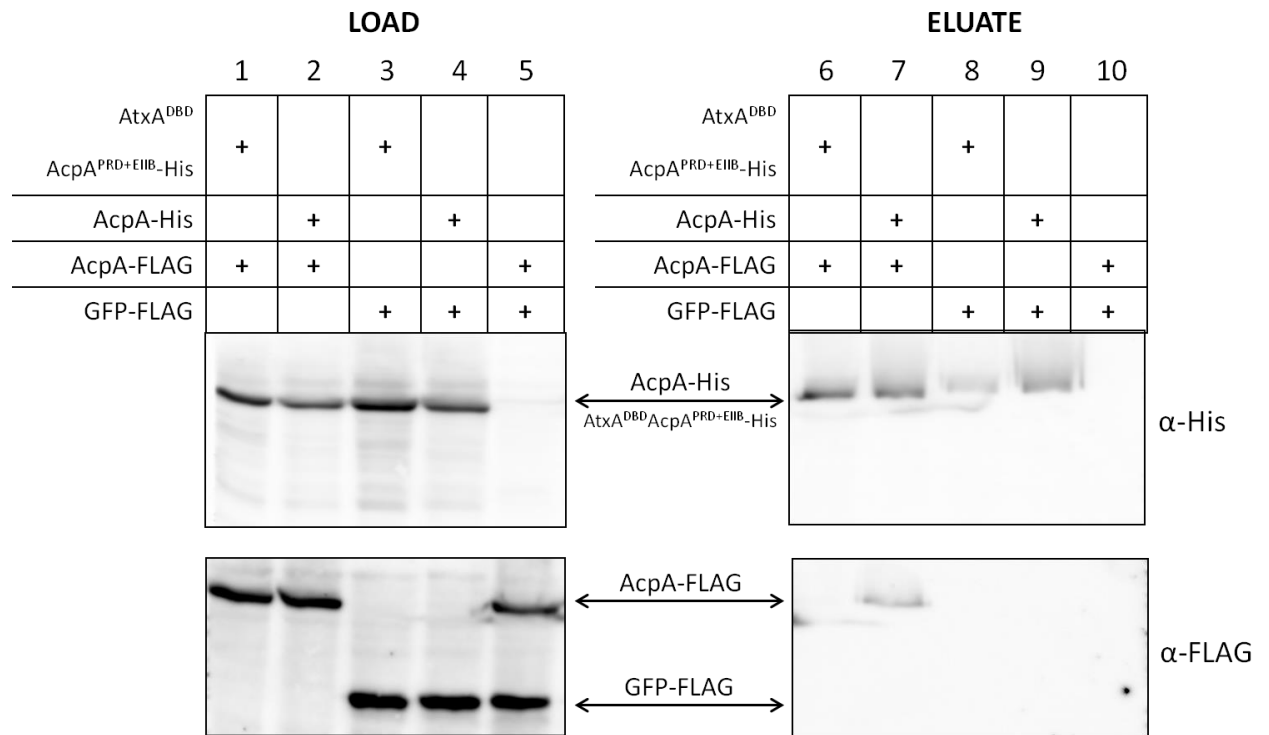


**Figure 4-11.** PCVR chimera multimerization

Lysates from *B. anthracis* strains producing AtxA<sup>DBD</sup>AcpA<sup>PRD+EIIB-His</sup> (pUTE1123), AcpA-His (pUTE1090), AcpA-FLAG (pUTE1073), and GFP-FLAG (pUTE1013) induced with 50-100  $\mu$ M IPTG were used in co-affinity purification with a NTA-Ni resin. Westerns blots of soluble cell lysates (lanes 1-5) and eluted proteins (lanes 6-10) were probed with  $\alpha$ -His and  $\alpha$ -FLAG antibodies.

#### 4.2.6 Heteromultimerization of PCVRs

Given the amino acid sequence similarity between AtxA, AcpA, and AcpB and the formation of homomultimers, I questioned whether the PCVRs could interact with each other to form heteromultimers. As done for the homomultimerization assays, I tested mixed culture lysates containing recombinant proteins with C-terminal 6xHis or FLAG epitopes for co-affinity purification with NTA-Ni resin. The lysates contained pairs of differentially tagged PCVRs. Results are shown in **Figure 4-12**. AcpA-FLAG co-eluted from the NTA-Ni resin with AtxA-His (lane 5), indicating that these two proteins can interact. The amount of co-eluted AcpA-FLAG was small compared to the amount of eluted AtxA-His. Increasing the ratio of AcpA-FLAG to AtxA-His by using a higher IPTG concentration to induce the AcpA-FLAG (lane 2) level yielded an increased amount of co-eluted AcpA-FLAG (lane 6). AcpA-FLAG was not detected in eluates lacking AtxA-His (lane 7) indicating non-specific resin binding did not account for the presence of AcpA-FLAG in eluates. In similar experiments, I tested for AtxA-AcpB and AcpA-AcpB interactions, but no heteromeric protein interactions were detected.

The complex interdependent control of *atxA*, *acpA*, and *acpB* gene expression and the formation of PCVR homo- and hetero-multimers suggest that the stoichiometry of the regulators is important for optimal transcription of target genes. I tested for the effect of AtxA over-expression on transcription from the *capB* promoter, which in my RNA-Seq experiments was highly regulated by AcpA and AcpB, but showed a much lower induction by AtxA (**Table 3-1**). We cultured strains that co-expressed AtxA and AcpA (**Figure 4-13A**), or AtxA and AcpB (**Figure 4-13B**) in strain UT423 which carries the transcription reporter *PcapB::lacZ*. AtxA expression was controlled by an IPTG-inducible promoter, while AcpA and AcpB expression was under the control of a xylose-inducible promoter. AcpA and AcpB levels were monitored using western blotting, and *capB* promoter activity was quantified as  $\beta$ -galactosidase activity. Increasing levels of AtxA relative to AcpA correlated with a decrease in  $\beta$ -galactosidase activity

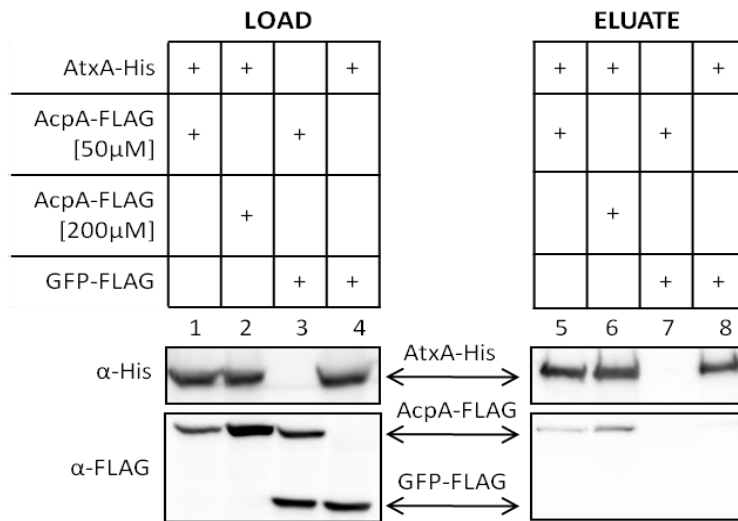


**Figure 4-12. Heteromultimerization by PCVRs**

Lysates from *B. anthracis atxA*-null pXO1+ pXO2- strains (UT423) containing plasmids that encode IPTG-inducible AtxA-His (pUTE991), AcpA-FLAG (pUTE1079), or GFP-FLAG (pUTE1013); were co-incubated as indicated, then co-affinity purified with Ni-NTA resin. Proteins present in the mixed lysates prior to (Load, lanes 1-3) and after purification (Eluate, lanes 4-6) were subjected to SDS-PAGE and Western blot with  $\alpha$ -His and  $\alpha$ -FLAG antibodies as indicated. Arrows indicate the predicted sizes of AtxA, AcpA, and GFP.

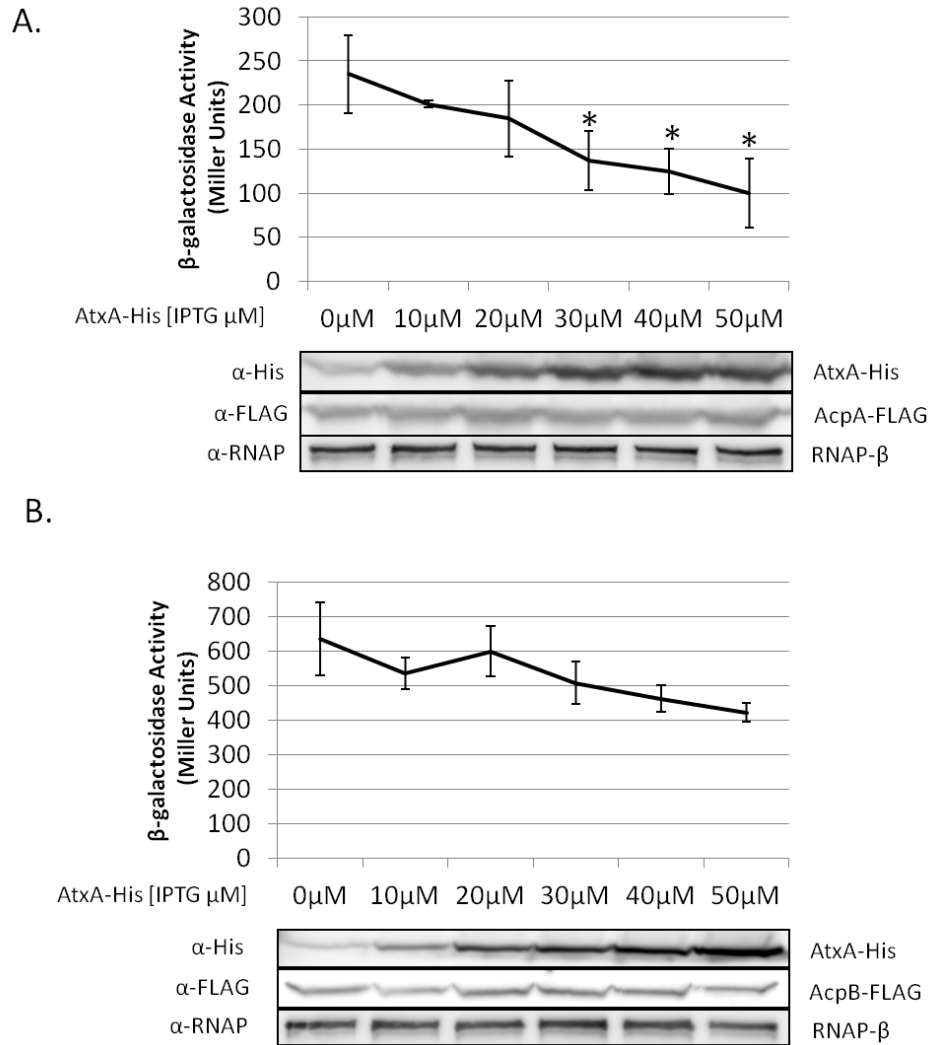


**Figure 4-13.** AtxA effect on AcpA and AcpB activity

UT423 strains co-expressing AtxA-His (pUTE991) from an IPTG inducible promoter and AcpA-FLAG (pUTE1099) or AcpB-FLAG (pUTE1100) from a xylose inducible promoter were cultured in  $\text{CACO}_3$  in 5%  $\text{CO}_2$  atmosphere. Across six cultures IPTG was added in the indicated concentrations to incrementally increased AtxA-His expression, while AcpA-FLAG or AcpB-FLAG expression levels were kept constant with 1% xylose in all cultures. Asterisks represent a significant decrease in activity at the indicated [IPTG] compared to 10  $\mu\text{M}$  IPTG (P value <0.05).  $\beta$ -galactosidase activity of these strains harboring the *PcapB-lacZ* reporter was determined as described previously (95). Error bars represent  $\pm 1$  SD.

(**Figure 4-13A**). At IPTG concentrations of 30  $\mu\text{M}$ , 40  $\mu\text{M}$ , and 50  $\mu\text{M}$ , AtxA significantly decreased AcpA activity on *PcapB::lacZ* compared to an uninduced culture (0  $\mu\text{M}$ ). Although the data trended toward a modest affect of AtxA overexpression on AcpB activity, no statistically significant difference was observed (**Figure 4-13B**). These data indicate that PCVR function is affected by regulator stoichiometry in cell cultures.

### 4.3 Discussion

My data reveal that *atxA*, *acpA*, and *acpB* are regulated at the translational level, and culture in 5% atmospheric  $\text{CO}_2$  positively affects AcpA and AcpB activity, as shown previously for AtxA. Neither the solubility nor stability of the PCVRs was affected by culture in ambient air relative to elevated  $\text{CO}_2$ . I have determined that AcpA and AcpB form homomultimers, and like AtxA, multimerization is required for activity of these two proteins. Importantly, I show that heteromultimers of AtxA and AcpA could be detected *in vitro*, and this interaction may result in modulation of AcpA activity.

Culturing in 5% or greater  $\text{CO}_2$  atmosphere in medium supplemented with 0.8% bicarbonate results in optimal toxin and capsule synthesis (57) presumably by increasing the activities of AtxA, AcpA, and AcpB. Culture in 20%  $\text{CO}_2$  did not significantly increase regulator activity above the level observed during culture in 5%  $\text{CO}_2$  suggesting that the effect  $\text{CO}_2$  has on activity is saturated at a concentration of 5%. The molecular mechanism by which  $\text{CO}_2$  affects the activity of these regulators is unknown. With regard to AtxA, *B. anthracis* cultures grown in elevated  $\text{CO}_2$ -bicarbonate contain more dimers of AtxA compared to cultures grown in air leading to an increase in AtxA activity (64). It is possible that AtxA binds bicarbonate or  $\text{CO}_2$ . There are precedents for  $\text{CO}_2$ /bicarbonate affecting protein activity. With regard to transcription factors, the *Citrobacter rodentium* protein RegA is a regulator that has increased binding affinity for target DNA in the presence of bicarbonate (133). Bicarbonate is thought to enhance the DNA binding affinity of RegA by inducing a conformational change, however a defined bicarbonate binding pocket has yet to be identified (134). RegA does not share significant



amino acid sequence homology to AtxA, AcpA, nor AcpB, and it is unknown whether similar conformational changes occur in these regulators when bicarbonate is present.

Another possible mechanism for CO<sub>2</sub>-controlled PCVR activity is that CO<sub>2</sub> competes with another ligand at a binding pocket within AtxA, AcpA, and AcpB. AtxA dimerization occurs constitutively in ambient air, but it is the ratio of dimers to monomers that increases with elevated CO<sub>2</sub>. It is possible that a small molecule binds to AtxA causing some level of constitutive dimerization that is increased competitively by CO<sub>2</sub> at high concentration. The enzyme RuBisCo which functions in carbon fixation in some species of bacteria competitively binds oxygen and CO<sub>2</sub> at its active site. Increasing the CO<sub>2</sub> concentration increases the carbon fixation ability of RuBisCo (135). AtxA structural predictions have not identified any regions similar to the RuBisCo CO<sub>2</sub> binding pocket, leaving the mechanism of CO<sub>2</sub>/bicarbonate influence on AtxA dimerization unknown.

Clues to how CO<sub>2</sub> influences dimerization may be found in the family of enzymes called  $\beta$ -carbonic anhydrases. These enzymes catalyze the reversible interconversion of CO<sub>2</sub> and HCO<sub>3</sub><sup>-</sup>. A member of the  $\beta$ -carbonic anhydrase family in *Pseudomonas aeruginosa*, psCA3, was crystallized in complex with CO<sub>2</sub> using pressurized cryo-cooled crystallography. The enzyme crystallized as a dimer with a CO<sub>2</sub> molecule in the active site of each monomer. A third CO<sub>2</sub> molecule was detected buried in the dimer interface. The location of the third CO<sub>2</sub> molecule was expected to be more stable due to multiple stabilizing interactions compared to the CO<sub>2</sub> molecule in the active site (136). The AtxA crystal structure was not solved using these crystallization conditions, but it is possible that CO<sub>2</sub> may bind within the AtxA dimer interface providing increased stability.

Previous investigations and my current results show that the increase in regulator activity observed when *B. anthracis* is cultivated in elevated CO<sub>2</sub> compared to ambient air is likely due to increased dimer stabilization and not changes in PCVR stability or solubility. Modified pulse-chase experiments designed to assess whether PCVR stability was affected by culture in CaCO<sub>3</sub> in 5% CO<sub>2</sub> compared to CA-Air showed switching cultures from CaCO<sub>3</sub> in 5%

CO<sub>2</sub> to CA-Air did not affect the stability of these proteins compared to cultures maintained in CACO<sub>3</sub> in 5% CO<sub>2</sub> throughout growth. In fact, both AcpA and AtxA appear to be very stable following removal of IPTG and cessation of protein synthesis by chloramphenicol. These results are similar to steady state AtxA-FLAG and AcpA-FLAG levels expressed from their respective native loci throughout the growth phase in fully virulent *B. anthracis* Ames strain (pXO1<sup>+</sup> pXO2<sup>+</sup>). During culture in CACO<sub>3</sub>, samples taken at hourly intervals from one hour after the start of culture to six hours after culture initiation show that AcpA-FLAG levels are consistent at all time points. AtxA-FLAG levels increase from one hour to three hours after culture initiation and then remain steady through six hours. I could not detect AcpB-FLAG in these experiments. These data indicate that *atxA* and *acpA* expressed from their respective native loci produce proteins that are detectable throughout exponential and stationary growth phase, suggesting that the activities of these proteins are beneficial to the cell during these stages of growth in these culture conditions.

Structure/function studies to elucidate the function of intrinsic domains within the PCVRs indicate that, like AtxA, the EIIB-like domain of AcpA and AcpB functions in multimerization, and that multimerization is required for activity. Predictions from the AtxA crystal structure relate phosphorylation of H199 within PRD1 may affect positioning of the DNA-binding domain and influence target specificity. Phosphorylation of AcpA and AcpB has not been demonstrated. Although comparisons of the AcpA and AcpB amino acid sequences and structure predictions are highly suggestive of the presence of PRDs, the placement of histidines within the PRDs differ between the three regulators, suggesting large differences in the potential phosphorylation sites (**Figure 3-1**) (66). If indeed the AcpA and AcpB PRDs control PCVR function, the relationships between phosphorylation and protein structure may differ between the PCVRs, affecting their target specificity and relative activity.

Experiments designed to test the target specificity of chimeric regulators in which the DNA-binding domain was swapped with that of other PCVRs were unsuccessful. The AtxA<sup>DBD</sup>AcpA<sup>PRD+EIIB</sup> and AtxA<sup>DBD</sup>AcpB<sup>PRD+EIIB</sup> chimeras were detected in soluble cell lysates but

did not have activity on either *in vivo* reporter possibly due to improper folding. Chimeras with either the AcpA<sup>DBD</sup> or AcpB<sup>DBD</sup> were not detected in soluble cell lysates. The lack of AcpA and AcpB crystal structures complicates identification of unstructured regions in which to make domain boundaries to generate chimeras. Once the crystal structures of AcpA and AcpB are solved, accurate domain interfaces can be determined which will likely increase the stability of chimeric proteins.

In addition to experiments designed to assess how individual domains affect PCVR activity, I also examined interactions between different PCVRs and assessed effects of interactions on PCVR activity. Results from my co-affinity purification experiments reveal that AtxA can interact with AcpA, and the relative amounts of FLAG-tagged PCVRs in eluates suggested that AtxA has a stronger affinity for itself than for AcpA. I was unable to detect AtxA-AcpB or AcpA-AcpB interactions in the same conditions. The AtxA homodimer structure suggests interactions between amino acids within PRD2 of one monomer and amino acids of the EIIB-like domain of the other monomer (65). Of the eight amino acids implicated in the AtxA-AtxA interaction; L375, T382, L386 and N389 of one monomer, and I403, Y407, E413 and K414 of the second monomer, three of these residues are dissimilar in AcpA and AcpB. T382 of AtxA is a glutamic acid residue in AcpA and AcpB, and L386 of AtxA is a lysine in AcpA and AcpB. N389 of AtxA is an isoleucine residue in AcpA and a serine in AcpB. These differences may contribute to the apparent weak heteromeric interaction between AtxA-AcpA relative to the AtxA-AtxA interaction.

I artificially altered AtxA/AcpA stoichiometry and assessed the effect on expression of the co-regulated gene, *capB*. In my experiment, increasing AtxA expression decreased AcpA activity on the *PcapB-lacZ* reporter. The data support a model in which *in vivo* PCVR stoichiometry can alter expression of PCVR targets. My RNA-Seq data show that *capB* transcription is more strongly affected by AcpA than by AtxA. When both PCVRs are present, an *in vivo* heteromeric interaction may result in reduced AcpA activity. Interestingly, AcpB activity on the transcriptional reporter was not significantly decreased by co-expression of AtxA,

in agreement with a model in which AtxA-AcpB heteromultimer formation is weak or does not occur. Alternatively, AtxA may compete with AcpA, but not AcpB, for occupancy of the *capB* promoter. Further investigation of protein-protein and protein-DNA interactions will probe the molecular basis for *cap* operon control by the three PCVRs.

# Chapter V

## The roles of AtxA orthologs in an anthrax-like *Bacillus cereus* strain

*NOTE: This work was performed in collaboration with Dr. Allison O'Brien's group at The Uniformed Services University of the Health Sciences. In the Introduction of this chapter (5.1) I summarize work performed in the O'Brien laboratory. My work is presented in the Results (5.2). Portions of the writing in this chapter were drawn from:*

*Scarff, J.M., Raynor, M.J., Seldina, Y., Ventura, C.L., Koehler, T.M., O'Brien, A.D. (2016) The Roles of AtxA Orthologs in Virulence of Anthrax-like Bacillus cereus G9241. Molecular Microbiology. doi: 10.1111/mmi.13478*

*I have received permission by the publisher of Molecular Microbiology, John Wiley and Sons, to reproduce all of the manuscript in print or electronically for the purposes of my dissertation (License Number: 4284271503886)*

## 5.1 Introduction

*Bacillus anthracis* and *Bacillus cereus* are pathogenic members of the *B. cereus* subgroup of related Bacilli. *B. anthracis* is the causative agent of anthrax, and *B. cereus* is frequently associated with food poisoning as well as opportunistic and nosocomial infections. Many virulence factors produced by these organisms are plasmid-associated, and plasmid number in *B. cereus* group members varies ranging from 1 to 12 with sizes from 2 to 600 kb (137). The anthrax toxin structural genes and capsule biosynthesis operon are located on plasmids pXO1 and pXO2, respectively in *B. anthracis*. *B. cereus* produces an emetic toxin, cereulide, the gene of which is encoded by plasmid pCER270 (16, 138).

Plasmids with high sequence identity to pXO1 and pXO2 have been found in other *B. cereus* group members. Several *B. cereus* isolates from food, dairy, and clinical samples carry plasmids with large regions of homology and synteny to pXO1, but lack the 44.8-kb pathogenicity island containing the toxin structural genes and *atxA* (137). Plasmids with high identity to pXO1 and pXO2 have been detected in *B. cereus* strains recovered from great apes that succumbed to an anthrax-like disease. These plasmids contained genes encoding the anthrax toxins, poly- $\gamma$ -D-glutamic acid capsule, and the respective regulatory genes (*atxA*, *acpA*, and *acpB*) (18).

One particular *B. cereus* strain with a pXO1-like plasmid is of particular interest as it contains two *atxA* alleles. *B. cereus* strain G9241 was obtained from a welder in Louisiana afflicted by an anthrax-like respiratory illness. Strain G9241 contains three plasmids, pBCXO1, pBC210, and pBClin29. Plasmid pBCXO1 has high sequence similarity to pXO1 and encodes homologues of the anthrax toxin genes with more than 96% amino acid identity to the *B. anthracis* toxin genes. An *atxA* allele (*atxA1*) is also encoded by pBCXO1, producing AtxA1 predicted to have 100% amino acid identity to AtxA produced by *B. anthracis*. Genes required for synthesis of a hyaluronic acid capsule are encoded by the *hasACB* operon also located on pBCXO1. Plasmid pBC210 does not have homology to pXO2 and does not encode *acpA*, *acpB*, nor genes to produce a polyglutamate capsule. In addition to genes encoding a

protective antigen paralogue, PA2, an ADP-ribosyltransferase, Certhrax, and the *bps* locus required for synthesis of a tetrasaccharide capsule, pBC210 harbors an *atxA* allele, *atxA2*. The *atxA2* gene product has 79% amino acid identity and 91% similarity to AtxA produced by *B. anthracis* (**Figure 5-1**). The discovery of AtxA2, an orthologue of AtxA, provides an opportunity to assess how amino acid differences between the two proteins affect activity and multimerization.

To study the roles of the AtxA orthologs in capsule and toxin expression, Dr. O'Brien's group created isogenic single and double mutants of *atxA1* and *atxA2* in strain G9241. The impact of AtxA1 and AtxA2 on production of the hyaluronic acid (HA) capsule encoded by *hasACB*, and the tetrasaccharide (TS) capsule encoded by the *bps* locus was assessed using the quantitative real-time polymerase chain reaction (qRT-PCR) and by observing capsule phenotypes of the mutants. AtxA1 positively affected expression of *hasACB* and *bpsA*. AtxA2 promoted expression of *bpsA*, but did not affect expression of *hasACB*. Capsule visualization data were consistent with the qRT-PCR results. The HA capsule was only produced in strains containing AtxA1. The TS capsule was detected in strains containing either AtxA1 or AtxA2 indicating functional similarity with respect to expression of this capsule. The *atxA1atxA2* double mutant had reduced transcripts of *hasACB* and *bpsA* compared to the parent, and neither capsule was produced by the double mutant. These data demonstrate that AtxA1 regulates HA capsule production, and that either AtxA1 or AtxA2 is adequate for TS capsule production.

To assess the roles of AtxA1 and AtxA2 in toxin expression in strain G9241, Dr. O'Brien's group measured transcript levels of the protective antigen homologue *pagA* located on pBCXO1 in the *atxA1* and *atxA2* mutants. Transcripts of *pagA* were reduced by 19-fold in the *atxA1* mutant and 58-fold in the *atxA1atxA2* mutant, relative to the parent strain. The *atxA2* mutant did not affect *pagA* expression. However, complementation of the *atxA1atxA2* mutant with either *atxA1* or *atxA2* restored parent levels of *pagA*. Western blots of culture supernates from the different strains show that toxin levels from the *atxA1* and *atxA1atxA2* mutants were

less abundant than from the parent. The *atxA2* mutant and parent strains produced similar toxin levels. These data indicate that toxin production is primarily regulated by AtxA1 in *B. cereus* strain G9241.

Given the different effects of AtxA1 and AtxA2 on toxin and capsule production, Dr. O'Brien's group tested the virulence of the different mutants in two murine models of anthrax; A/J mice which are immunodeficient and susceptible to toxigenic but noncapsulated *B. anthracis* strains, and C57BL/6 mice which are immunocompetent and susceptible to *B. anthracis* strains that produce toxin and capsule (139–143). A/J mice inoculated subcutaneously with spores of the *atxA1* mutant exhibited a mean time-to-death (MTD) that was approximately two days later than that observed for mice inoculated with an equivalent dose of parent strain spores. The MTD for A/J mice challenged with spores from the *atxA2* mutant did not differ from the parent strain. There were no survival differences following intranasal inoculation of A/J mice with spores of the parent, *atxA1*, and *atxA2* mutants. The *atxA1atxA2* mutant was avirulent when inoculated subcutaneously or intranasally.

Immunocompetent C57BL/6 mice challenged intranasally with spores of the *atxA1* mutant had a significantly longer MTD relative to the parent strain, but no difference in MTD was observed when spores of the parent and *atxA2* strains were administered. There was no difference in MTD of C57BL/6 mice challenged subcutaneously with spores of the parent, *atxA1*, or *atxA2* strains. *In vivo* capsule production in mice challenged subcutaneously with spores of the parent and mutant strains indicate that AtxA1 is required for HA capsule formation and either AtxA1 or AtxA2 is sufficient for elaboration of the TS capsule. These virulence studies show that at least one AtxA ortholog is required for virulence in *B. cereus* strain G9241, and that AtxA1 may play a larger role in virulence than AtxA2.

In this chapter I discuss my contributions to the collaborative effort to investigate the roles of AtxA1 and AtxA2 in the regulation of capsule and toxin expression in *B. cereus* strain G9241. I measured and compared AtxA1 and AtxA2 activity on the lethal factor promoter. I also assessed the multimerization capabilities of AtxA2.



## 5.2 Results

### 5.2.1 Activity of AtxA and AtxA2

To assess whether AtxA2 can act as a transcriptional regulator I used the *P<sub>lef</sub>-lacZ* reporter (UT376) to measure transcriptional activity, as was done previously for AtxA in *B. anthracis* (Hammerstrom 2011). I measured the activity of AtxA-His and AtxA2-His expressed from a plasmid-borne IPTG-inducible promoter in cultures of UT376. Previous investigations showed that addition of the 6xHis epitope to the carboxy terminus of AtxA did not affect activity of AtxA (Hammerstrom 2011). Expression of AtxA-His and AtxA2-His was induced to similar levels with IPTG (30  $\mu$ M and 100  $\mu$ M, respectively) as shown by western blot probed with an antibody against the 6xHis epitope (**Figure 5-2**). I found that  $\beta$ -galactosidase activity in the AtxA2-His expression strain was approximately five-fold lower than activity in the AtxA-His expression strain (**Figure 5-2**). These data indicate that AtxA positively affects *lef* transcription to a significantly greater degree than does AtxA2-His. Moreover, AtxA2-His required three-fold more IPTG to reach levels comparable to AtxA-His, which suggest that AtxA2-His is less stable than AtxA in *B. anthracis*.

### 5.2.2 Multimerization of AtxA proteins.

AtxA activity requires dimerization of the protein and mutants that fail to dimerize are inactive (Hammerstrom 2011). To test homomultimer formation by AtxA2, I used co-affinity purification to detect protein-protein interactions. *B. anthracis* ANR-1 *atxA*-null strains that expressed AtxA-His, AtxA-FLAG, AtxA2-His, AtxA2-FLAG, or GFP-FLAG were pooled and lysed in pairs: (1) AtxA2-His and AtxA2-FLAG, (2) AtxA-His and AtxA-FLAG, (3) AtxA2-His and GFP-FLAG, and (4) AtxA2-FLAG and GFP-FLAG, as indicated in **figure 5-3A**. AtxA dimerization has been demonstrated previously, so pair (2) served as a positive control (64). GFP-FLAG was used as a negative control. His-tagged proteins were



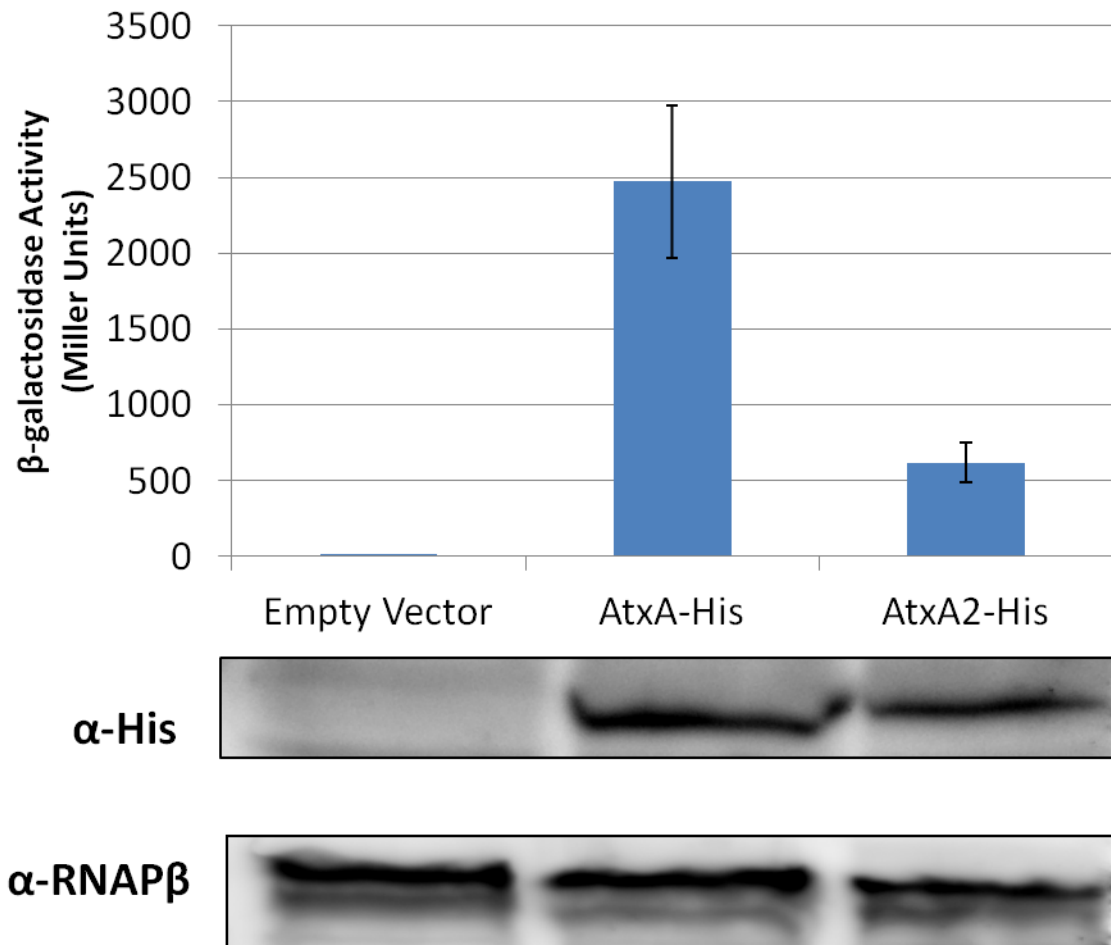


**Figure 5-2.** *In vivo* activity of AtxA-His and AtxA2-His

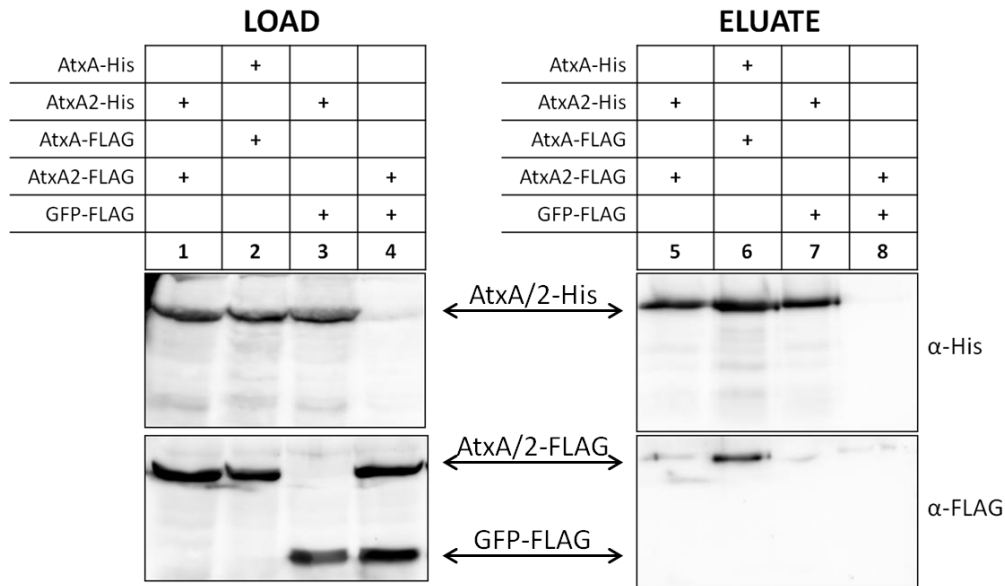
The  $\beta$ -galactosidase activity of *B. anthracis* strains harboring the *P<sub>lef</sub>-lacZ* reporter and IPTG-inducible *atxA* alleles was determined as described previously (95). In an *atxA*-null strain (UT376), production of AtxA-His (pUTE1097) and AtxA2-His (pUTE1096) was induced using 30  $\mu$ M and 100  $\mu$ M IPTG respectively during growth in  $\text{CaCO}_3$ . The empty vector sample was derived from UT376 (pUTE657) that lacks *atxA*. Samples were obtained at the transition to stationary phase (4h;  $\text{OD}_{600}$  1.2-1.7). Standard error shown.

captured with NTA-Ni resin, eluted with imidazole, and detected by western blot. All of the appropriate tagged proteins were present in pooled lysates prior to incubation with the NTA-Ni resin (**Figure 5-3A**, lanes 1-4). Protein complexes that contained a 6xHis epitope bound to the NTA-Ni resin were eluted with imidazole (**Figure 5-3A**, lanes 5-8). As expected, AtxA-FLAG co-eluted with AtxA-His (**Figure 5-3A**, lane 6). AtxA2-FLAG co-eluted with AtxA2-His, represented by a faint band in the anti-His western blot (**Figure 5-3A**, lane 5). The AtxA2-FLAG band was much less intense than that of the AtxA-FLAG band that co-eluted with AtxA-His (**Figure 5-3A**, lane 5 versus lane 6). These data suggest that AtxA2 can form homomultimers, but that the AtxA2 homomeric interaction is weaker than that of AtxA homomultimers.

As a parallel approach to test AtxA2 homomultimerization, I employed protein crosslinking with bis(maleimido)hexane (BMH). BMH reacts specifically with free cysteines within 13 Å to irreversibly crosslink the residues. AtxA has cysteines at positions 96, 161, 202, 356, 370, and 402, and crosslinking by BMH at C402 results in homomeric protein dimers (64). AtxA2 has the same cysteine residues as AtxA, except for C161, which is an alanine residue. Cell lysates from individual cultures that expressed 6xHis-tagged recombinant AtxA, AtxA-H379D, and AtxA2 were treated with BMH, subjected to SDS-PAGE, and probed with an anti-His antibody via western blot. In the absence of the crosslinker, AtxA-His migrated as a dense band near the 50-kDa marker in each of the lysates (**Figure 5-3B**). The predicted molecular weights of the three AtxA variants is 55.6 kDa. The crosslinking of two AtxA-His proteins was indicated by a band of the size commensurate with an AtxA dimer (110 kDa) detected in the AtxA-His lysate treated with BMH (**Figure 5-3B**). The H379D amino acid mutation in AtxA abolishes dimerization (65), and only monomer was detected in the BMH-treated lysate from the AtxA-H379D-His mutant (**Figure 5-3B**). Similarly, BMH treatment of lysates containing AtxA2-His did not produce a band suggestive of a dimer. Smears of apparent high molecular weight cross-reactive protein were present in the cross-linked AtxA-His and AtxA2-His lysates, an observation that suggests that each AtxA protein has the capacity to form some higher-ordered protein-protein interactions.

The capacity for AtxA and AtxA2 to form heterodimers was also investigated with co-affinity purification. *B. anthracis* ANR-1 *atxA*-null strains that expressed AtxA-His, AtxA-FLAG, AtxA2-His, or GFP-FLAG via an IPTG-inducible expression plasmid were pooled and lysed in pairs as depicted in **figure 5-4**. Lysates were incubated with NTA-Ni resin and eluted with imidazole, then separated by SDS-PAGE and analyzed by western blot. As expected, AtxA multimerization was demonstrated by detection of AtxA-FLAG in AtxA-His eluates (**Figure 5-4**; lane 6). GFP-FLAG was not detected in any eluates, which indicated that non-specific proteins were washed from the NTA-Ni resin and that the 6xHis and FLAG epitopes did not interact. The presence of AtxA-FLAG in AtxA2-His eluates revealed that, in these conditions, AtxA-FLAG formed a stable interaction with AtxA2-His. Taken together, the BMH crosslinking and co-affinity purification data suggest a model in which AtxA2 forms weak or unstable homomultimers relative to AtxA homomultimers, and AtxA2 forms a relatively stable heteromultimer with AtxA.

A.



B.

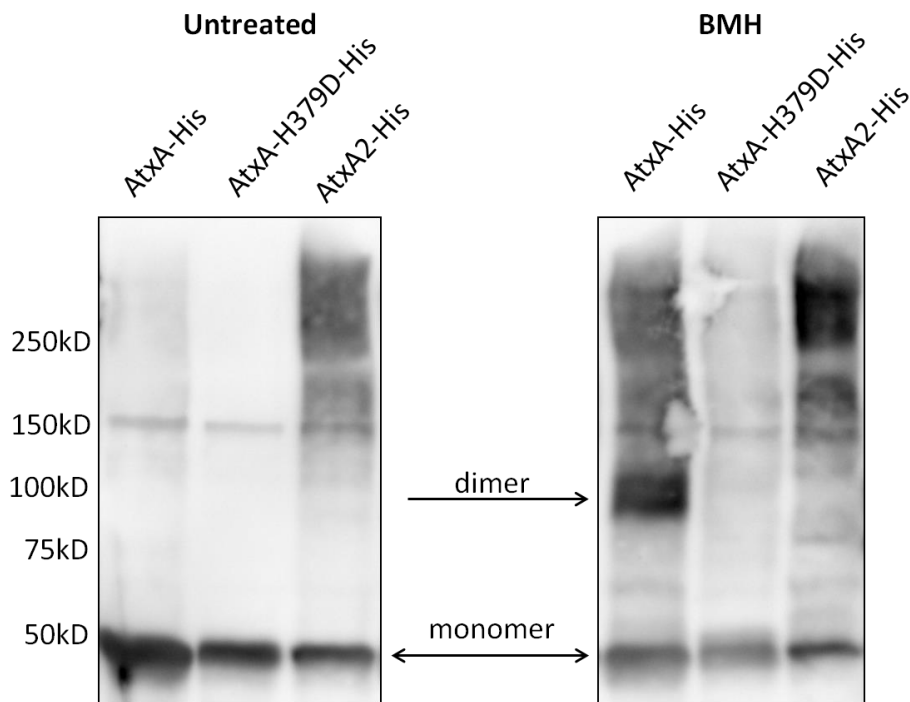


**Figure 5-3.** Dimerization of AtxA2

(A) Lysates from *B. anthracis* *atxA*-null strains (UT376) containing AtxA2-His (pUTE1096), AtxA2-FLAG (pUTE1122), AtxA-His (pUTE991), AtxA-FLAG (pUTE992), or GFP-FLAG (pUTE1013) induced with IPTG were subjected to co-affinity purification using NTA-Ni resin. western blots probed with  $\alpha$ -His or  $\alpha$ -FLAG were performed on soluble cell lysates (Load, lanes 1-4) and purified proteins (Eluate, Lanes 5-8). (B) Cultures of UT376 containing AtxA-His, AtxA-H379D-His, or AtxA2-His (pUTE1096) were induced with 50  $\mu$ M, 50  $\mu$ M, and 100  $\mu$ M IPTG respectively. Cell lysates were treated with cross-linking agent BMH. SDS-PAGE (4-15%) and western blots using anti-His antibody were used to detect AtxA-His and AtxA2-His.

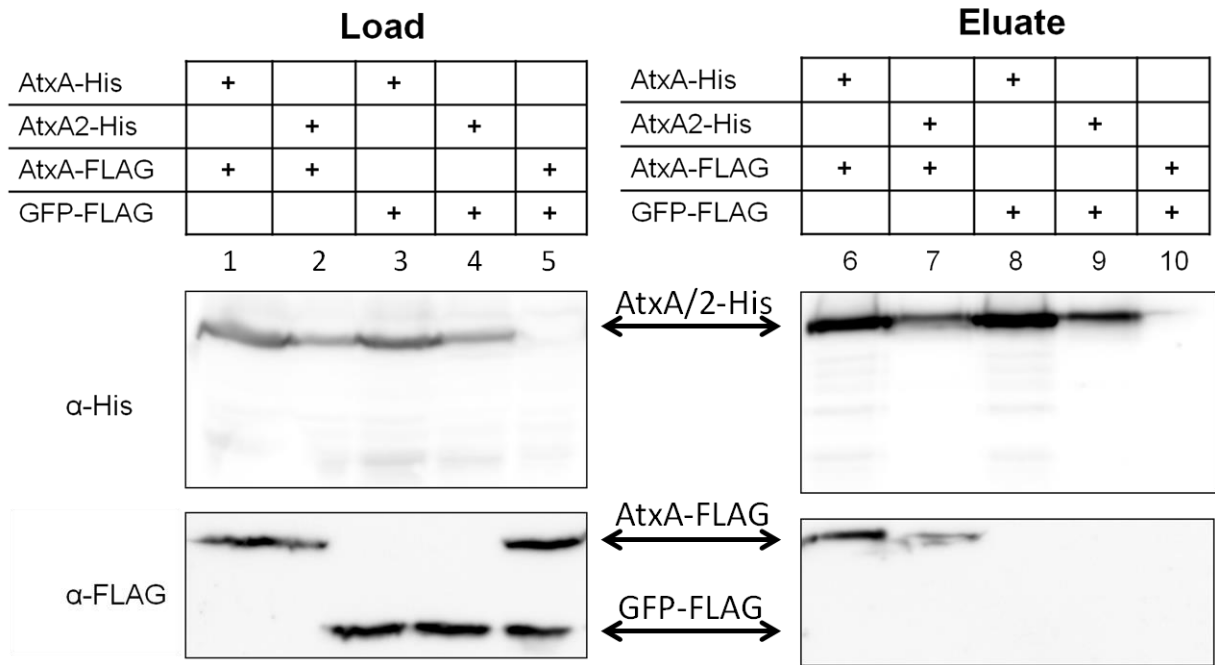


**Figure 5-4.** Specific binding of AtxA2-His to AtxA-FLAG  
 Lysates from *B. anthracis atxA*-null strains (UT376) containing AtxA-His (pUTE991), AtxA2-His (pUTE1096), AtxA-FLAG (pUTE992), or GFP-FLAG (pUTE1013) induced with IPTG were subjected to co-affinity purification using NTA-Ni resin. Western blots probed with  $\alpha$ -His or  $\alpha$ -FLAG were performed on soluble cell lysates (Load, lanes 1-5) and purified proteins (Eluate, Lanes 6-10).

### 5.3 Discussion

In this chapter I have presented my data comparing the activity and multimerization states of the AtxA orthologs, AtxA1 and AtxA2, from *B. cereus* strain G9241. My data reveal differences in activity and multimerization of the two AtxA orthologs which are likely mediated by dissimilarities in the amino acid sequences of AtxA and AtxA2.

There are clear similarities with regard to functional relationships that exist among the *B. anthracis* PCVRs and the *B. cereus* strain G9241 AtxA orthologs. In *B. anthracis*, my RNA-Seq and transcriptional reporter data indicate that AtxA controls toxin gene expression, with AcpA and AcpB having little to no effect (-), yet several other genes are coregulated by all three proteins. Toxin western blots from *atxA1*- and *atxA2*-null *B. cereus* strains indicate that AtxA1 primarily regulates toxin expression with AtxA2 having no effect on toxin production. Considering that AtxA1 and AtxA2 share 76% amino acid identity and 91% similarity, and share greater sequence conservation than AtxA has to AcpA and AcpB, the molecular requirements for toxin expression appear considerably stringent. Despite AtxA2 having no effect on toxin expression, either AtxA1 or AtxA2 was sufficient for expression of the TS capsule indicating functional similarity with regard to expression of the *bps* locus and suggests that AtxA2 functionality is promoter dependent.

A linear representation of the five domains of AtxA and a comparison of AtxA and AtxA2 amino acid sequences is shown in **figure 5-1**. There are 37 amino acids that are not conserved between AtxA and AtxA2, only four of which are in the amino-terminal DNA-binding domains of the protein. The remainder of the non-conserved amino acids are located in the PRDs and the EIIb-like multimerization domain. Notably, the phosphorylation sites of AtxA, H199 of PRD1 and H379 of PRD2, that are known to affect AtxA activity (65, 66) are conserved in AtxA and AtxA2 (represented in bold in **figure 5-1**). In the current model for AtxA structure and function, phosphorylation of H199 enhances AtxA activity, while phosphorylation at H379 prevents dimerization and abrogates AtxA function (65). The crystal structure of AtxA shows that several amino acids interact at the dimer interface, and, with the exception of the asparagine to serine



change at position 389, these residues are conserved among the proteins. Nevertheless, despite this conservation of residues, I was unable to detect robust homomultimerization of AtxA2 using coaffinity purification and crosslinking. Amino acid differences in AtxA2 may result in conformational changes that affect accessibility of the histidine residues for phosphorylation and/or alter the positions of residues that interact at the dimer interface and lead to reduced dimerization and activity of AtxA2. It is also possible that a slight alteration in the AtxA2 structure changes the position of C402, a residue that is required for BMH-mediated crosslinking of two AtxA molecules (64).

My data also suggest that AtxA2 may be less stable than AtxA. When *atxA* and *atxA2* expression were controlled by the same IPTG-inducible promoter, three-fold more IPTG was required to induce AtxA2 to a level comparable to AtxA. Finally, it is also possible that, for reasons not yet clear, dimerization may not be essential for AtxA2 function. Future studies of AtxA2 should involve phosphomimetic and phosphoablative mutations at positions 199 and 379 to determine whether potential phosphorylation at these sites affects AtxA2 in a manner comparable to AtxA in *B. anthracis*.

My data support a model in which AtxA/AtxA homomultimers have the highest activity and AtxA2/AtxA2 homomultimers have the lowest activity. I propose that AtxA/AtxA2 heteromultimers have an intermediate activity that does not have a dramatic impact on AtxA-mediated transcriptional regulation due to low abundance and/or stability of the heteromultimer. Given that it is unknown how the amino acid differences alter activity between the two AtxA orthologs it is important to identify other pXO1-like plasmids harboring *atxA* alleles with sequence changes from *atxA* in *B. anthracis*. Examining amino acid conservation between orthologs coupled with activity assays could identify specific amino acids required for optimal activity.

Plasmids with homology to pXO1 and pXO2, encoding PCVR orthologs, have been identified in pathogenic bacilli other than *B. anthracis*. In Cameroon and the Ivory Coast, *B. cereus* strains harboring pXO1-like and pXO2-like plasmids were recovered from great apes

that succumbed to an anthrax-like disease. These strains contained homologues of the anthrax toxin genes, poly- $\gamma$ -D-glutamic acid capsule biosynthesis genes, in addition to *atxA*, *acpA*, and *acpB*. However, regulation of capsule expression in these strains is distinct from that of *B. anthracis*. Culture of the CA and CI *B. cereus* strains on bicarbonate agar in a CO<sub>2</sub>-enriched atmosphere resulted in encapsulated cells. Interestingly, capsule formation was also observed when the CA and CI strains were cultured on blood or LB agar in ambient air, while *B. anthracis* control cultures did not form capsules in these culture conditions. The ability to synthesize a capsule in subclones of the CA and CI strains correlated with the presence or absence of *capBCADE* suggesting that the observed capsule is not the result of other capsule biosynthesis genes. Toxin production by the CI strain was akin to that of *B. anthracis* and dependent on culture conditions inclusive of bicarbonate and elevated CO<sub>2</sub> (18). The uncoupling of capsule formation and culture conditions containing bicarbonate and CO<sub>2</sub> is both novel and interesting, and suggest that regulatory elements aside from AcpA and AcpB control capsule expression in the CA and CI strains. My research into AcpA and AcpB function show that these two regulators have low activity in strains cultured in medium lacking bicarbonate and ambient air. It is unlikely that the capsule regulators in the *B. cereus* have gain of function mutations enabling increased activity in ambient air as the sequence conservation with the *B. anthracis* homologues is almost identical. Future studies on capsule expression in this strain should compare the regulatory region of *capBCADE* from the CA and CI strains with that of *B. anthracis*. Clues to *cis* and/or *trans*-acting factors that influence *capBCADE* expression could be identified.

# Chapter VI

## Dual role for AtxA: control of sporulation and anthrax toxin production

*NOTE: This work was performed in collaboration with Dr. Jennifer Dale and others at The University of Texas Health Science Center at Houston. In the Introduction of this chapter (6.1) I summarize work performed with the coauthors. My work is presented in the Results (5.2). Portions of the writing in this chapter were drawn from:*

Dale, J.L., Raynor, M.J., Dwivedi, P., and Koehler, T.M. (2012) cis-acting Elements Controlling Expression of the Master Virulence Regulatory Gene *atxA* in *Bacillus anthracis*. *Journal of Bacteriology*. doi:10.1128/JB.00776-12.

Dale, J.L., Raynor, M.J., Ty, M.C., Hadjifrangiskou, M., Koehler, T.M. (2018) A dual role for the *Bacillus anthracis* master virulence regulator AtxA: control of sporulation and anthrax toxin production. *Frontiers in Microbiology*. doi: 10.3389/fmicb.2018.00482.

## 6.1 Introduction

While *B. anthracis* is commonly thought of as the anthrax pathogen, this bacterium also occupies niches outside of mammalian hosts. Vegetative cells of *B. anthracis* have been recovered on and around plant roots in the soil, and from the guts of earthworms (24, 144). The spore, however, is thought to be the primary form of *B. anthracis* outside the host environment. Spores are resistant to heat, desiccation, and other environmental conditions. The spore is the infectious form of the bacterium and enters the host via inhalation, ingestion, or skin abrasion leading to different types of anthrax dependent on the route of infection. Spores of *B. anthracis* have not been observed within infected hosts where conditions that promote virulence factor expression, such as high partial pressure of CO<sub>2</sub>, diminish sporulation efficiency (145). It is not until the host succumbs to anthrax and begins to decompose, exposing *B. anthracis* to the exterior environment, that vegetative cells begin to form spores. The cycling between spore and vegetative forms is an important part of the bacterial lifestyle and is necessary for transfer of the bacterium to new hosts.

Control of sporulation is managed by several *trans*-acting factors that have been characterized primarily in the model *Bacillus*, *Bacillus subtilis*. CodY is a pleiotropic regulator of stationary phase genes and is highly conserved in *Bacillus* species. In *B. subtilis*, CodY repressed expression of genes required for sporulation during exponential growth phase when nutrients were in excess (146). AbrB is a transition-state regulator that prevents untimely expression of genes required for survival in stationary phase, including sporulation genes (147). During the transition into stationary phase, AbrB-mediated repression of genes necessary for sporulation is relieved by inhibition of *abrB* expression by Spo0A (148). Spo0A is the master response regulator for expression of genes required for survival in stationary phase. Spo0A is activated following phosphorylation by a complex phosphorelay that is initiated in response to nutrient limitation (149). The phosphorelay is triggered by autophosphorylation of sensor histidine kinases, and the specific signal of nutrient limitation required for induction is

unknown. Homologues of CodY, AbrB, and Spo0A are present in *B. anthracis* and are thought to play similar roles to those demonstrated in *B. subtilis*.

*B. anthracis* produces a unique pXO2-encoded element of the sporulation pathway, pXO2-0075 annotated as SkiA for "sporulation kinase inhibitor" (the gene encoding SkiA is referenced in the literature as pXO2-61). SkiA shares homology with the signal sensor domain of the *B. anthracis* sensor histidine kinase BA2291, and overexpression of *skiA* negatively affects sporulation. It is hypothesized that overexpression of *skiA* titrates away a signal from BA2291 negatively affecting the phosphorelay required to phosphorylate and activate Spo0A (150). Expression of *skiA* was shown to be positively regulated by AtxA in previous microarray studies (56) and in my RNA-Seq experiment, thus SkiA may provide a mechanism for AtxA to regulate sporulation.

In a joint effort with Dr. Jennifer Dale, Dr. Maria Hadjifrangiskou, and Maureen Ty we used two different culture conditions to model growth of *B. anthracis* in the host and *ex vivo* environments and examined sporulation efficiency, toxin production, and *atxA* expression. Dr. Dale is the primary author of the publication resulting from these experiments. To examine sporulation in *B. anthracis* two culture conditions were employed: a rich medium in air (PA-air), and a semi-defined minimal medium containing dissolved bicarbonate and incubated in 5% atmospheric CO<sub>2</sub> (CACO<sub>3</sub>). Culture in PA-air has been shown to promote efficient sporulation as observed outside the host environment, whereas culture in CACO<sub>3</sub> has been used to model the host environment and is conducive to toxin and capsule expression (44, 49, 151, 152). Culture in PA-air resulted in an increase heat-resistant colony forming units (CFU) over time, a result consistent with sporulation. However, culture in CACO<sub>3</sub> yielded heat-resistant CFU less than 1% of that measured in PA-air cultures indicating growth in CACO<sub>3</sub> is not conducive for sporulation. Western blots to show lethal factor levels in culture supernates indicate lethal factor is not detectable in samples taken from PA-air cultures, but were abundant in CACO<sub>3</sub>-grown cultures. Consistent with AtxA control of lethal factor production, AtxA was detected in low levels and decreased over time during culture in PA-air. Conversely, AtxA levels increased

during culture in CACO<sub>3</sub> and peaked at the transition to stationary growth phase. These data reveal an inverse relationship between sporulation and toxin production. Moreover, production of AtxA is dependent upon culture conditions.

To delineate the relationship between AtxA and sporulation in the fully virulent *B. anthracis* Ames strain (pXO1<sup>+</sup> pXO2<sup>+</sup>) mutants that express AtxA at different levels were employed. Parent, *atxA*-null, and *atxA*-up (contains a mutation in the *atxA* promoter resulting in 5- and 7-fold increases in lethal factor and AtxA levels, respectively, relative to the parent) strains were grown in CACO<sub>3</sub> and PA-air and spores were visualized by phase contrast microscopy. Compared to the parent and *atxA*-null strains, the *atxA*-up mutant exhibited both a delay and decrease in sporulation efficiency in both culture conditions. In the ANR-1 background (pXO1<sup>+</sup> pXO2<sup>-</sup>) the *atxA*-up mutant did not exhibit a defect in sporulation, suggesting that factors on pXO2 contribute to the *atxA*-up sporulation defect in the Ames strain.

A pXO2-encoded gene, *pXO2-0075* (previously designated *pXO2-61*), is predicted to encode a protein with homology to the signal sensor domain of sporulation sensor histidine kinase, an integral component of the sporulation phosphorelay. Previous studies indicate that AtxA positively regulates *pXO2-0075*, and that *pXO2-0075* overexpression results in a significant decrease in sporulation (56, 150). A *pXO2-0075*-null mutant exhibits sporulation patterns similar to the parent and *atxA*-null strains when cultured in PA-air, and early endospore formation in CACO<sub>3</sub> cultures. Importantly, the sporulation defect in the *atxA*-up mutant is suppressed by deletion of *pXO2-0075*, indicating pXO2-0075 mediates the defect in sporulation. Given this activity *pXO2-0075* was renamed *skiA* for "sporulation kinase inhibitor".

The possible link between AtxA and sporulation extends beyond regulation of *skiA* expression. Many regulators that control expression of genes necessary for sporulation also influence *atxA* at the level of transcription or posttranslationally. CodY, which represses genes needed in stationary phase during exponential growth, controls AtxA protein levels posttranscriptionally by an unknown mechanism. A *codY*-null mutant has diminished AtxA levels and is avirulent in a murine model of anthrax (69). AbrB is the only *trans*-acting factor

demonstrated to bind directly to the *atxA* promoter region, and represses transcription during early exponential growth phase. An *abrB*-null mutant exhibited increased AtxA levels in soluble cell lysates compared to the parent. Spo0A also increases *atxA* expression by repressing transcription of *abrB* (61, 62, 75).

The *atxA* promoter region provides limited clues about other factors affecting *atxA* expression. Transcription of *atxA* initiates from two start sites; P1, the dominant start site, positioned 99 nucleotides upstream of the translational start codon, and P2 located 650 nucleotides upstream of P1 (30, 66) (**Figure 6-1A**). The AbrB consensus sequence consists of 43 nucleotides and resides 25 to 67 nucleotides upstream of the P1 transcriptional start site (61). A putative consensus sequence for the housekeeping sigma factor SigA is upstream of the P1 and P2 transcription start sites (30),

In a collaborative effort involving Dr. Jennifer Dale, Dr. Prabhat Dwivedi, and me, we sought to delineate roles for *cis*-acting elements associated with regulation of *atxA* transcription, and to test for other *trans*-acting factors affecting *atxA* expression. Dr. Dale is the primary author for this work and completed the majority of the experiments. As an initial experiment to determine roles for *cis*-acting elements in the *atxA* promoter the putative SigA consensus sequence at the dominant *atxA* transcription start site, P1, was mutated. Mutation of the consensus sequence abolished transcription from P1. These results suggest that SigA-RNAP transcribes *atxA* from the P1 transcription initiation site.

Next Dr. Dale tested whether *trans*-acting factors other than AbrB bind the *atxA* promoter. Electrophoretic mobility shift assays (EMSA) using *abrB*- and *sigH*-null soluble cell lysates and a radiolabeled *atxA* promoter probe indicated a *trans*-acting factor other than AbrB and SigH bound specifically to the *atxA* promoter resulting in a DNA mobility shift. Similar experiments with an *atxA* probe containing a mutated SigA consensus sequence resulted in a DNA mobility shift indicating the *trans*-acting factor was a regulatory element other than SigA-RNAP.

To map the putative binding site of the *trans*-acting factor, 5' and 3' deletions of the *atxA* promoter were fused to a promoterless *lacZ* gene. Loss of DNA sequences -13 to +31, relative to the P1 transcription start site (+1) resulted in a 15-fold increase in  $\beta$ -galactosidase activity compared to the full length promoter, suggesting a repressor binds downstream of the *atxA* promoter. In EMSA experiments deletion of sequences -13 to +31 resulted in a nonspecific DNA shift suggesting the sequence is required for repressor site binding.

*In silico* analysis of the *atxA* promoter revealed an imperfect 9-bp palindrome within the sequences -13 to +31. A specific DNA shift was not observed in EMSAs using an *atxA* promoter probe containing a partial mutation of the palindromic sequence. Mutation of the palindromic sequence resulted in a 7-fold increase in  $\beta$ -galactosidase activity when the mutated *atxA* promoter was transcriptionally fused to a promoterless *lacZ* gene and introduced into *B. anthracis*.

To test whether the increase in *atxA* promoter activity results in elevated AtxA protein levels the palindromic sequence was mutated in the native *atxA* promoter. AtxA protein levels in the mutant (renamed *atxA-up*) were 6.6-fold higher than that of the parent. Toxin levels in culture supernates of the *atxA-up* mutant increased relative to the parent; lethal factor (5.4-fold), edema factor (8.9-fold), and protective antigen (2-fold). These data show that a partial mutation of the *atxA* repressor binding site results in elevated production of AtxA and the anthrax toxin genes.

In this chapter, I present my data in which I examined the effect AtxA has on sporulation through transcriptional control of *skiA*. I show sporulation efficiencies of *skiA* and *atxA* mutants in conditions favorable to toxin expression and conditions that favor sporulation. I measured transcript levels of *skiA* in *atxA* mutant backgrounds in both culture conditions. I also assessed the virulence of the *atxA-up* mutant in a murine model of anthrax.



## 6.2 Results

### 6.2.1 AtxA modulates sporulation efficiency through SkiA

To elucidate the relationship between AtxA, SkiA, and sporulation I cultured strains harboring deletions of *atxA* or *skiA*, or that overexpressed *atxA* in culture conditions conducive to either sporulation or toxin expression and quantified the respective sporulation efficiencies at different time points. Sporulation efficiency was quantified by enumeration of heat-resistant (HR) colony forming units/ml (CFU). During culture in PA medium in ambient air (PA-air) (sporulation conditions), the most striking observation is the dramatic difference in HR CFU between the *atxA*-up mutant and the parent strain (Ames) (**Figure 6-2A**). Cultures of the parent strain produced approximately  $1 \times 10^5$  HR CFU to  $1 \times 10^8$  HR CFU over the time course, while the *atxA*-up mutant produced 2- to 3-log fewer HR CFU. As stated in section 6.1, the *atxA*-up mutant exhibited increased steady state AtxA levels relative to the parent strain. Deletion of *skiA* in the *atxA*-up background resulted in near parent levels of HR CFU. Complementation with *skiA* in the  $\Delta skiA/atxA$ -up background restored the sporulation defect demonstrating that increasing *atxA* expression negatively affects sporulation efficiency via SkiA. Single and double mutants of *atxA* and *skiA* did not cause dramatic alterations in sporulation efficiencies.

I measured *skiA* expression levels in the different *atxA* mutants to examine whether increases and decreases in *atxA* expression modulated *skiA* transcription. Reverse transcriptase polymerase chain reaction (RT-PCR) results show *skiA* transcripts were 5-fold more abundant in the *atxA*-up mutant and seven-fold lower in the *atxA*-null mutant compared to the parent strain at 4h (**Figure 6-2B**). At 7h, *skiA* transcripts were more abundant than at 4h. Transcripts of *skiA* were 11-fold greater in the *atxA*-up mutant relative to the parent strain, while *skiA* transcripts in the *atxA*-null mutant were comparable to those of the parent strain. These

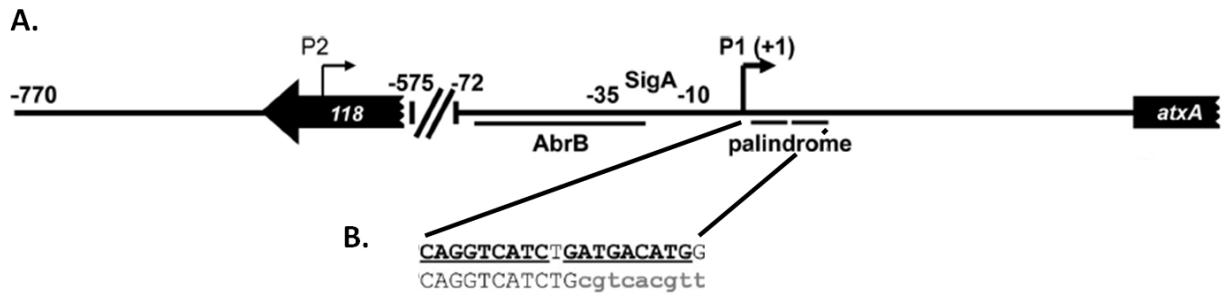


**Figure 6-1.** Schematic representation of the *atxA* promoter region

(A) Transcription start sites are indicated as P1 or P2. The nine base pair palindrome is indicated between +3 and +21 relative to the P1 transcription start site. (B) The palindromic sequence is denoted by bold, underlined letters. Nucleotides mutated using site-directed mutagenesis are denoted by lowercase, gray lettering. Modified from a publication I co-authored with Jennifer Dale. She created this schematic and I have used it with her permission.

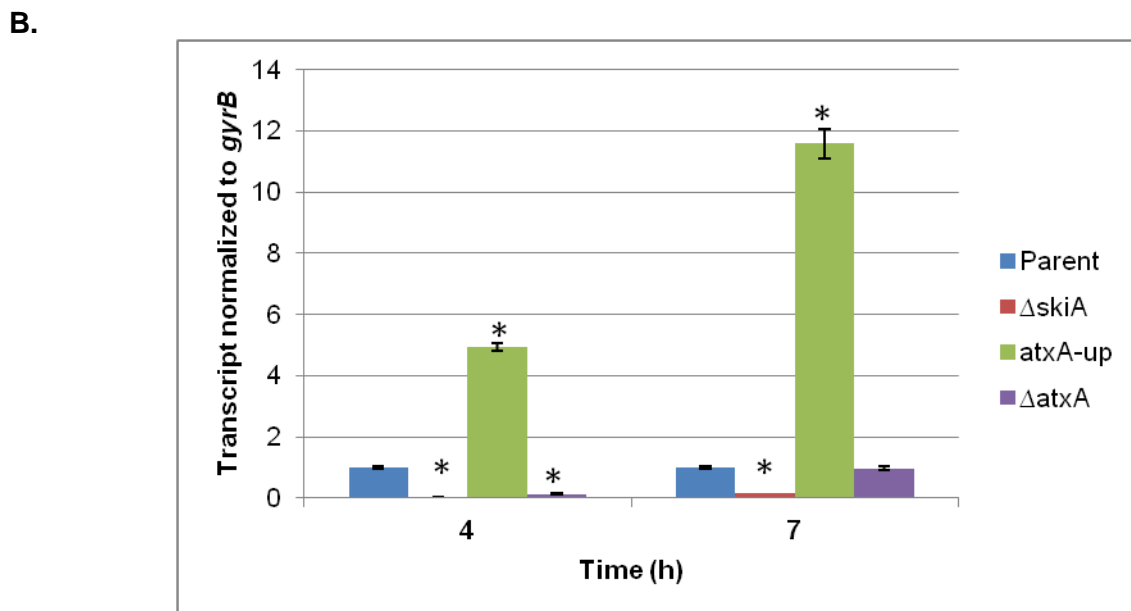
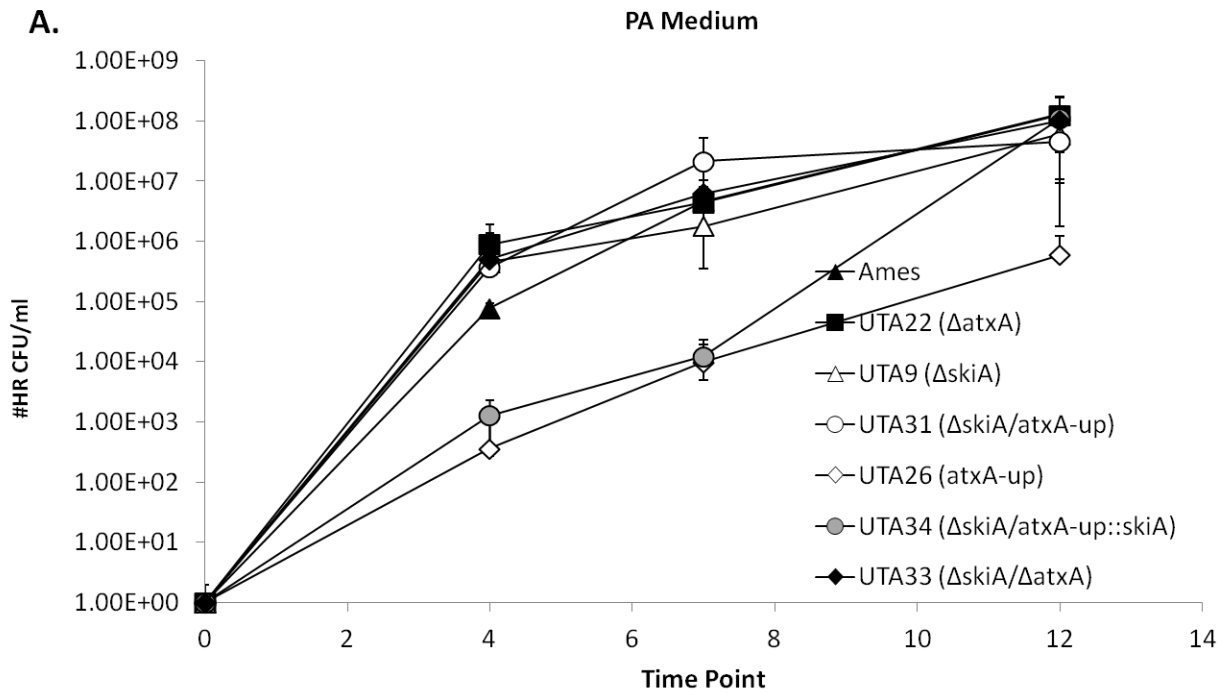


**Figure 6-2.** Spore quantification and *skiA* transcript levels in PA-air  
 (A) Heat-resistant CFU/ml of parent and mutant derivatives. (B) RT-qPCR of *skiA* transcripts at transition-to-stationary (4h) and stationary (7h) phases of growth normalized to the parent control. These data represent average values of detectable transcripts from three independent cultures. Asterisks denote p-values  $\leq 0.05$  relative to parent.

results demonstrate when *B. anthracis* is cultured in PA-air (sporulation conditions) overexpression of *atxA* leads to an increase in *skiA* transcription, causing a *skiA*-dependent defect in sporulation efficiency.

Next, I quantified sporulation efficiencies of the *atxA* and *skiA* mutants in CA medium supplemented with bicarbonate in 5% CO<sub>2</sub> atmosphere (CACO<sub>3</sub>) (toxin-inducing conditions). Culture in CACO<sub>3</sub> yielded less HR CFU, indicative of reduced sporulation efficiency, compared to culture in PA-air. Numbers of HR CFU for CACO<sub>3</sub> cultures were 1- to 2-log fewer than PA-air cultures. Interestingly, cultures of the *atxA*-up strain did not have a defect in sporulation efficiency until stationary phase (7h) (**Figure 6-3A**). The *atxA*- and *skiA*-null mutants had significantly higher sporulation efficiency than the parent at 7h. A 2-log difference in HR CFU was observed between the mutants and the parent strain. As observed during culture in PA-air, the  $\Delta$ *skiA/atxA*-up mutant produced HR CFU similar to that of the parent strain, and complementation with *skiA* restored the sporulation defect.

To assess *skiA* expression in the mutant backgrounds during culture in CACO<sub>3</sub> I measured transcript levels using RT-PCR. Transcript levels of *skiA* produced by the parent and *atxA*-up mutant were similar, with less than a 2-fold difference in relative levels (**Figure 6-3B**). The *atxA* mutant showed a dramatic decrease in *skiA* transcript levels, roughly 57-fold lower at transition phase (4h) and 25-fold lower at stationary phase (7h) compared to the parent strain. In summary, strains with low or undetectable *skiA* transcripts (*atxA*- and *skiA*-null strains) exhibited increased numbers of HR CFU compared to strains with native or elevated *skiA* expression (parent and *atxA*-up strains). These data suggest that culture in conditions mimicking the host environment (toxin induction conditions) results in decreased sporulation efficiency relative to culture in conditions conducive to sporulation, and the influence AtxA has on sporulation is likely mediated through SkiA.

### 6.2.2 Elevated *atxA* expression does not result in increased virulence.

Given the increases in AtxA and toxin levels observed in samples from the *atxA*-up mutant (91), in addition to the sporulation defect, **we** tested whether the mutant exhibited increased virulence in a murine model of anthrax (**Figure 6-4**). I injected vegetative cells of *B. anthracis* parent strain (ANR-1), and isogenic *atxA*-null and *atxA*-up strains into the tail veins of 6- to 8-week old female A/J mice. A/J mice are complement deficient and therefore more susceptible to toxigenic *B. anthracis* strains compared to murine models with intact immune systems (141). Mean time to death (MTD) did not differ significantly between mice inoculated with  $10^2$  CFU of the parent or *atxA*-up mutant. Mice succumbed to infection with the parent and *atxA*-up strains with a MTD of approximately 113 and 119h, respectively. The *atxA*-null mutant was avirulent. These results indicate that increases in AtxA protein and toxin levels observed in the *atxA*-up mutant *in vitro* do not result in a virulence phenotype.

### 6.3 Discussion

In this chapter, I have presented data indicating *atxA* expression levels are important for proper cell development in different environments. Conditions within the mammalian host environment are ideal for both *atxA* expression and activity. Body temperatures within mammals can range from 36°C to 39°C and expression of *atxA* increases six-fold when *B. anthracis* is incubated at 37°C compared to 30°C (59). Carbon dioxide concentrations within the blood of mammals is around 40 mmHg, which is close to 5% and 85-90% of CO<sub>2</sub> within mammals exists in the form of bicarbonate HCO<sub>3</sub><sup>-</sup> (153). AtxA dimerization and activity increase when *B. anthracis* is cultured in medium containing dissolved bicarbonate in 5% CO<sub>2</sub> atmosphere (64). The availability of nutrients in the host environment due to the activity of lethal toxin and other virulence factors produced by *B. anthracis* (see section 1.4) may lead to a physiological state in which genes required during stationary phase, notably sporulation genes, are repressed by transition state regulators. Nutrient availability, temperature, and high partial pressure of CO<sub>2</sub> may result in

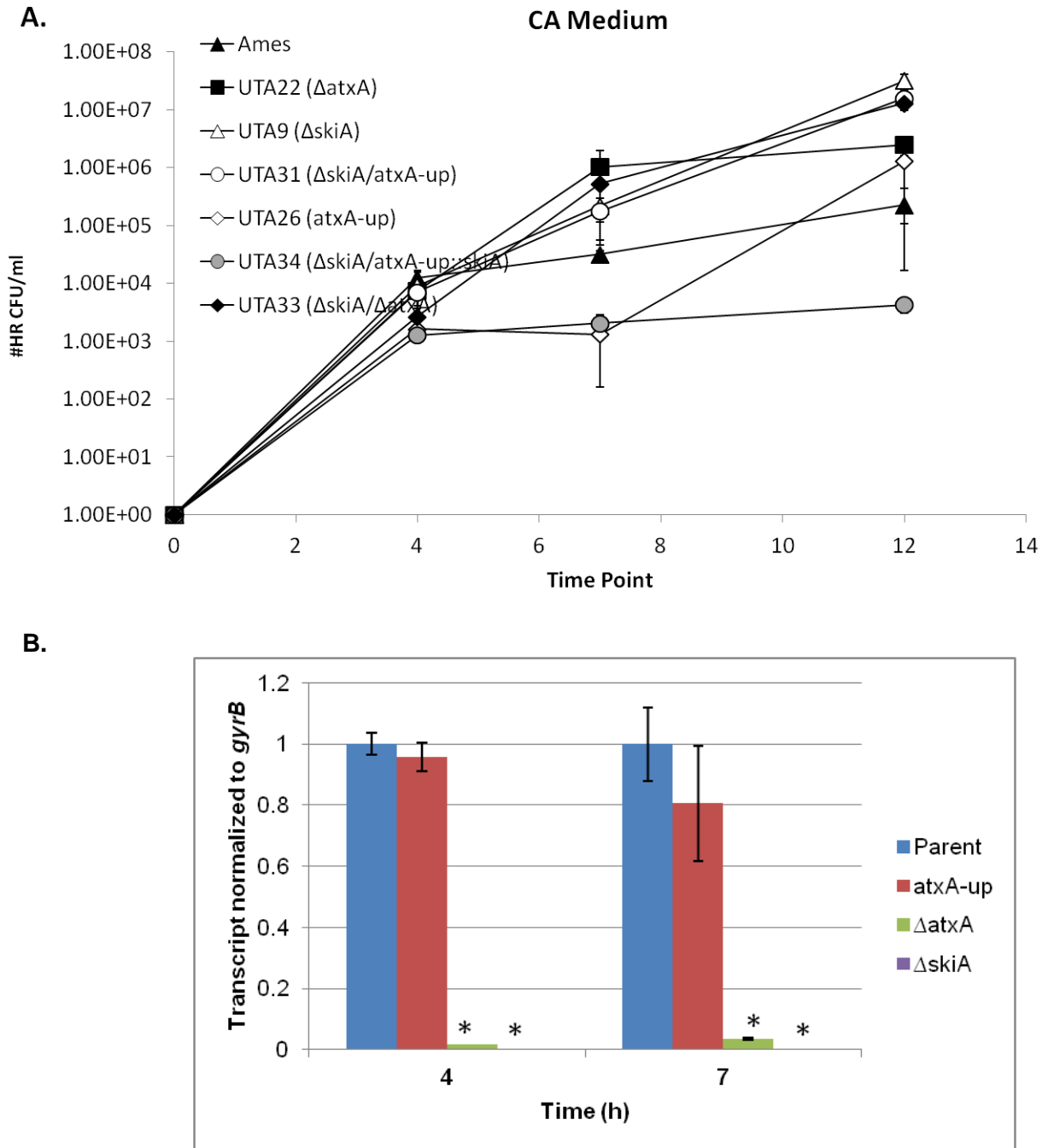


**Figure 6-3.** Spore quantification and *skiA* transcript levels in CACO<sub>3</sub> (A) Heat-resistant CFU/ml of parent and mutant derivatives. (B) RT-qPCR of *skiA* transcripts at transition-to-stationary (4h) and stationary (7h) phases of growth normalized to the parent control. These data represent average values of detectable transcripts from three independent cultures. Asterisks denote p-values  $\leq 0.05$  relative to parent.

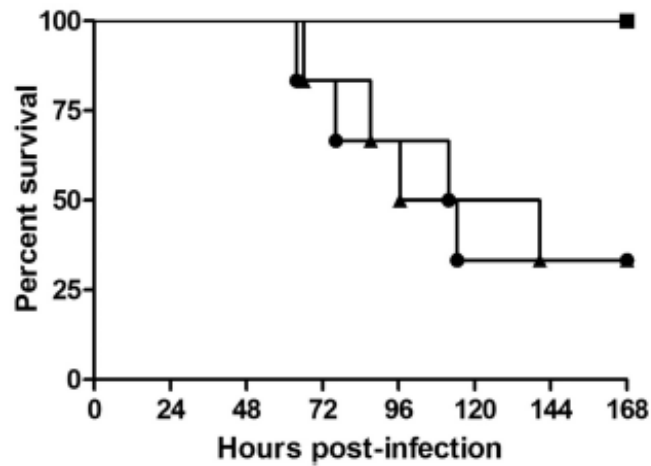


**Figure 6-4.** Virulence of parent and *atxA* mutants

Survival curves of A/J mice inoculated intravenously with vegetative *B. anthracis* are shown. Mice were injected via the tail vein with inocula of following strains: parent (circles; n = 6) inoculum =  $1.5 \times 10^2$  CFU, *atxA*-up (triangles; n = 6) inoculum =  $1.9 \times 10^2$  CFU, and *atxA*-null (squares; n = 3) inoculum =  $1.5 \times 10^3$  CFU. I performed the animal infections used to generate these data. Jennifer Dale created this figure and I have used it with her permission.

increased *atxA* expression and protein activity, resulting in expression of *skiA* and inhibition of sporulation. Moreover, the cerebrospinal fluid and blood from mammals that succumbed to anthrax corroborate *in vitro* studies as vegetative bacilli have been detected in these samples, but not spores (154).

In contrast to culture conditions that induce toxin expression, conditions conducive to sporulation (PA-air) include low CO<sub>2</sub> partial pressure (145). The CO<sub>2</sub> concentration in ambient air is at roughly 0.04%, more than 100-fold lower than what is observed within the host environment (155). AtxA activity is low in these conditions as referenced by the absence of lethal factor in culture supernates from *B. anthracis* strains cultured in PA-air. Interestingly, AtxA protein levels are also reduced in *B. anthracis* strains cultured in PA-air compared to culture in CACO<sub>3</sub> despite incubation of both cultures at 37°C (156). Transcription of *skiA* in the parent strain during culture in PA-air is similar levels observed in the *atxA*-null strain indicating that *skiA* expression is low in these culture conditions. These data are particularly relevant since *B. anthracis* resides in the soil environment where environmental conditions can quickly become unfavorable for survival of vegetative cells. The low CO<sub>2</sub> concentration of ambient air in the soil environment may result in *B. anthracis* vegetative cells with low AtxA activity, and by extension low *skiA* expression. The transition state regulators, which respond to nutrient availability, could function as the primary key holders for sporulation when *B. anthracis* is in the soil environment. In the host environment, when AtxA is more active, positive regulation of *skiA* could function as an added inhibitor of sporulation.

In addition to the influence AtxA has on sporulation via *skiA*, a more well-known role for AtxA is as a positive regulator of toxin expression. Mutation of a putative repressor binding site in the *atxA* promoter led to a seven-fold increase in β-galactosidase activity from a *PatxA-lacZ* reporter. Importantly, AtxA protein levels and toxin production were increased in the "*atxA*-up" strain harboring the repressor site mutation compared to the parent strain (91). Despite elevated toxin production detected during *in vitro* culture of the *atxA*-up mutant, an increase in virulence was not observed in this strain relative to the parent in a murine model of anthrax. It is



possible that the increases in *atxA* expression and toxin production observed *in vitro* do not occur *in vivo*. Alternatively, AtxA and toxin production by the parent strain *in vivo* may not be limiting for anthrax disease progression, and increases in toxin levels have no effect.

The other *B. anthracis* PCVRs, AcpA and AcpB, do not have a significant effect on *skiA* expression. Sporulation efficiency in strains with altered *acpA* or *acpB* expression has not been quantified, however abnormalities in sporulation have not been observed in sporulating cultures of these strains. Capsule production was unaffected in the *atxA*-up and *skiA* mutants. It is curious that lethal factor levels were elevated in the *atxA*-up mutant relative to the parent, but capsule thickness was unaffected. Expression of *acpA* was not measured in the *atxA*-up mutant, and it is possible that the 6.6-fold increase in AtxA in this mutant does not result in an increase in *acpA* transcripts which would suggest AtxA levels are not limiting for *acpA* expression. My data support the interpretation that overexpression of AcpA results in cells with increased capsule thickness compared to native *acpA* expression.

With respect to PCVR function, these data suggest a model in which AtxA plays an important role in toxin expression and suppression of sporulation in toxin inducing conditions through control of *skiA*. AcpA and AcpB appear to play more limited roles and function primarily in capsule production having no apparent effect on sporulation. Future studies should focus on *in silico* analysis of genes with unknown functions in the AcpA and AcpB regulons. Analysis of the predicted amino acid sequences for these AcpA- and AcpB-regulated genes may reveal homology to proteins of known function ascribed to specific gene networks or cellular processes. These studies could highlight other impacts AcpA and AcpB have on cellular physiology.

# **Chapter VII**

## **Discussion**

## 7.1 Noteworthy results and significance of *B. anthracis* PCVRs

*Bacillus anthracis* produces three proteins that are members of an emerging class of Gram-positive transcriptional regulators termed PRD-Containing Virulence Regulators (PCVRs). A defining characteristic of this class of regulators is the presence of phosphoenolpyruvate:carbohydrate phosphotransferase system regulatory domains (PRD). The phosphotransferase system, generally involved in the transfer of phosphate to incoming sugar molecules, may also play a role in virulence. AtxA, named for its control of anthrax toxin gene expression, is the master virulence regulator in *B. anthracis* and is the archetype PCVR. Cells lacking *atxA* are significantly attenuated in murine models of anthrax (30, 91). AtxA shares amino acid similarity with two less well-studied regulators, AcpA and AcpB, which independently positively control transcription of the capsule biosynthetic operon, *capBCADE*. Deletion of *acpA* results in cells with smaller capsule diameters, and *acpB*-null strains have reduced dissemination compared to the parent strain in a murine model of anthrax. An *acpAacpB* mutant is non-capsulated and avirulent in a murine infection model (29, 107).

My research has revealed similarities and differences among AtxA, AcpA, and AcpB with regard to gene regulation and structure-function relationships. In chapter three I describe my efforts to determine the regulons of the PCVRs in strains expressing individual regulators at near native levels. My data show that multiple plasmid and chromosomal genes are PCVR controlled, with AtxA, AcpA, and AcpB having a  $\geq 4$ -fold effect on transcript levels of 145, 130, and 49 genes respectively. Several genes are coregulated by two or three PCVRs. In chapter four I present data concerning the relative *in vivo* activities of each PCVR on *PcapB-lacZ* and *Plef-lacZ* reporter fusions in *B. anthracis*, the effect of CO<sub>2</sub> on the solubility and stability of the PCVRs, the impact functional domains have on regulator activity, and finally multimerization studies. *In vivo* reporter results are largely consistent with RNA-Seq data such that AtxA alone had activity on *Plef-lacZ*, and AcpA and AcpB had more activity on *PcapB-lacZ* than AtxA. The concentration of CO<sub>2</sub> during culture did not affect PCVR stability nor solubility. Similar to AtxA, homodimer formation was observed for AcpA and AcpB and was dependent on the EIIb-like

domains. In co-expression experiments, AcpA activity was reduced by increased levels of AtxA. Experiments presented in chapter five characterize the activity and multimerization potential of an *atxA* orthologue, AtxA2, identified in a virulent *B. cereus*. Compared to AtxA from *B. anthracis*, AtxA2 has less activity. The reduced activity of AtxA2 is potentially due to reduced homodimer formation. Data presented in chapter six further define the effects of AtxA expression levels on virulence and sporulation. *B. anthracis* mutants that overexpress *atxA*, resulting in increased AtxA and toxin production *in vitro*, do not have increased virulence in a murine model of anthrax. Finally, AtxA protein levels can alter sporulation efficiency through control of *skiA* expression.

The presence of three PCVRs in *B. anthracis* provides the opportunity to perform a comparative analysis of paralogues with shared and different functions. My studies, focusing on the mechanistic basis for overlapping and distinct target genes of AtxA, AcpA, and AcpB advance our knowledge of virulence gene expression in *B. anthracis*, while contributing to our understanding of this newly-discovered class of transcriptional regulators. My work defining the regulons of these proteins combined with protein-protein interaction experiments hone our model for PCVR-mediated gene expression in *B. anthracis*. PCVR activity is increased in the presence of bicarbonate and high CO<sub>2</sub> concentration affecting expression of genes located on the chromosome, pXO1, and pXO2. Expression of co-regulated genes can be affected differently by each PCVR. Homodimers of each PCVR are the most prevalent, but a small percentage of AtxA-AcpA heteromultimers may be present affecting expression of select genes. In **Figure 7-1** I present a model for virulence gene expression in *B. anthracis* which is based on previous data and new revelations discovered during my dissertation research.

## **7.2 Model for virulence gene regulation in *B. anthracis***

AtxA is epistatic to AcpA and AcpB, and transcription of *atxA* is influenced by environmental and physiological signals. Many of these signals are related to conditions

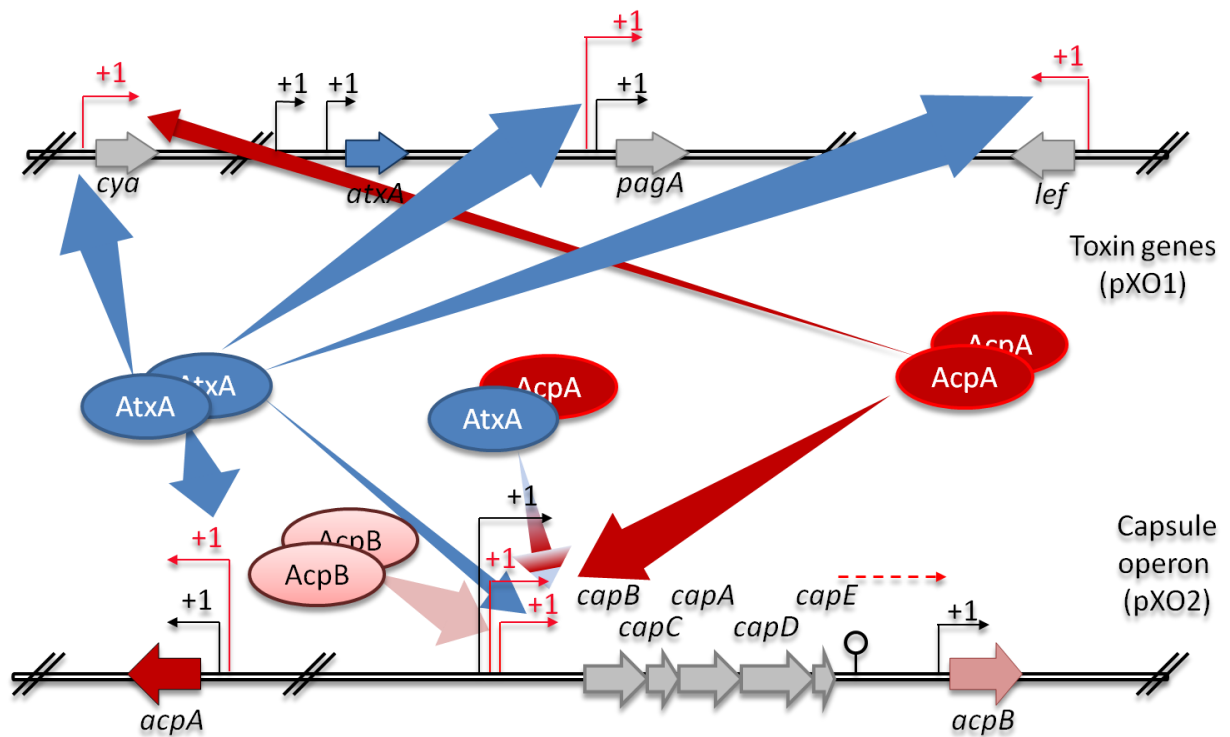


**Figure 7-1.** Comprehensive model of virulence gene regulation in *B. anthracis*. CO<sub>2</sub>-dependent transcriptional start sites are red, and low-level constitutive start sites are black. Thickness of arrows from proteins to transcript start sites show degree of regulation with thick arrows indicating a large effect and thin arrows representing a small effect on expression. The multicolored arrow from AtxA-AcpA to the *capBCADE* transcript start site denotes the AtxA-mediated decrease of AcpA activity on *PcapB*. Protein interactions determined for each PCVR are denoted. The broken arrow from *capE* to *acpB* transcriptional start site represents a low level of transcriptional read through.

encountered within the host environment. The median range for mammalian body temperature is between 35°C and 37.9°C (157), and glucose is the energy source used for cellular respiration in animals. Growth of *B. anthracis* at 37°C and in medium containing glucose are two environmental conditions that promote *atxA* transcription (59, 63). Temporal regulation of *atxA* expression is affected by cellular redox state and growth phase such that AtxA levels increase during early exponential growth phase (60, 61). An undefined repressor also affects *atxA* expression and is thought to function primarily in conditions favoring sporulation ((91), Dale 2018 *in revision*).

Following translation, AtxA is subject to other mechanisms that alter steady-state protein levels and activity. The transition-state regulator CodY indirectly influences AtxA protein levels post-translationally in soluble cell lysates. In a *codY*-null strain, AtxA was not detected in cell lysates by western blot (69). AtxA activity is affected by phosphorylation of H199 and H379 within PRD1 and PRD2, respectively. Phosphomimetic and phosphoablative mutations at H199 and H379 suggest that phosphorylation at H199 allows for optimal AtxA activity, whereas phosphorylation at H379 abolishes AtxA activity (65, 66). Carbon dioxide/bicarbonate are physiological signals positively affecting AtxA activity by increasing the dimer-to-monomer ratio (64). When conditions required for optimal expression and activity of AtxA are met, AtxA-regulated genes, including the toxin structural genes, are expressed.

Expression of *acpA* and *acpB* is presumed to be much less complex than *atxA*. A low basal level of expression of *acpA* and *acpB* is maintained by constitutive promoters at each gene locus. This low level of expression is insufficient for capsule production (29, 70). In conditions suitable for AtxA activity (an environment with elevated CO<sub>2</sub>/bicarbonate), AtxA promotes *acpA* expression from an AtxA-dependent promoter. My RNA-Seq data show that AtxA promotes transcription of *acpA*; transcripts increase by a log 2-fold change of 4.2. AcpA promotes expression of the capsule biosynthetic operon, *capBCADE*, and increases transcripts by a log 2-fold change of 8.7. Cotranscription of *acpB* with *capBCADE* was reported to occur in

roughly ten percent of *capBCADE* transcripts (70). AcpB increased transcripts of *capBCADE* by a log 2-fold change of 8.2.

AtxA positively affects capsule synthesis indirectly through control of *acpA* and *acpB*, yet some capsule production is observed in strains lacking AtxA. In a *B. anthracis* strain containing pXO1 and pXO2, deletion of *atxA* results in cells that produce little to no capsule when cultured in CA medium supplemented with bicarbonate in 5% CO<sub>2</sub> atmosphere (capsule-inducing conditions) (29, 56). Although expression of *acpA* and *acpB* is significantly lower in the *atxA*-null strain compared to the parent, AcpA and AcpB are likely present in low abundance. My results show culture in CACO<sub>3</sub> increases AcpA and AcpB activity compared to culture in CA-Air, and suggest that the thin capsule produced by an *atxA*-null strain is due to "active" AcpA and AcpB present in low quantities.

### **7.3 AtxA, AcpA, and AcpB: a case for divergent evolution**

Similarities with regard to PCVR activity and protein interactions suggest the PCVRs have related ancestry. Analysis of the amino acid sequence of AtxA, AcpA, and AcpB indicate that AcpA and AcpB are more closely related to each other than either is to AtxA. AcpA and AcpB have 40% amino acid sequence identity and 62% similarity, while AtxA shares about 27% amino acid sequence identity and close to 50% amino acid sequence similarity with AcpA and AcpB. Consistent with amino acid sequence conservation, structural models of AcpA and AcpB suggest that both proteins have similar domain organization to AtxA. Functionally, the three proteins are all able to form homodimers and their respective activities are increased when cells containing each protein are cultured in 5% CO<sub>2</sub> in medium containing dissolved bicarbonate. Strong sequence similarity alone is considered to be sufficient evidence for common ancestry (158). Phylogenetic analysis of amino acid sequences models the substitutions that have occurred over the course of evolution and derives a representation of evolutionary relationships between sequences (159–161).

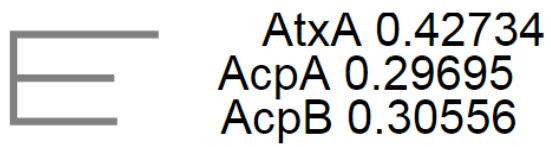


**Figure 7-2.** Phylogram of AtxA, AcpA, and AcpB  
Numbers indicate phylogenetic distances. Phylogenetic analysis completed using Simple Phylogeny.



Analysis of the AtxA, AcpA, and AcpB amino acid sequences supports AcpA and AcpB being more closely related to each other, than either are to AtxA (**Figure 7-2**).

Gene duplication and successive divergence is a mechanism to generate genes with novel functions within genomes, and *acpA* and *acpB* likely result from an *atxA* gene duplication event. Gene duplication can occur by at least two mechanisms: homologous recombination and replicative transposition. For homologous recombination to occur, >100 bp direct-order sequence repeats must exist between potential sites for recombination (162). *B. anthracis* is characterized as a low G-C organism with an average A-T content of 66.5%. Some loci encompassing genetic rearrangements can have enriched A-T content as high as 70% (163). It's a miracle *B. anthracis* can keep its genome together. Given the abundance of A-T rich loci in the *B. anthracis* genome it is possible that regions of homology exist between the *atxA* locus on pXO1 and the *capBCADE* locus on pXO2 allowing for homologous recombination to occur and duplication of *atxA*. This initial gene duplication event likely resulted in the progenitor gene for *acpA* as AtxA and AcpA coregulate more targets than AtxA and AcpB. A second duplication event likely created *acpB* from *acpA*.

Alternatively, *atxA* gene duplication could have occurred by replicative transposition. Transposition is dependent upon a recognizable target sequence and insertion elements (ISs), and a functional transposase. Several putative ISs and genes annotated as integrases and transposases have been identified on pXO1 (109). In replicative transposition, DNA sequences containing *atxA* could be duplicated and inserted into a target DNA sequence on pXO2. In this model, DNA sequences containing *atxA* would be duplicated by replicative transposition and inserted into a target upstream of the *capBCADE* locus on pXO2 to create the progenitor for *acpA*. Successive replicative transposition or homologous recombination events could have led to duplication of *acpA* to create *acpB*. This potential mechanism for gene duplication is plausible because pXO2 also contains several annotations for putative ISs and transposases, many near the capsule biosynthetic operon locus. Interestingly, transposable elements can also support homologous recombination by serving as movable regions of homology (162).

Following duplication of *atxA*, I propose that the resulting copy (the progenitor of *acpA*) assumed both novel and shared functionality compared to AtxA through the accumulation of mutations over time. Following some degree of functional divergence of AcpA from AtxA, a duplication event created the progenitor of *acpB* which accumulated mutations to have shared and unique function compared to AtxA and AcpA. Phylogenetic analysis of PCVR amino acid sequences and RNA-Seq support my model for the order of PCVR gene duplication events in *B. anthracis* (**Figures 7-2, 3-5**). AtxA and AcpA significantly coregulate expression of 31 genes (log 2-fold  $\geq 4$ ), compared to 15 genes controlled by both AtxA and AcpB. Five genes were coregulated by AcpA and AcpB. Assuming symmetrical divergence, equivalent accumulation of mutations over time between paralogues, I would have expected AcpA and AcpB to have a greater number of shared targets. However, the number of coregulated genes is likely low due to the dramatically fewer number of genes controlled by AcpB compared to AtxA and AcpA.

Future studies aimed at understanding the divergence of AtxA, AcpA, and AcpB should focus on identifying genes targets that are regulated directly by the PCVRs. My regulon studies were unable to differentiate direct versus indirect effects on gene expression. ChIP-Seq would identify direct PCVR targets and would define more clearly regulon profiles. Hierarchical clustering data presented in **figure 3-6** is likely skewed by genes regulated indirectly by the PCVRs. Hierarchical clustering of gene expression profiles regulated directly by each PCVR may more closely align with amino acid sequence conservation, such that AcpA and AcpB expression profiles are the most similar on all three genetic elements.

#### **7.4 Evolutionary advantage to cross-talk between genetic elements**

The influence of plasmid-encoded PCVRs on chromosome-encoded branched chain amino acid genes is one of several examples of cross-talk between genetic elements in *B. anthracis*. My RNA-Seq data reveal that cross-talk appears to be multi-directional. In one direction, plasmid-encoded AtxA, AcpA and AcpB affect expression of genes located on the chromosome. In another direction, the well-studied chromosome-encoded transition state

regulator, AbrB, affects expression of *atxA* on pXO1 (61). It is unclear whether chromosome-encoded factors regulate any pXO2-encoded genes. However, intra-genomic gene regulation may serve as a mechanism to coordinate expression of several gene networks required for host colonization. Given that many virulence factors are acquired by horizontal gene transfer and plasmid acquisition, it is reasonable to postulate that these factors are added gradually over time and that transcriptional regulators associated with these factors both gain and lose functionality. Considering *atxA*, *acpA*, and *acpB* are located in apparent pathogenicity islands, over the course of evolution they may have gained functionality to control expression of genes outside of their original/initial targets providing a fitness advantage.

### **7.5 PCVR paralogues in other organisms may have shared functionality**

The *B. anthracis* PCVRs represent a unique opportunity to study the interplay of three paralogues in one organism. My research regarding AtxA, AcpA, and AcpB functionality has identified functions unique to each regulator as well activities shared among all three proteins. However, *B. anthracis* is not the only bacterium to produce PCVR paralogues. Group A streptococcus (GAS) is a pathogenic bacterium that causes several diseases including strep throat, impetigo, and necrotizing fasciitis. Like *Bacillus anthracis*, GAS can colonize a wide range of host tissues and must regulate virulence factor expression in response to host cues (117). Virulence determinants produced by GAS include a hyaluronic acid capsule, secreted proteases, and cell wall-anchored proteins that inhibit host defenses (12). GAS produces two PCVRs, Mga and RivR, that share 22% amino acid sequence identity and 49% similarity. Mga is the most well-characterized PCVR in GAS, and regulates expression of M protein; a major adhesin used during host colonization, a complement factor C5a peptidase, and other virulence factors (117). RivR is a negative regulator of the *hasABC* operon, encoding a hyaluronic acid capsule, and *grab* which encodes a protein G-related  $\alpha_2$ -macroglobulin-binding protein (GRAB) that binds a human protease inhibitor. There are conflicting reports of RivR having either a

positive effect or no effect on expression of two genes in the Mga regulon; *scpA*, encoding the C5a peptidase, and the gene encoding M protein *emm* (12, 116).

Comprehensive transcriptomic studies and biochemical assays elucidated the Mga regulon and molecular mechanism for activity. While RivR has not been studied to the same extent as Mga, similarities and difference between the *B. anthracis* PCVRs and GAS PCVRs are apparent. Both Mga and AtxA promote expression of adhesins in their respective organisms; M protein in GAS, BslA in *B. anthracis*. PCVRs of both organisms affect capsule expression; *B. anthracis* regulators promote capsule production and RivR of GAS negatively affects capsule synthesis. Negative regulation of capsule production by RivR is thought to play an important role in GAS infection. A GAS *rivR* deletion mutant has reduced adherence to a keratinocyte cell line relative to that of the parent strain due to the enhanced capsule elaborated by the mutant strain. Treatment with hyaluronidase restored adherence of the *rivR* mutant indicating that capsule production is a tradeoff between immune avoidance and adherence to host cells (12). Considering my data demonstrating that AtxA alone cannot promote capsule expression and can negatively affect AcpA activity on *PcapB-lacZ*, similar considerations regarding optimal capsule expression may be applicable to *B. anthracis*.

## 7.6 Concluding remarks

Future studies of the *B. anthracis* PCVRs should aim to build on my work to uncover molecular mechanisms that account for the overlapping and divergent function of the regulators. AtxA is likely the progenitor PCVR in *B. anthracis* and *acpA* and *acpB* genes likely arose from gene duplication events. The regulators retained some initial functionality, but also developed specific functions through the accumulation of mutations over time. Undoubtedly, the molecular basis behind functional similarity and differences resides in amino acid conservation among the regulators. Amino acid differences exist in all five predicted domains among AtxA, AcpA, and AcpB, but I propose that dissimilarities in the DNA-binding domains and/or PRDs are responsible for PCVR functional differences. My approach to determine the

specific effects of the DNA-binding domains and PRDs on PCVR activity involved creation of protein chimeras. However, my results were inconclusive due to two chimeric regulators,  $AcpA^{DBD}AtxA^{PRD+EIIB}$  and  $AcpB^{DBD}AtxA^{PRD+EIIB}$ , that were not detectable in soluble cell lysates. The two other chimeras,  $AtxA^{DBD}AcpA^{PRD+EIIB}$  and  $AtxA^{DBD}AcpB^{PRD+EIIB}$ , were detectable in cell lysates, but did not have activity on *PcapB-lacZ* or *Plef-lacZ*.

Future studies to define the impact the DNA-binding domain and PRDs have on PCVR activity would be aided by two advancements: (1) the crystal structures of AcpA and AcpB need to be solved, and (2) the phosphorylation states of AcpA and AcpB need to be determined. Crystal structures for AcpA and AcpB would define domain boundaries and unstructured regions more definitively than structural predictions and alignments with the AtxA crystal structure. These data would facilitate the creation of more stable, and potentially more active, chimeras. It is possible that the redesigned chimeras would be transcriptionally inactive as was observed with the  $AtxA^{DBD}AcpA^{PRD+EIIB}$  and  $AtxA^{DBD}AcpB^{PRD+EIIB}$  proteins. These results would suggest that specific DNA-binding-domain - PRD1 pairing is required for activity. Heteromultimerization experiments with chimeric and full-length PCVR proteins could indicate whether the chimeras are folded properly.

Determination of the phosphorylation states of AcpA and AcpB would complement any results relating the PRDs of these proteins with activity. PRD-containing transcriptional regulators have been shown to be phosphorylated at specific histidines within the PRDs and in EIIA- and EIIB-like domains (9). If AcpA and AcpB are phosphorylated, phosphoablative mutations at amino acids likely to be phosphorylated (histidines within PRDs, and cysteines or histidines within the EIIB-like domain) would indicate at which residue phosphorylation occurred. These data, combined with AcpA and AcpB crystal structures, would illuminate how phosphorylation ultimately affects PCVR activity. Predictions from the AtxA crystal structure suggest that phosphorylation of H199 within PRD1 may affect positioning of the DNA-binding domain and influence target specificity. It is hypothesized that phosphorylation of H379 abolishes dimer formation by destabilizing the interaction between PRD2 of monomer one and

the EIIB-like domain of monomer two (65). Amino acid alignments show that histidines within the PRDs of AcpA and AcpB do not align with phosphorylated histidines in AtxA, and whether or not the residues occupy similar locations in 3D space has not been determined. Differences in the locations of phosphorylated histidines in AcpA and AcpB could affect positioning of the respective DNA-binding domains, and/or the stability of multimeric protein interactions. Alternatively, AcpA or AcpB may not be phosphorylated suggesting that the DNA-binding domain alone confers target specificity.

PCVR expression is complex and different *cis*- and *trans*-acting factors contribute to different relative amounts of AtxA, AcpA, and AcpB within cells of *B. anthracis* (**Figure 3-3**). My results show that artificially altering PCVR stoichiometry can effect expression of target genes (**Figure 4-13**). One way to test whether the complex regulation of PCVR expression is relevant for virulence is to swap PCVR gene loci. PCVR open reading frames could be swapped among PCVR loci such that *cis*- and *trans*-acting factors that control the expression of one PCVR would control the expression of a different PCVR (**Figure 7-3**). This would likely lead to altered PCVR protein levels in addition to dramatic changes in virulence gene expression. In the strain depicted in **Figure 7-3B**, *acpA* is in the native *atxA* locus, *acpB* is in the native *acpA* locus, and *atxA* is in the native *acpB* locus. Given the relative PCVR protein levels observed in the parent strain (**Figure 7-3A, 3-3**), I would expect AcpA to be the most abundant PCVR during culture in CACO<sub>3</sub>. High levels of AcpA would lead to elevated expression of *capBCADE* as well as cotranscription of *atxA*. AtxA would positively regulate *acpB* expression and AcpB would further promote capsule production. This strain would likely exhibit a thicker capsule and reduced toxin expression compared to the parent strain. The strain represented in **Figure 7-3C** would presumably have high levels of AcpB leading to high expression of *capBCADE* and cotranscription of *acpA*. The *atxA* gene is in the native *acpA* locus and AtxA positively regulates *acpA* expression. Thusly, in this mutant AtxA would be in a positive feedback loop. I predict this

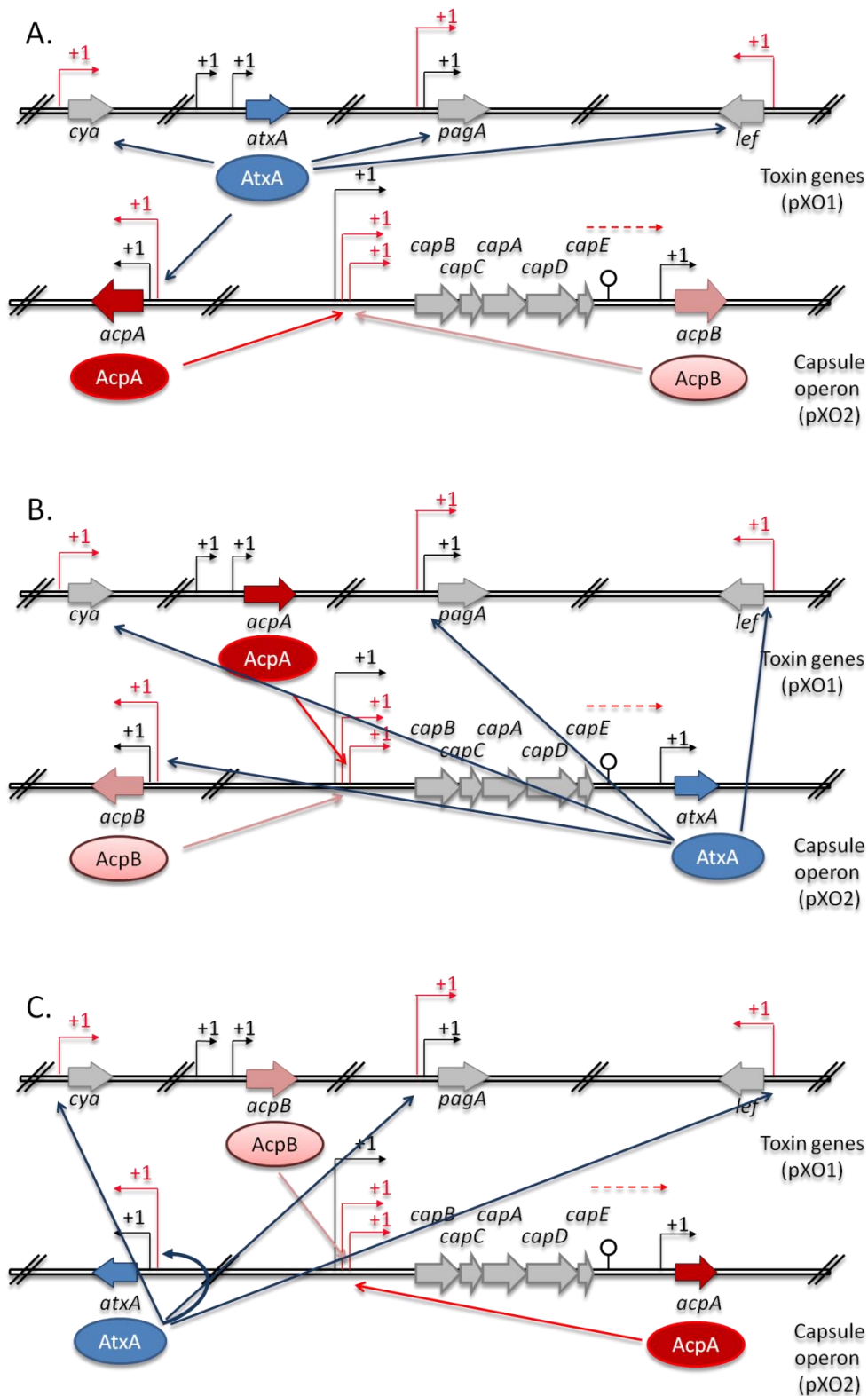


**Figure 7-3.** PCVR locus-activity relationships

CO<sub>2</sub>-dependent transcriptional start sites are red, and low-level constitutive start sites are black. Arrows from proteins to transcript start sites indicate positive regulation. The broken arrow from *capE* to *acpB* transcriptional start site represents a low level of transcriptional read through. (A) PCVR loci in the parent strain. (B & C) Strains in which the open reading frames encoding *AtxA*, *AcpA*, and *AcpB* have been exchanged.

strain would express a thicker capsule than the parent strain, in addition to higher toxin levels.

The impact these locus mutations could have on various cellular processes would be extremely interesting to explore. Modulation of AtxA levels has already been demonstrated to impact sporulation efficiency. The effects on virulence of these mutant strains could be tested in animal models of anthrax. The results of these studies could indicate an optimal level of expression for each PCVR that allows the bacterium to thrive in the host and soil environments.

The ability of an organism to thrive depends to a large extent on its ability to adapt to changing environments and successfully colonize new niches. Adaptation can spawn the creation of genes with new functions to cope with the environmental changes. For the two most well-characterized virulence factors in *B. anthracis*, AtxA has sole control over expression of anthrax toxin, but is a poor regulator of capsule expression. Duplication of *atxA* eventuated the creation of *acpA* and *acpB*. Positive regulation of *acpA* by AtxA allows for AtxA control of toxin and capsule synthesis. AcpA and AcpB expanded their roles beyond regulators of capsule production to control expression of non AtxA-regulated genes. Future investigations addressing domain-specific differences among the regulators will broaden our understanding of the molecular bases for PCVR activity and provide insight into the physiological and evolutionary significance of these major gene control elements of *B. anthracis* and other pathogens.



## References

1. Fuqua, C., S. C. Winans, and E. P. Greenberg. 1996. CENSUS AND CONSENSUS IN BACTERIAL ECOSYSTEMS: The LuxR-LuxI Family of Quorum-Sensing Transcriptional Regulators. *Annu. Rev. Microbiol.* 50: 727–751.
2. Waters, C. M., and B. L. Bassler. 2005. QUORUM SENSING: Cell-to-Cell Communication in Bacteria. *Annu. Rev. Cell Dev. Biol.* 21: 319–346.
3. Miller, M. B., and B. L. Bassler. 2001. Ensing in. *Annu. Rev. Microbiol.* 55: 165–99.
4. Mascher, T., J. D. Helmann, and G. Uden. 2006. Stimulus Perception in Bacterial Signal-Transducing Histidine Kinases. *Microbiol. Mol. Biol. Rev.* 70: 910–938.
5. Capra, E. J., and M. T. Laub. 2012. Evolution of Two-Component Signal Transduction Systems. *Annu. Rev. Microbiol.* 66: 325–347.
6. Wolanin, P. M., P. A. Thomason, and J. B. Stock. 2002. Histidine protein kinases: key signal transducers outside the animal kingdom. *Genome Biol.* 3: REVIEWS3013.
7. Deutscher, J., C. Francke, and P. W. Postma. 2006. How Phosphotransferase System-Related Protein Phosphorylation Regulates Carbohydrate Metabolism in Bacteria. *Microbiol. Mol. Biol. Rev.* 70: 939–1031.
8. Misko, T. P., W. J. Mitchell, N. D. Meadow, and S. Roseman. 1982. Sugar Transport by the Bacterial Phosphotransferase System. *J. Biol. Chem.* 257: 14526–14537.
9. Deutscher, J., F. M. D. Aké, M. Derkaoui, A. C. Zébré, T. N. Cao, H. Bouraoui, T. Kentache, A. Mokhtari, E. Milohanic, and P. Joyet. 2014. The Bacterial Phosphoenolpyruvate:Carbohydrate Phosphotransferase System: Regulation by Protein Phosphorylation and Phosphorylation-Dependent Protein-Protein Interactions. *Microbiol. Mol. Biol. Rev.* 78: 231–256.
10. Hondorp, E. R., and K. S. McIver. 2007. The Mga virulence regulon: Infection where the grass is greener. *Mol. Microbiol.* 66: 1056–1065.
11. Hondorp, E. R., S. C. Hou, L. L. Hause, K. Gera, C. E. Lee, and K. S. Mciver. 2013. PTS phosphorylation of Mga modulates regulon expression and virulence in the group A streptococcus. *Mol. Microbiol.* 88: 1176–1193.
12. Treviño, J., Z. Liu, T. N. Cao, E. Ramirez-Peña, and P. Sumbly. 2013. RivR is a negative regulator of virulence factor expression in group a Streptococcus. *Infect. Immun.* 81: 364–372.
13. Kelley, L. A., S. Mezulis, C. M. Yates, M. N. Wass, and M. J. E. Sternberg. 2015. Europe PMC Funders Group The Phyre2 web portal for protein modelling , prediction and analysis. *Nat. Protoc.* 10: 845–858.
14. Solano-Collado, V., R. Lurz, M. Espinosa, and A. Bravo. 2013. The pneumococcal MgaSpn virulence transcriptional regulator generates multimeric complexes on linear double-stranded DNA. *Nucleic Acids Res.* 41: 6975–6991.
15. Baum, M., M. Watad, S. N. Smith, C. J. Alteri, N. Gordon, I. Rosenshine, H. L. Mobley, and O. Amster-Choder. 2014. PafR, a novel transcription regulator, is important for pathogenesis in

uropathogenic *Escherichia coli*. *Infect. Immun.* 82: 4241–4252.

16. Koehler, T. M. 2009. *Bacillus anthracis* physiology and genetics. *Mol. Aspects Med.* 30: 386–396.

17. Keim, P., J. M. Gruendike, A. M. Klevytska, J. M. Schupp, J. Challacombe, and R. Okinaka. 2009. The genome and variation of *Bacillus anthracis*. *Mol. Aspects Med.* 30: 397–405.

18. Klee, S. R., M. Özel, B. Appel, C. Boesch, H. Ellerbrok, D. Jacob, G. Holland, F. H. Leendertz, G. Pauli, R. Grunow, and H. Nattermarm. 2006. Characterization of *Bacillus anthracis*-like bacteria isolated from wild great apes from Côte d'Ivoire and Cameroon. *J. Bacteriol.* 188: 5333–5344.

19. Breezillon, C., M. Haustant, S. Dupke, J. P. Corre, A. Lander, T. Franz, M. Monot, E. Couture-Tosi, G. Jouvion, F. H. Leendertz, R. Grunow, M. E. Mock, S. R. Klee, and P. L. Goossens. 2015. Capsules, Toxins and AtxA as Virulence Factors of Emerging *Bacillus cereus* Biovar anthracis. *PLoS Negl. Trop. Dis.* 9: 1–27.

20. Hoffmaster, A. R., K. K. Hill, J. E. Gee, C. K. Marston, B. K. De, T. Popovic, D. Sue, P. P. Wilkins, S. B. Avashia, R. Drumgoole, C. H. Helma, L. O. Ticknor, R. T. Okinaka, and P. J. Jackson. 2006. Characterization of *Bacillus cereus* isolates associated with fatal pneumonias: Strains are closely related to *Bacillus anthracis* and Harbor *B. anthracis* virulence genes. *J. Clin. Microbiol.* 44: 3352–3360.

21. Cardazzo, B., E. Negrisolò, L. Carraro, L. Alberghini, T. Patarnello, and V. Giaccone. 2008. Multiple-locus sequence typing and analysis of toxin genes in *Bacillus cereus* food-borne isolates. *Appl. Environ. Microbiol.* 74: 850–860.

22. Swick, M. C., T. M. Koehler, and A. Driks. 2016. Surviving Between Hosts: Sporulation and Transmission. *Virulence Mech. Bact. Pathog. Fifth Ed.* 4: 529–566.

23. Dragon, D. C., and R. P. Rennie. 1995. The ecology of anthrax spores: Tough but not invincible. 36.

24. Saile, E., and T. M. Koehler. 2006. *Bacillus anthracis* multiplication, persistence, and genetic exchange in the rhizosphere of grass plants. *Appl. Environ. Microbiol.* 72: 3168–3174.

25. Weiner, Z. P., and I. J. Glomski. 2012. Updating perspectives on the initiation of *Bacillus anthracis* growth and dissemination through its host. *Infect. Immun.* 80: 1626–1633.

26. Organization, W. H. 2008. *Anthrax in humans and animals*,. Geneva, Switzerland.

27. Prevention, C. for D. C. and. 2013. Gastrointestinal Anthrax. .

28. Brookmeyer, R. 2002. Prevention of Inhalational Anthrax in the U.S. Outbreak. *Science (80- .)*. 295: 1861–1861.

29. Drysdale, M., A. Bourgogne, S. G. Hilsenbeck, and T. M. Koehler. 2004. atxA Controls *Bacillus anthracis* Capsule Synthesis via acpA and a Newly Discovered Regulator, acpB. *J. Bacteriol.* 186: 307–315.

30. Dai, Z., J. C. Sirard, M. Mock, and T. M. Koehler. 1995. The atxA gene product activates transcription of the anthrax toxin genes and is essential for virulence. *Mol. Microbiol.* 16: 1171–

1181.

31. Artenstein, A. W., and S. M. Opal. 2012. Novel approaches to the treatment of systemic anthrax. *Clin. Infect. Dis.* 54: 1148–1161.
32. Bradley, K. A., J. Mogridge, M. Mourez, R. J. Collier, and J. A. T. Young. 2001. Identification of the cellular receptor for anthrax toxin. *Nature* 414: 225–229.
33. Friedman, T., V. Gordon, S. Leppla, K. Klimpel, N. P. Birch, and P. Y. Loh. 1995. In vitro Processing of Anthrax Toxin Protective Antigen by Recombinant PC1SPC3 and Bovine Intermediate Lobe Secretory Vesicles Membranes. *Arch. Biochem. Biophys.* 316: 5–13.
34. Milne, J. C., D. Furlong, P. C. Hanna, J. S. Wall, and R. J. Collier. 1994. Anthrax protective antigen forms oligomers during intoxication of mammalian cells. *J. Biol. Chem.* 269: 20607–20612.
35. Beauregard, K. E., S. Wimer-Mackin, R. J. Collier, and W. I. Lencer. 1999. Anthrax toxin entry into polarized epithelial cells. *Infect. Immun.* 67: 3026–3030.
36. Friedlander, A. 1986. Macrophages are sensitive to anthrax lethal toxin through an acid-dependent process. *J. Biol. Chem.* 261: 7123–7126.
37. Gordon, V. M., S. H. Leppla, and E. L. Hewlett. 1988. Inhibitors of receptor-mediated endocytosis block the entry of *Bacillus anthracis* adenylate cyclase toxin but not that of *Bordetella pertussis* adenylate cyclase toxin. *Infect. Immun.* 56: 1066–1069.
38. Krantz, B. A., A. Finkelstein, and R. J. Collier. 2006. Protein translocation through the anthrax toxin transmembrane pore is driven by a proton gradient. *J. Mol. Biol.* 355: 968–979.
39. Krantz, B. A., A. D. Trivedi, K. Cunningham, K. A. Christensen, and R. J. Collier. 2004. Acid-induced unfolding of the amino-terminal domains of the lethal and edema factors of anthrax toxin. *J. Mol. Biol.* 344: 739–756.
40. Collier, R. J., and J. A. T. Young. 2003. Anthrax Toxin. *Annu. Rev. Cell Dev. Biol.* 19: 45–70.
41. Leppla, S. H. 1982. Anthrax toxin edema factor: a bacterial adenylate cyclase that increases cyclic AMP concentrations of eukaryotic cells. *Proc. Natl. Acad. Sci. U. S. A.* 79: 3162–3166.
42. Hochstrasser, M., and D. Kornitzer. 1998. Ubiquitin-Dependent Degradation of Transcription Regulators. In *Ubiquitin and the Biology of the Cell* J. Peters, and J. Harris, eds. Boston, MA.
43. Smith, H., J. Keppie, and J. L. Stanley. 1953. The Chemical Basis of the Virulence of *Bacillus anthracis*. I: Properties of Bacteria Grown in vivo and Preparation of Extracts. *Br. J. Exp. Pathol.* 34: 477–485.
44. Makino, S. I., I. Uchida, N. Terakado, C. Sasakawa, and M. Yoshikawa. 1989. Molecular characterization and protein analysis of the *cap* region, which is essential for encapsulation in *Bacillus anthracis*. *J. Bacteriol.* 171: 722–730.
45. Ashiuchi, M., K. Shimanouchi, H. Nakamura, T. Kamei, K. Soda, C. Park, M. Sung, and H.

Misono. 2004. Enzymatic synthesis of high-molecular-mass poly-g-glutamate and regulation of its stereochemistry. *Appl. Environ. Microbiol.* 70: 4249–4255.

46. Record, B. R., and R. G. Wallis. 1955. Physicochemical Examination of Polyglutamic Acid from *Bacillus anthracis* Grown in vivo. *Biochem. J.* 63: 443–447.

47. Candela, T., M. Mock, and A. Fouet. 2005. CapE, a 47-amino-acid peptide, is necessary for *Bacillus anthracis* polyglutamate capsule synthesis. *J. Bacteriol.* 187: 7765–7772.

48. Scorpio, A., D. J. Chabot, W. A. Day, T. A. Hoover, and A. M. Friedlander. 2010. Capsule depolymerase overexpression reduces *Bacillus anthracis* virulence. *Microbiology* 156: 1459–1467.

49. Uchida, I., J. A. N. M. Hornung, C. B. Thorne, K. R. Klimpel, and S. H. Lepplal. 1993. Cloning and Characterization of a Gene Whose Product Is a trans-Activator of Anthrax Toxin Synthesis. 175: 5329–5338.

50. Jelacic, T. M., D. J. Chabot, J. A. Bozue, S. A. Tobery, M. W. West, K. Moody, D. Yang, J. J. Oppenheim, and A. M. Friedlander. 2014. Exposure to bacillus anthracis capsule results in suppression of human monocyte-derived dendritic cells. *Infect. Immun.* 82: 3405–3416.

51. Chitlaru, T., G. Zaide, S. Ehrlich, I. Inbar, O. Cohen, and A. Shafferman. 2011. HtrA is a major virulence determinant of *Bacillus anthracis*. *Mol. Microbiol.* 81: 1542–1559.

52. Gat, O., I. Mendelson, T. Chitlaru, N. Ariel, Z. Altboum, H. Levy, S. Weiss, H. Grosfeld, S. Cohen, and A. Shafferman. 2005. The solute-binding component of a putative Mn(II) ABC transporter (MntA) is a novel *Bacillus anthracis* virulence determinant. *Mol. Microbiol.* 58: 533–551.

53. McGillivray, S. M., C. M. Ebrahimi, N. Fisher, M. Sabet, D. X. Zhang, Y. Chen, N. M. Haste, R. V. Aroian, R. L. Gallo, D. G. Guiney, A. M. Friedlander, T. M. Koehler, and V. Nizet. 2009. ClpX contributes to innate defense peptide resistance and virulence phenotypes of *Bacillus anthracis*. *J. Innate Immun.* 1: 494–506.

54. Cendrowski, S., W. MacArthur, and P. Hanna. 2004. *Bacillus anthracis* requires siderophore biosynthesis for growth in macrophages and mouse virulence. *Mol. Microbiol.* 51: 407–417.

55. Kern, J. W., and O. Schneewind. 2008. BslA, a pXO1-encoded adhesin of *Bacillus anthracis*. *Mol. Microbiol.* 68: 504–515.

56. Bourgogne, A., M. Drysdale, S. G. Hilsenbeck, S. N. Peterson, T. M. Koehler, A. Bourgogne, M. Drysdale, S. G. Hilsenbeck, S. N. Peterson, and T. M. Koehler. 2003. Global Effects of Virulence Gene Regulators in a *Bacillus anthracis* Strain with Both Virulence Plasmids Global Effects of Virulence Gene Regulators in a *Bacillus anthracis* Strain with Both Virulence Plasmids. .

57. Koehler, T. M., Z. Dai, and M. Kaufman-Yarbray. 1994. Regulation of the *Bacillus anthracis* protective antigen gene: CO<sub>2</sub> and a trans-acting element activate transcription from one of two promoters. *J. Bacteriol.* 176: 586–595.

58. Hadjifrangiskou, M., and T. M. Koehler. 2008. Intrinsic curvature associated with the coordinately regulated anthrax toxin gene promoters. *Microbiology* 154: 2501–2512.

59. Dai, Z., and T. M. Koehler. 1997. Regulation of anthrax toxin activator gene (*atxA*) expression in *Bacillus anthracis*: Temperature, not CO<sub>2</sub>/bicarbonate, affects *atxA* synthesis. *Infect. Immun.* 65: 2576–2582.
60. Wilson, A. C., J. A. Hoch, and M. Perego. 2009. Two small c-type cytochromes affect virulence gene expression in *Bacillus anthracis*. *Mol. Microbiol.* 72: 109–123.
61. Strauch, M. A., P. Ballar, A. J. Rowshan, and K. L. Zoller. 2005. The DNA-binding specificity of the *Bacillus anthracis* AbrB protein. *Microbiology* 151: 1751–1759.
62. Saile, E., and T. M. Koehler. 2002. Control of Anthrax Toxin Gene Expression by the Transition State Regulator *abrB*. *Control of Anthrax Toxin Gene Expression by the Transition State Regulator *abrB**. 184: 370–380.
63. Chiang, C., C. Bongiorno, and M. Perego. 2011. Glucose-dependent activation of *Bacillus anthracis* toxin gene expression and virulence requires the carbon catabolite protein CcpA. *J. Bacteriol.* 193: 52–62.
64. Hammerstrom, T. G., J. H. Roh, E. P. Nikonowicz, and T. M. Koehler. 2011. *Bacillus anthracis* virulence regulator AtxA: Oligomeric state, function and CO<sub>2</sub>-signalling. *Mol. Microbiol.* 82: 634–647.
65. Hammerstrom, T. G., L. B. Horton, M. C. Swick, A. Joachimiak, J. Osipiuk, and T. M. Koehler. 2015. Crystal structure of *Bacillus anthracis* virulence regulator AtxA and effects of phosphorylated histidines on multimerization and activity. *Mol. Microbiol.* 95: 426–441.
66. Tsvetanova, B., A. C. Wilson, C. Bongiorno, C. Chiang, J. A. Hoch, and M. Perego. 2007. Opposing effects of histidine phosphorylation regulate the AtxA virulence transcription factor in *Bacillus anthracis*. *Mol. Microbiol.* 63: 644–655.
67. Sirard, J. C., M. Mock, and A. Fouet. 1994. The three *Bacillus anthracis* toxin genes are coordinately regulated by bicarbonate and temperature. *J. Bacteriol.* 176: 5188–5192.
68. Shivers, R. P., and A. L. Sonenshein. 2004. Activation of the *Bacillus subtilis* global regulator CodY by direct interaction with branched-chain amino acids. *Mol. Microbiol.* 53: 599–611.
69. van Schaik, W., A. Château, M.-A. Dillies, J.-Y. Coppée, A. L. Sonenshein, and A. Fouet. 2009. The global regulator CodY regulates toxin gene expression in *Bacillus anthracis* and is required for full virulence. *Infect. Immun.* 77: 4437–4445.
70. Drysdale, M., A. Bourgogne, and T. M. Koehler. 2005. Transcriptional Analysis of the *Bacillus anthracis* Capsule Regulators. 187: 5108–5114.
71. Uchida, I., S. I. Makino, T. Sekizaki, and N. Terakado. 1997. Cross-talk to the genes for *Bacillus anthracis* capsule synthesis by *atxA*, the gene encoding the trans-activator of anthrax toxin synthesis. *Mol. Microbiol.* 23: 1229–1240.
72. Drobniowski, F. A. 1993. *Bacillus cereus* and Related Species. *Microbiology* 6: 324–338.
73. Hoffmaster, A. R., J. Ravel, D. a Rasko, G. D. Chapman, M. D. Chute, C. K. Marston, B. K. De, C. T. Sacchi, C. Fitzgerald, L. W. Mayer, M. C. J. Maiden, F. G. Priest, M. Barker, L. Jiang,

- R. Z. Cer, J. Rilstone, S. N. Peterson, R. S. Weyant, D. R. Galloway, T. D. Read, T. Popovic, and C. M. Fraser. 2004. Identification of anthrax toxin genes in a *Bacillus cereus* associated with an illness resembling inhalation anthrax. *Proc. Natl. Acad. Sci. U. S. A.* 101: 8449–54.
74. Thorne, C. B., and F. C. Belton. 1957. An agar-diffusion method for titrating *Bacillus anthracis* immunizing antigen and its application to a study of antigen production. *J. Gen. Microbiol.* 17: 505–516.
75. Hadjifrangiskou, M., Y. Chen, and T. M. Koehler. 2007. The Alternative Sigma Factor H Is Required for Toxin Gene Expression by *Bacillus anthracis*. *J. Bacteriol.* 189: 1874–1883.
76. Britton, R. a, P. Eichenberger, J. Eduardo, P. Fawcett, R. Monson, A. D. Grossman, J. E. Gonzalez-pastor, and R. Losick. 2002. Genome-Wide Analysis of the Stationary-Phase Sigma Factor ( Sigma-H ) Regulon of *Bacillus subtilis* Genome-Wide Analysis of the Stationary-Phase Sigma Factor ( Sigma-H ) Regulon of *Bacillus subtilis*. *Society* 184: 4881–4890.
77. Welkos, S., S. Little, A. Friedlander, D. Fritz, and P. Fellows. 2001. The role of antibodies to *Bacillus anthracis* and anthrax toxin components in inhibiting the early stages of infection by anthrax spores. *Microbiology* 147: 1677–1685.
78. Sambrook, J., and D. W. Russell. 2001. *Molecular Cloning - Sambrook & Russel*,
79. Marrero, R., and S. L. Welkos. 1995. The transformation frequency of plasmids into *Bacillus anthracis* is affected by adenine methylation. *Gene* 152: 75–78.
80. Pflughoeft, K. J., P. Sumby, and T. M. Koehler. 2011. *Bacillus anthracis* sin locus and regulation of secreted proteases. *J. Bacteriol.* 193: 631–639.
81. Horton, R. M., H. D. Hunt, S. N. Ho, J. K. Pullen, and L. R. Pease. 1989. Engineering hybrid genes without the use of restriction enzymes: gene splicing by overlap extension. *Gene* 77: 61–68.
82. Agaisse, H., and D. Lereclus. 1994. Expression in *Bacillus subtilis* of the *Bacillus thuringiensis* cryIIIA toxin gene is not dependent on a sporulation-specific sigma factor and is increased in a spo0A mutant. *J. Bacteriol.* 176: 4734–4741.
83. Thorvaldsdóttir, H., J. T. Robinson, and J. P. Mesirov. 2013. Integrative Genomics Viewer (IGV): High-performance genomics data visualization and exploration. *Brief. Bioinform.* 14: 178–192.
84. Quinlan, A. R., and I. M. Hall. 2010. BEDTools: A flexible suite of utilities for comparing genomic features. *Bioinformatics* 26: 841–842.
85. Langmead, B., and S. L. Salzberg. 2012. Fast gapped-read alignment with Bowtie 2. *Nat. Methods* 9: 357–359.
86. Liao, Y., G. K. Smyth, and W. Shi. 2014. FeatureCounts: An efficient general purpose program for assigning sequence reads to genomic features. *Bioinformatics* 30: 923–930.
87. Love, M. I., W. Huber, and S. Anders. 2014. Moderated estimation of fold change and dispersion for RNA-seq data with DESeq2. *Genome Biol.* 15.
88. Wattam, A. R., D. Abraham, O. Dalay, T. L. Disz, T. Driscoll, J. L. Gabbard, J. J. Gillespie,

- R. Gough, D. Hix, R. Kenyon, D. MacHi, C. Mao, E. K. Nordberg, R. Olson, R. Overbeek, G. D. Pusch, M. Shukla, J. Schulman, R. L. Stevens, D. E. Sullivan, V. Vonstein, A. Warren, R. Will, M. J. C. Wilson, H. S. Yoo, C. Zhang, Y. Zhang, and B. W. Sobral. 2014. PATRIC, the bacterial bioinformatics database and analysis resource. *Nucleic Acids Res.* 42.
89. Green, B. D., L. Battisti, T. M. Koehler, C. B. Thorne, and B. E. Ivins. 1985. Demonstration of a capsule plasmid in *Bacillus anthracis*. *Infect. Immun.* 49: 291–297.
90. Ivins, B. E., S. L. Welkos, G. B. Knudson, and S. F. Little. 1990. Immunization against anthrax with aromatic compound-dependent (Aro-) mutants of *Bacillus anthracis* and with recombinant strains of *Bacillus subtilis* that produce anthrax protective antigen. *Infect. Immun.* 58: 303–308.
91. Dale, J. L., M. J. Raynor, P. Dwivedi, and T. M. Koehler. 2012. cis-acting elements that control expression of the master virulence regulatory gene *atxA* in *Bacillus anthracis*. *J. Bacteriol.* 194: 4069–4079.
92. Han, H., and A. C. Wilson. 2013. The two *CcdA* proteins of *Bacillus anthracis* differentially affect virulence gene expression and sporulation. *J. Bacteriol.* 195: 5242–5249.
93. Scarff, J. M., M. J. Raynor, Y. I. Seldina, C. L. Ventura, T. M. Koehler, and A. D. O'Brien. 2016. The roles of *AtxA* orthologs in virulence of anthrax-like *Bacillus cereus* G9241. *Mol. Microbiol.* 102: 545–561.
94. Stenz, L., P. Francois, K. Whiteson, C. Wolz, P. Linder, and J. Schrenzel. 2011. The *CodY* pleiotropic repressor controls virulence in gram-positive pathogens. *FEMS Immunol. Med. Microbiol.* 62: 123–139.
95. Miller, J. H. 1972. Assay of b-galactosidase. In *Experiments in molecular genetics* 352–355.
96. Thorne, C. B. 1993. *Bacillus anthracis*. In *Bacillus subtilis and Other Gram-Positive Bacteria: Biochemistry, Physiology and Molecular Genetics* A. L. Sonenshein, J. A. Hoch, and R. Losick, eds. American Society for Microbiology, Washington, DC. 113–124.
97. Carr, K. A., S. R. Lybarger, E. C. Anderson, B. K. Janes, and P. C. Hanna. 2010. The role of *Bacillus anthracis* germinant receptors in germination and virulence. *Mol. Microbiol.* 75: 365–375.
98. Hoffmaster, A. R., and T. M. Koehler. 1999. Control of virulence gene expression in *Bacillus anthracis*. 279–281.
99. Liang, X., E. Zhang, H. Zhang, J. Wei, W. Li, and J. Zhu. 2016. Involvement of the *pagR* gene of *pXO2* in anthrax pathogenesis. *Nat. Publ. Gr.* 1–10.
100. Fouet, A., and M. Mock. 1996. Differential Influence of the Two *Bacillus anthracis* Plasmids on Regulation of Virulence Gene Expression. 64: 4928–4932.
101. Guignot, J., M. Mock, and A. Fouet. 1997. *AtxA* activates the transcription of genes harbored by both *Bacillus anthracis* virulence plasmids. *FEMS Microbiol. Lett.* 147: 203–207.
102. Sirard, J., C. Guidi-Rontani, A. Fouet, and M. Mock. 2000. Characterization of a plasmid region involved. *Int. J. Med. Microbiol.* 290: 313–316.

103. Mignot, T., M. Mock, and A. Fouet. 2003. A plasmid-encoded regulator couples the synthesis of toxins and surface structures in *Bacillus anthracis*. *Mol. Microbiol.* 47: 917–927.
104. Makino, S., C. Sasakawa, I. Uchida, N. Terakado, and M. Yoshikawa. 1988. Cloning and CO<sub>2</sub>-dependent expression of the genetic region for encapsulation from *Bacillus anthracis*. *Mol. Microbiol.* 2: 371–376.
105. Meynell, E., and G. G. Meynell. 1964. The roles of serum and carbon dioxide in capsule formation by *Bacillus anthracis*. *J. Gen. Microbiol.* 34: 153–164.
106. Ross, C. L., K. S. Thomason, and T. M. Koehler. 2009. An extracytoplasmic function sigma factor controls  $\beta$ -lactamase gene expression in *Bacillus anthracis* and other *Bacillus cereus* group species. *J. Bacteriol.* 191: 6683–6693.
107. Drysdale, M., S. Heninger, J. Hutt, Y. Chen, C. R. Lyons, and T. M. Koehler. 2005. Capsule synthesis by *Bacillus anthracis* is required for dissemination in murine inhalation anthrax. *EMBO J.* 24: 221–227.
108. Hondorp, E. R., S. C. Hou, A. D. Hempstead, L. L. Hause, D. M. Beckett, and K. S. McIver. 2012. Characterization of the Group A *Streptococcus* Mga virulence regulator reveals a role for the C-terminal region in oligomerization and transcriptional activation. *Mol. Microbiol.* 83: 953–967.
109. Okinaka, R. T., K. Cloud, O. Hampton, a. R. Hoffmaster, K. K. Hill, P. Keim, T. M. Koehler, G. Lamke, S. Kumano, J. Mahillon, D. Manter, Y. Martinez, D. Ricke, # R. Svensson, and P. J. Jackson. 1999. Sequence and organization of pXO1, the large *Bacillus anthracis* plasmid harboring the anthrax toxin genes. *J. Bacteriol.* 181: 6509–6515.
110. Van der Auwera, G. a, L. Andrup, and J. Mahillon. 2005. Conjugative plasmid pAW63 brings new insights into the genesis of the *Bacillus anthracis* virulence plasmid pXO2 and of the *Bacillus thuringiensis* plasmid pBT9727. *BMC Genomics* 6: 103.
111. Hava, D. L., C. J. Hemsley, and A. Camilli. 2003. Transcriptional regulation in the *Streptococcus pneumoniae* *rlrA* pathogenicity islet by RlrA. *J. Bacteriol.* 185: 413–421.
112. Panchaud, A., L. Guy, F. Collyn, M. Haenni, M. Nakata, A. Podbielski, P. Moreillon, and C. A. Roten. 2009. M-protein and other intrinsic virulence factors of *Streptococcus pyogenes* are encoded on an ancient pathogenicity island. *BMC Genomics* 10: 198.
113. Kongklom, N., H. Luo, Z. Shi, C. Pechyen, Y. Chisti, and S. Sirisansaneeyakul. 2015. Production of poly- $\gamma$ -glutamic acid by glutamic acid-independent *Bacillus licheniformis* TISTR 1010 using different feeding strategies. *Biochem. Eng. J.* 100: 67–75.
114. Urushibata, Y., S. Tokuyama, and Y. Tahara. 2002. Characterization of the *Bacillus subtilis* *ywsC* gene, involved in  $\gamma$ -polyglutamic acid production. *J. Bacteriol.* 184: 337–343.
115. Ribardo, D. A., and K. S. McIver. 2006. Defining the Mga regulon: Comparative transcriptome analysis reveals both direct and indirect regulation by Mga in the group A streptococcus. *Mol. Microbiol.* 62: 491–508.
116. Roberts, S. A., and J. R. Scott. 2007. RivR and the small RNA RivX: The missing links between the CovR regulatory cascade and the Mga regulon. *Mol. Microbiol.* 66: 1506–1522.



117. Cunningham, M. W. 2000. Pathogenesis of group A streptococcal infections. *Clin. Microbiol. Rev.* 13: 470–511.
118. Bisno, A. L. 2003. Diagnosing Strep Throat in the Adult Patient: Do Clinical Criteria Really Suffice? *Ann. Intern. Med.* 139: 150–151.
119. McLellan, L. K., and D. A. Hunstad. 2016. Urinary Tract Infection: Pathogenesis and Outlook. *Trends Mol. Med.* 22: 946–957.
120. Kirby, J. E. 2004. Anthrax lethal toxin induces human endothelial cell apoptosis. *Infect. Immun.* 72: 430–439.
121. Frankel, A., S.-R. Kuo, D. Dostal, L. Watson, N. Duesbery, C.-P. Cheng, H. J. Cheng, W.-J. Tang, and S. Leppla. 2014. NIH Public Access. *Front. Biosci.* 14: 4516–4524.
122. Terwilliger, A., M. C. Swick, K. J. Pflughoeft, A. Pomerantsev, C. R. Lyons, T. M. Koehler, and A. Maresso. 2015. Bacillus anthracis overcomes an amino acid auxotrophy by cleaving host serum proteins. *J. Bacteriol.* 197: 2400–2411.
123. Kaiser, J. C., S. Omer, J. R. Sheldon, I. Welch, and D. E. Heinrichs. 2015. Role of BrnQ1 and BrnQ2 in branched-chain amino acid transport and virulence in Staphylococcus aureus. *Infect. Immun.* 83: 1019–1029.
124. Belitsky, B. R. 2015. Role of branched-chain amino acid transport in Bacillus subtilis CodY activity. *J. Bacteriol.* 197: 1330–1338.
125. Lobel, L., N. Sigal, I. Borovok, B. R. Belitsky, A. L. Sonenshein, and A. A. Herskovits. 2015. The metabolic regulator CodY links Listeria monocytogenes metabolism to virulence by directly activating the virulence regulatory gene prfA. *Mol. Microbiol.* 95: 624–644.
126. Benson, D. A., I. Karsch-Mizrachi, D. J. Lipman, J. Ostell, and D. L. Wheeler. 2005. GenBank. *Nucleic Acids Res.* 33: 34–38.
127. Cottier, F., W. Leewattanapasuk, L. R. Kemp, M. Murphy, C. T. Supuran, O. Kurzai, and F. A. Mühlischlegel. 2013. Carbonic anhydrase regulation and CO<sub>2</sub>sensing in the fungal pathogen Candida glabrata involves a novel Rca1p ortholog. *Bioorganic Med. Chem.* 21: 1549–1554.
128. Cragg, P., A. B. C. MacKnight, and R. C. Mills. 1999. Estimating Plasma PH. In *Lecture Notes on Human Physiology* J. J. Bray, ed. Blackwell Science, Malden, MA. 556.
129. Yesudhas, D., M. Batoor, M. A. Anwar, S. Panneerselvam, and S. Choi. 2017. Proteins recognizing DNA: Structural uniqueness and versatility of DNA-binding domains in stem cell transcription factors. *Genes (Basel)*. 8.
130. Tschowri, N., M. A. Schumacher, S. Schlimpert, N. B. Chinnam, K. C. Findlay, R. G. Brennan, and M. J. Buttner. 2014. Tetrameric c-di-GMP mediates effective transcription factor dimerization to control streptomyces development. *Cell* 158: 1136–1147.
131. Bouraoui, H., M. Ventroux, M. F. Noirot-Gros, J. Deutscher, and P. Joyet. 2013. Membrane sequestration by the EIIB domain of the mannitol permease MtlA activates the Bacillus subtilis mtl operon regulator MtlR. *Mol. Microbiol.* 87: 789–801.

132. Gottesman, S., M. Gottesman, J. E. Shaw, and M. L. Pearson. 1981. Protein degradation in *E. coli*: The lon mutation and bacteriophage lambda N and cII protein stability. *Cell* 24: 225–233.
133. Yang, J., E. Hart, M. Tauschek, G. D. Price, E. L. Hartland, R. A. Strugnell, and R. M. Robins-Browne. 2008. Bicarbonate-mediated transcriptional activation of divergent operons by the virulence regulatory protein, RegA, from *Citrobacter rodentium*. *Mol. Microbiol.* 68: 314–327.
134. Yang, J., C. Dogovski, D. Hocking, M. Tauschek, M. Perugini, and R. M. Robins-Browne. 2009. Bicarbonate-Mediated Stimulation of RegA, the Global Virulence Regulator from *Citrobacter rodentium*. *J. Mol. Biol.* 394: 591–599.
135. Farazdaghi, H. 2011. The single-process biochemical reaction of Rubisco: A unified theory and model with the effects of irradiance, CO<sub>2</sub> and rate-limiting step on the kinetics of C<sub>3</sub> and C<sub>4</sub> photosynthesis from gas exchange. *BioSystems* 103: 265–284.
136. Aggarwal, M., T. K. Chua, M. A. Pinard, D. M. Szebenyi, and R. McKenna. 2015. Carbon Dioxide “Trapped” in a  $\beta$ -Carbonic Anhydrase. *Biochemistry* 54: 6631–6638.
137. Kolstø, A.-B., N. J. Tourasse, and O. A. Økstad. 2009. What Sets *Bacillus anthracis* Apart from Other *Bacillus* Species? *Annu. Rev. Microbiol.* 63: 451–476.
138. Ehling-Schulz, M., M. Fricker, H. Grallert, P. Rieck, M. Wagner, and S. Scherer. 2006. Cereulide synthetase gene cluster from emetic *Bacillus cereus*: Structure and location on a mega virulence plasmid related to *Bacillus anthracis* toxin plasmid pXO1. *BMC Microbiol.* 6: 1–11.
139. Cinader, B., S. Dubiski, and A. C. Wardlaw. 1964. Distribution, inheritance, and properties of an antigen, MuB1, and its relation to hemolytic complement. *J. Exp. Med.* 120: 897–924.
140. Welkos, S. L., and A. M. Friedlander. 1988. Pathogenesis and genetic control of resistance to the Sterne strain of *Bacillus anthracis*. *Microb. Pathog.* 4: 53–69.
141. Welkos, S. L., T. J. Keener, and P. H. Gibbs. 1986. Differences in susceptibility of inbred mice to *Bacillus anthracis*. *Infect. Immun.* 51: 795–800.
142. Welkos, S. L., R. W. Trotter, D. M. Becker, and G. O. Nelson. 1989. Resistance to the Sterne strain of *B. anthracis*: phagocytic cell responses of resistant and susceptible mice. *Microb. Pathog.* 7: 15–35.
143. Wetsel, R. A., D. T. Fleischer, and D. L. Haviland. 1990. Deficiency of the murine fifth complement component (C5): A 2-base pair gene deletion in A 5???-exon. *J. Biol. Chem.* 265: 2435–2440.
144. Schuch, R., and V. A. Fischetti. 2009. The secret life of the anthrax agent *Bacillus anthracis*: Bacteriophage-mediated ecological adaptations. *PLoS One* 4.
145. Hugh-Jones, M., and J. Blackburn. 2009. The ecology of *Bacillus anthracis*. *Mol. Aspects Med.* 30: 356–367.
146. Ratnayake-Lecamwasam, M., P. Serror, K. W. Wong, and A. L. Sonenshein. 2001. *Bacillus subtilis* CodY represses early-stationary-phase genes by sensing GTP levels. *Genes*

*Dev.* 15: 1093–1103.

147. Smith, I., I. Mandić-Mulec, and N. Gaur. 1991. The role of negative control in sporulation. *Res. Microbiol.* 142: 831–839.

148. Strauch, M., V. Webb, G. Spiegelman, and J. A. Hoch. 1990. The SpoOA protein of *Bacillus subtilis* is a repressor of the *abrB* gene. *Proc. Natl. Acad. Sci.* 87: 1801–1805.

149. Burbulys, D., K. A. Trach, and J. A. Hoch. 1991. Initiation of sporulation in *B. subtilis* is controlled by a multicomponent phosphorelay. *Cell* 64: 545–552.

150. White, A. K., J. A. Hoch, M. Grynberg, A. Godzik, and M. Perego. 2006. Sensor domains encoded in *Bacillus anthracis* virulence plasmids prevent sporulation by hijacking a sporulation sensor histidine kinase. *J. Bacteriol.* 188: 6354–6360.

151. Bartkus, J. M., and S. H. Leppla. 1989. Transcriptional regulation of the protective antigen gene of *Bacillus anthracis*. *Infect. Immun.* 57: 2295–2300.

152. Cataldi, A., A. Fouet, and M. Mock. 1992. Regulation of *pag* gene expression in *Bacillus anthracis*: use of a *pag-lacZ* transcriptional fusion. *FEMS Microbiol Lett* 77: 89–93.

153. Geers, C., and G. Gros. 2000. Carbon dioxide transport and carbonic anhydrase in blood and muscle. *Physiol. Rev.* 80: 681–715.

154. Bush, L. M., B. H. Abrams, A. Beall, and C. C. Johnson. 2001. Index Case of Fatal Inhalational Anthrax due to Bioterrorism in the United States. *NEJM New Engl. J. Med.* 345: 1607–1610.

155. Dlugokencky, E., and P. Tans. 2013. Trends in Carbon Dioxide. *NOAA /ESRL* .

156. Dale, J. L., M. J. Raynor, M. C. Ty, M. Hadjifrangiskou, and T. M. Koehler. 2018. A dual role for the *Bacillus anthracis* master virulence regulator AtxA: Control of sporulation and anthrax toxin production. *Front. Microbiol.* 9: 1–12.

157. Lovegrove, B. G. 2012. The evolution of mammalian body temperature: The Cenozoic supraendothermic pulses. *J. Comp. Physiol. B Biochem. Syst. Environ. Physiol.* 182: 579–589.

158. Murzin, A. G. 1998. How far divergent evolution goes in proteins. *Curr. Opin. Struct. Biol.* 8: 380–387.

159. Larkin, M. A., G. Blackshields, N. P. Brown, R. Chenna, P. A. Mcgettigan, H. McWilliam, F. Valentin, I. M. Wallace, A. Wilm, R. Lopez, J. D. Thompson, T. J. Gibson, and D. G. Higgins. 2007. Clustal W and Clustal X version 2.0. *Bioinformatics* 23: 2947–2948.

160. Goujon, M., H. McWilliam, W. Li, F. Valentin, S. Squizzato, J. Paern, and R. Lopez. 2010. A new bioinformatics analysis tools framework at EMBL-EBI. *Nucleic Acids Res.* 38: 695–699.

161. McWilliam, H., W. Li, M. Uludag, S. Squizzato, Y. M. Park, N. Buso, A. P. Cowley, and R. Lopez. 2013. Analysis Tool Web Services from the EMBL-EBI. *Nucleic Acids Res.* 41: 597–600.

162. Reams, A. B., and J. R. Roth. 2015. Mechanisms of gene duplication and amplification. *Cold Spring Harb Perspect Biol* 7: a016592.

163. Hurtle, W., E. Bode, D. A. Kulesh, R. S. Kaplan, J. Garrison, D. Bridge, M. House, M. S. Frye, B. Loveless, and D. Norwood. 2004. Detection of *Bacillus anthracis*gyrA gene by using a minor groove binder probe. *J. Clin. Microbiol.* 42.

## **Vita**

Malik Jamaal Raynor was born October 18, 1980 in Atlanta, Georgia to Robert L. Raynor and Shirley L. Raynor. He graduated from Druid Hills High School (Atlanta, GA) in 1999 before attending Emory University (Atlanta, GA). In 2003, he received the Bachelors of Science degree in biology. Starting fall of 2010, he attended The University of Texas Health Science Center at Houston MD Anderson Cancer Center UHealth Graduate School of Biomedical Sciences.

Permanent address:

2465 Fairview Lane

Jonesboro, GA 30236